

## Digital Surveys and BIM Modelling Processes and Semi-Automation

**VINÍCIUS DO VALE FERREIRA**

agosto de 2024

# **Digital Surveys and BIM Modelling: processes and semi-Automation**

**Vinícius do Vale Ferreira**

**Dissertation for the attainment of the  
Master's Degree in Civil Engineering,  
Specialization in Construction**

**Advisor: Prof. Dr. Diogo Rodrigo Ferreira Ribeiro**

**Co-advisor: Prof. Ricardo Manuel Pereira Santos**

**Co-advisor: Eng. Rafael de Araújo Cabral (FEUP)**

**Comitee:**

Chairperson:

Prof. Dra. Maria do Rosário Santos Oliveira, Professora-adjunta, ISEP

Examiners:

Prof. Dr. Diogo Rodrigo Ferreira Ribeiro, Professor-adjunto, ISEP

Prof. Dr. Rodrigo Esmeriz Falcão Moreira, Professor-adjunto, ISEP

July, 2024

## DECLARAÇÃO DE INTEGRIDADE

---

### DECLARAÇÃO DE INTEGRIDADE

Declaro ter conduzido este trabalho académico com integridade. Não plagiei ou apliquei qualquer forma de uso indevido de informações ou falsificação de resultados ao longo do processo que levou à sua elaboração.

Declaro que o trabalho apresentado neste documento é original e de minha autoria, não tendo sido utilizado anteriormente para nenhum outro fim.

Declaro ainda que tenho pleno conhecimento do Código de Conduta Ética do P.PORTO.



ISEP, Porto, 29 de Julho de 2024





## GENERAL INDEX

General Index .....	iii
Abstract .....	v
Resumo .....	vii
Acknowledgments.....	ix
Table of Contents .....	xi
List of Figures .....	xiii
List of Tables.....	xvii
Acronyms and Symbols .....	xix
1.Introduction .....	1
2.Literature Review .....	5
3. Methodology.....	31
4. Case Studies .....	47
5.Discussion.....	61
6.Final remarks.....	63
References.....	65
Annex A .....	71
Annex B .....	73
Annex C .....	75



## **ABSTRACT**

This study aims to enhance the use of advanced technologies to improve the accuracy and efficiency of 3D geometric surveys in civil engineering applications. The thesis proposes a workflow that includes in situ surveys, with and without topographic support, 2D and 3D modeling from point clouds, as well as a contribution to the automation of 3D modeling through a dedicated algorithm developed in VPL and Python.

Digital surveys represent a significant advancement in documenting existing constructions, providing faster, safer, and more accurate measurements compared to traditional methods. The development of the script seeks to facilitate the modeling of structural elements from point clouds, optimizing time and reducing human errors, allowing for minor adjustments to the final model. This script has been detailed so that future work can continue to automate this workflow, which consequently increases productivity in the construction sector.

The first stage of this study, conducted in collaboration with the Warsaw University of Technology, focused on a comparative analysis between the design dimensions and the actual dimensions of a structural connection plate of a railway bridge, using photogrammetry and laser scanning. In the photogrammetry process, photographs obtained from a drone without GNSS were used to create a point cloud, referenced and adjusted iteratively. The point cloud was segmented using the RANSAC method to facilitate 2D modeling.

The second part aimed at semi-automatic 3D modeling, creating an algorithm based on visual programming and Python, using the results of a survey of an industrial warehouse with georeferenced photographs, laser scanning, and topographic support. This point cloud also had to be segmented using the RANSAC method to be used as input for the semi-automatic 3D modeling script

**Keywords:** Photogrammetry, Laser scanner, 2D and 3D Modeling, Visual Programming, RANSAC, Point Cloud, Workflow, Topographic Support.



## RESUMO

Esse estudo visa aprimorar o uso de tecnologias avançadas para melhorar a precisão e eficiência de levantamentos geométricos 3D em aplicações de engenharia civil. A tese propõe um fluxo de trabalho que inclui levantamentos in situ, com e sem apoio topográfico, modelação 2D e 3D a partir de nuvens de pontos, além de um contributo para a automatização da modelação 3D por intermédio de um algoritmo dedicado desenvolvido em VPL e Python.

Os levantamentos digitais são um grande avanço na documentação de construções existentes, proporcionando medições mais rápidas, seguras e precisas comparativamente aos métodos tradicionais. O desenvolvimento do script busca facilitar a modelação de elementos estruturais a partir de nuvens de pontos, otimizando tempo e reduzindo erros humanos, permitindo pequenos ajustes no modelo final. Esse script foi destrinchado para que futuros trabalhos continuem e automatizem cada vez mais esse fluxo de trabalho que gera por consequência maior produtividade no setor da construção civil.

A primeira etapa desse estudo, realizada em colaboração com a Universidade Tecnológica de Varsóvia, focou-se na análise comparativa entre as dimensões de projeto e as reais de uma chapa de conexão estrutural de uma ponte ferroviária, recorrendo a fotogrametria e laser scanner. No processo de fotogrametria, as fotografias obtidas a partir de um drone sem GNSS foram usadas para criar uma nuvem de pontos, referenciadas e ajustadas iterativamente. A nuvem foi segmentada usando o método de RANSAC para facilitar a modelagem 2D.

A segunda parte visou a modelação 3D semi automática, criando um algoritmo baseado em programação visual e Python, a partir dos resultados de um levantamento de um armazém industrial com fotografias georreferenciadas, laser scanner e apoio topográfico. Essa nuvem de pontos também teve de ser segmentada recorrendo ao método de RANSAC para ser usada como input para o script semi automático para modelação 3D.

Palavras-chave: Fotogrametria, Laser scanner, Modelação 2D e 3D, Programação Visual, RANSAC, Nuvem de Pontos, Fluxo de trabalho, Apoio topográfico.



## ACKNOWLEDGMENTS

This work would not have been possible without the support of key individuals who influenced, supported, and inspired me along the way, and I take this opportunity to express my gratitude.

Firstly, to my advisors, Eng Diogo Ribeiro, who gave me the unique opportunity to undertake a study on a subject that is dear to me. Eng Ricardo Santos, who provided the necessary support at key moments for the execution of this thesis, and finally to Eng Rafael Cabral, who provided guidance and support to ensure that the thesis achieved its objective at the highest level; I consider his presence in this work essential.

I thank the Postgraduate Course in BIM Coordination, which sparked my interest in learning more about BIM in general and provided me with the opportunity to meet my advisor, Eng. Diogo Ribeiro.

I would like to express my sincere gratitude to the "Scientific Cooperation Project between Portugal and Poland (FCT-NAWA) titled 'Intelligent Structural Condition Assessment of Existing Steel Railway Bridges,' Ref. 2021.09571.CBM, funded by the Foundation for Science and Technology (FCT)." The collaboration facilitated by this project significantly contributed to the successful development of this dissertation.

Additionally, I wish to acknowledge the "R&D activity contract 'MAPDRONE - Mapping Anomalies in the Exterior Surroundings of Industrial Buildings Based on Photogrammetric 3D Models,'" funded by Multiprojectus, and the collaboration of the contractor company García García. Their support were crucial for the practical aspects of this work.

I thank my family, my mother, father, and brother, who have always supported me during the execution of this work, without which this study would not have been possible.

Finally, I thank the man who inspired me to pursue the profession of civil engineering, whom I have the honor to call my grandfather, Eng. Benedito Ferreira.





## TABLE OF CONTENTS

General Index .....	iii
Abstract .....	v
Resumo .....	vii
Acknowledgments.....	ix
Table of Contents .....	xi
List of Figures .....	xiii
List of Tables.....	xvii
Acronyms and Symbols .....	xix
1.Introduction .....	1
1.1    Motivation .....	1
1.2.    Objectives .....	2
1.2.1    General objectives.....	2
1.2.2    Specific objectives .....	2
1.3    Structure of the dissertation .....	3
2.Literature Review .....	5
2.1    Photogrammetry .....	5
2.2    Laser scanner .....	9
2.3    Practical examples .....	12
2.3.1Photogrammetry case studies .....	12
2.3.2 Laser scanner case studies.....	16
2.4    Data Fusion .....	20

## TABLE OF CONTENTS

2.5	Semi-automatic modelling from point clouds .....	24
3.	Methodology .....	31
3.1	General aspects.....	31
3.2	Components.....	34
3.3	Semi-automatic 3D modelling script .....	39
4.	Case Studies.....	47
4.1	Gousset Plate From Gdański Railway Bridge (Poland).....	47
4.1.1	General description.....	47
4.1.2	Framework implementation .....	49
4.1.3	2D Modeling.....	51
4.2	Industrial warehouse (Portugal) .....	52
4.2.1	General description .....	52
4.2.2	Framework implementation .....	53
4.2.3	3D Modeling.....	58
5.	Discussion.....	61
6.	Final remarks .....	63
	References.....	65
	Annex A .....	71
	Annex B.....	73
	Annex C.....	75

## LIST OF FIGURES

Figure 1 – Aerial triangulation theory (He <i>et al.</i> , 2022) .....	6
Figure 2-Photogrammetry framework (Iglhaut <i>et al.</i> , 2019) .....	7
Figure 3 -SIFT example (Iglhaut <i>et al.</i> , 2019).....	7
Figure 4-Interactive SfM (Jiang, Jiang e Jiang, 2020) .....	8
Figure 5 - 3D reconstruction Via Meshroom (Chen e Rakha, 2021) .....	9
Figure 6- Laser Scanner and CCD example (Fontana <i>et al.</i> , 2003) .....	10
Figure 7-Laser scanner positioning for building survey example (Castellazzi <i>et al.</i> , 2015).....	10
Figure 8-ToF schema (Pfeifer e Briesse, 2007) .....	11
Figure 9-Phase shift waves schema (Pfeifer e Briesse, 2007).....	12
Figure 10-Existing condenser (Zicarelli, 1992) .....	12
Figure 11- 3D CAD model of condenser replacement (Zicarelli, 1992).....	12
Figure 12- Example of traditional agro-industrial building and camera positions for data acquisition (Arias <i>et al.</i> , 2007). .....	12
Figure 13- Side views of traditional agro-industrial building (Arias <i>et al.</i> , 2007).....	12
Figure 14- 3D model of traditional agro-industrial building (Arias <i>et al.</i> , 2007).....	12
Figure 15-Hospital construction monitoring workflow (Jadon e Patil, 2020) .....	12
Figure 16- Quantity comparison (Jadon e Patil, 2020).....	12
Figure 17- SPbPU Future Factory Point cloud (Badenko <i>et al.</i> , 2019).....	13
Figure 18- Proposed workflow (Badenko <i>et al.</i> , 2019) .....	14
Figure 19- Framework using laser scanner (Almukhtar <i>et al.</i> , 2021).....	15
Figure 20- Automatic cloud registration (Almukhtar <i>et al.</i> , 2021).....	15

Figure 21- The Headington Hill Building: (a) Before cleaning (b) After cleaning (Almukhtar <i>et al.</i> , 2021) .....	16
Figure 22-Integration with BIM process framework (Almukhtar <i>et al.</i> , 2021).....	17
Figure 23- Proposed framework for data fusion (Lee and Choi, 2004) .....	17
Figure 24-Building studied (Lee and Choi, 2004) .....	18
Figure 25- Proposed fusion workflow (Lee and Choi, 2004) .....	18
Figure 26- Comparison between derived model and planning model (Lee and Choi, 2004) ....	19
Figure 27- Case study bridge of Aveiro railway bridge (OLIVEIRA, 2022) .....	20
Figure 28- Comparison between bridge design solution and point clouds (OLIVEIRA, 2022) ...	20
Figure 29 - Fundamental LOD examples (BIMFORUM, 2023) .....	22
Figure 30 - RANSAC application: a) Point cloud; b) Geometries after RANSAC application (Schnabel, Wahl e Klein, 2007) .....	23
Figure 31 - Overview of VPL script (Xiong e Wang, 2021) .....	24
Figure 32 - Final model of the conference room (Xiong and Wang, 2021) .....	25
Figure 33 – Semi-automatic modelling framework (Jung <i>et al.</i> , 2014) .....	25
Figure 34 - South Korean university building (Jung <i>et al.</i> , 2014).....	26
Figure 35 - Refinement example a) point cloud; b) refined and boundary traced (Jung <i>et al.</i> , 2014) .....	26
Figure 36 - Comparison between study phases a) geometric model; b) as-built model; c) 3D rendered model (Jung <i>et al.</i> , 2014).....	27
Figure 37 - Proposed framework - Part 1 .....	29
Figure 38 - Proposed framework - Part 2 .....	31
Figure 39 – Softwares system requirements.....	36
Figure 40 – Dynamo script - part 1 .....	37
Figure 41 – Dynamo script - part 2 .....	38
Figure 42 – Dynamo script - part 3 .....	38
Figure 43 – Python script for walls, floors and roofs separation .....	39

Figure 44 – Python script for roofs and floors points separation .....	39
Figure 45 – Dynamo script - part 4.....	40
Figure 46 – Python script to order the 2D points .....	40
Figure 47 – Dynamo script - part 5.....	41
Figure 48 – Python script get first two items from every four items.....	42
Figure 49 – Dynamo script - part 6.....	42
Figure 50 – Python script for heights calculation.....	42
Figure 51 – Dynamo script - part 7.....	43
Figure 52 – Gdański bridge: span location .....	46
Figure 53 – Gousset plate location.....	46
Figure 54 – Gdański bridge: structural frames distances.....	47
Figure 55 - Bottom, top and front bridge’s photos.....	47
Figure 56 – Gdański bridge point cloud .....	48
Figure 57 - Gousset plate point cloud after applying RANSAC method.....	49
Figure 58 – Point cloud in CAD software aligned.....	49
Figure 59 – 2D modelling with polylines and circles.....	50
Figure 60 – Comparison of three models of the Gousset plate .....	50
Figure 61 - Warehouse overview .....	51
Figure 62 – References for topographic survey .....	52
Figure 63 - Control points coordinates .....	52
Figure 64 - Laser scanner survey of the warehouse .....	53
Figure 65 – Marking control points on laser scanner point cloud .....	53
Figure 66 - Flight plan software in use .....	54
Figure 67 - Drone surveys .....	54
Figure 68 – Final aerial triangulation .....	55
Figure 69 - Model reconstruction with noisy data.....	55

## LIST OF FIGURES

Figure 70 - Warehouse point cloud final version .....	56
Figure 71 - RANSAC method applied to the warehouse point cloud .....	56
Figure 72 – Script output.....	57
Figure 73 - Warehouse final 3D model.....	57
Figure 74 – Example of different LOD’s applied to buildings (Abualdenien and Borrmann, 2022) .....	59

## LIST OF TABLES

Table 1- Linear dimensions comparison (Lee and Choi, 2004) .....	19
Table 2 - LOD and corresponding contents (Gavina, 2023) .....	22
Table 3 – Aircrafts comparison .....	32
Table 4 – Systems comparison .....	33
Table 5 – Cameras comparison .....	33
Table 6 – Laser scanners comparison .....	34
Table 7 – Columns order .....	57





# Acronyms and Symbols

## List of Acronyms

<b>CAD</b>	Computer Aided Design
<b>BIM</b>	Building Information Modelling
<b>GPS</b>	Global Positioning System
<b>SFM</b>	Structure From Motion
<b>MVS</b>	Muti-view stereo matching
<b>SIFT</b>	Scale Invariant Feature Transform
<b>ToF</b>	Time of Flight
<b>PS</b>	Phase Shift
<b>AEC</b>	Architecture, Engineering and Construction
<b>IFC</b>	Industry Foundation Classes
<b>DWG</b>	Drawing Format
<b>RGC</b>	Refinement grid cell-size
<b>TGC</b>	tracing grid cell-size
<b>LOD</b>	Level of Development
<b>GCP</b>	Ground Control Points
<b>RANSAC</b>	Random Sample Consensus
<b>TLS</b>	Terrestrial Laser Scanner
<b>VPL</b>	Visual Programming Language
<b>WFD</b>	Wave Form Digitizing

**CSV**     comma-separated-values

**GNSS**    Global Navigation Satellite System

**ANAC**    National Civil Aviation Authority

**2D**       Two dimensional

**3D**       Three dimensional

**MLESAC**   Maximum Likelihood Estimation Sample Consensus

**MSAC**    M-estimator Sample Consensus

**AIA**       American Institute of Architects

**RIBA**     Royal Institute of British Architects

## **List of Symbols**

®           Registered Mark

# 1.INTRODUCTION

## 1.1 MOTIVATION

With the rapid advance of technologies in society, the construction industry is adapting itself, as other industries, to incorporate these new technologies into their processes, but unlike most of the industries, the construction must adapt to different scenarios, as each construction is unique. This incorporation happens with the use of new components and the automation of processes diminishing the human workforce needed to accomplish the tasks. This incorporation is in its early stages, presenting a vast field for research and significant potential for the development and enhancement of existing task frameworks.

The time decrease and higher precision in construction industry tasks are pursued all time, and the digital surveys are already a better solution for the documentation of existing buildings, decreasing the time between 50% to 70% compared to traditional solutions (Tang *et al.*, 2010) and developing the frameworks for these tasks may drop this time even more, however requiring dedicated research.

Another component that supports the research, development and use of digital surveys is to increase the safety in construction industry. This issue deserves attention since the traditional methods may expose construction workers to dangerous situations causing accidents with injuries or even fatalities. As an example, in the United States the construction industry falls are the leading cause of injuries, representing 48% of the total accidents with injury and 30% of fatalities (Nadhim *et al.*, 2016). Therefore, changing the traditional processes avoiding this high exposure to accidents is an important factor of development and research.

According to 2020 NBS report, that interviewed a thousand professionals related to construction industry, showed that 73% were using BIM methodology. Otherwise, the comparison between 2020 and 2011 report results, shows an impressive upgrade, since in the 2011 report only 13% of the interviewed were using the BIM methodology (*National BIM Report*

2020, 2020). This shows the increase of BIM use in construction sector and the rising need of new research also in this relatively new topic.

Following this idea that BIM use is new for most part of construction industry, the BIM processes automation using programming is a field even less explored than BIM itself. This aspect serve as motivation to develop this study and generate real impact on the future of construction.

In summary, the motivation behind this study is to contribute to the development of existing frameworks for field surveys and to enhance semi-automatic modeling procedures. Additionally, the study aims to create a concise body of research that is among the first to examine these processes together in detail.

### 1.2. OBJECTIVES

#### 1.2.1 General objectives

The general objectives are a framework proposal that encompasses field surveys, point clouds creation, point clouds processing and modelling. For the last task this study aims to create a script to semi-automatize this process.

#### 1.2.2 Specific objectives

To achieve the general objectives, this study aims to:

- Make a comparative analysis between Laser scanner and photogrammetry point clouds results applying these two methods in case studies.
- Apply digital field surveys methodologies processes with and without topographic support.
- Test the accuracy of digital field surveys methods.
- Analyze and apply 2D and 3D modelling from point clouds.
- Research and develop existent modelling automation methods.
- Research and apply point cloud processing methods.

The study focuses on research and application of the point cloud data fusion, the use of components such as laser scanners and drones, explaining how they work and using them in different case studies. Regarding automation, this study aimed to research processes that will

reduce the human workforce need for the tasks, including the application of a flight planning software, the use of RANSAC method and the creation of a script for 3D modelling based on point clouds.

Finally, connecting to the main objectives, this study is focused on a framework proposal that can be as much generic as possible, in other words, can be used in different situations with or without slightly changes. This framework shall include not only the 3D modelling but also the 2D modelling.

### **1.3 STRUCTURE OF THE DISSERTATION**

The dissertation is divided in six chapters.

The first chapter introduces the motivation and objectives of the study, including an overview of the contents of each chapter.

The second chapter is the literature review and provides the research basis for the study. It presents what are digital field surveys and its techniques and it is divided into photogrammetry and laser scanner, including case studies applying these techniques. This chapter shows the research on point cloud fusion and semi-automation for 3D modelling, that clearly are aligned with the objectives of this study.

The third chapter presents and explains step by step the proposed framework for field surveys and modelling from point clouds data. It includes two subchapters, one showing all the components used in the study, softwares, drones and laser scanners, and a brief description of each technology. The other subchapter explains in detail the created script for 3D modelling semi-automation based on VPL and Python.

The fourth chapter is focused on demonstrating two real case studies where all the knowledge acquired is applied. This includes the application of the proposed framework to the case of a railway bridge and an industrial warehouse.

The fifth chapter is the discussion and final considerations, where the results of both case studies are summarized and a link with the objectives of this study is performed, demonstrating what was accomplished and what can be improved on further studies.

The sixth chapter provides an overview of this study about its positioning within the construction industry and its potential to be implemented in real practices with the industry.

## *1. INTRODUCTION*

## **2.LITERATURE REVIEW**

This chapter provides an overview of the literature studied that served as basis for the case studies. It explains general concepts and definitions about photogrammetry and laser scanner techniques, including some practical examples. It also provides an overview about data fusion techniques between laser scanning and photogrammetry. Finally, it shows research related with semi-automation techniques for the creation of models from point clouds (scan to BIM).

### **2.1 PHOTOGRAMMETRY**

Photogrammetry is the process of computationally extracting a three-dimensional surface model from a set of two-dimensional photographs of an object or environment (Ruan *et al.*, 2018). To obtain a point cloud as a final product, it is possible to use cell phone cameras or even professional cameras. Typically, in the construction industry, photogrammetry is performed using cameras attached to drones. This method easily covers large buildings or other infrastructure constructions and is usually more economical when compared to other methods for obtaining a point cloud (OLIVEIRA, 2022).

The principles of photogrammetry and good practices are described in Bentley Context Capture guide for photo acquisition (Bentley, 2017). Data acquisition is an important step in obtaining a reliable photo-realistic model, i.e., the so-called mesh. It begins with the choice of the photography method, followed by the selection of cameras that suit the situation. If drones are chosen for the task, they also need to be selected based on the requirements of the task and local conditions. Once all equipment is selected, photos can be taken with or without topographic support, impacting the georeferencing of the resulting output. These decisions can significantly impact the result of the aerial triangulation.

Following the equipment selection, it is crucial to create a flight plan, presuming that drones will be used. This flight plan can be generated using software designed for this purpose based

on the georeferenced system. Once all preparations are completed, the photos should have minimum overlap and cover the entire building from different angles and positions.

Finally, with all the photos imported into a dedicated software, aerial triangulation is performed. This process involves using different photos and reference spots on the building surface. Reference spots can be created with tie points managed solely by the user or control points that utilize geographical coordinates, which can be combined with the drone's GPS support.

According to figure 1, each 2D image can undergo virtual stretching of the reference spots. With two or more photos, triangles can be formed, making it possible to obtain other building points with greater precision in three dimensions and measurements.

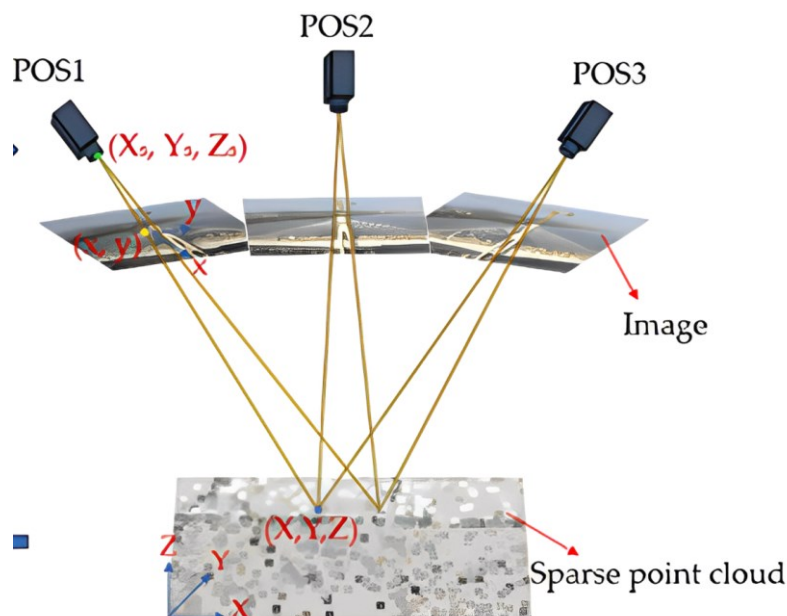


Figure 1 – Aerial triangulation theory (He *et al.*, 2022)

Based on the aerial triangulation, it is possible to see a pre model defined as a sparse point cloud. This point could permit to correct any mistake or see if it is necessary to do another data acquisition. If this model is fine, the reconstruction is done and transformed into dense point cloud, mesh or orthophotos models.

The process of creating a point cloud from a photo dataset can be done in many ways. The full process encompasses three main steps, one that identify and matches the key points, other for the bundle adjustment and another that densify the point cloud (Iglhaut *et al.*, 2019). This is



performed using common features using a Scale Invariant Feature Transform (SIFT), the structure from motion (SfM) and Multi-view stereo matching (MVS), as shown in figure 2.

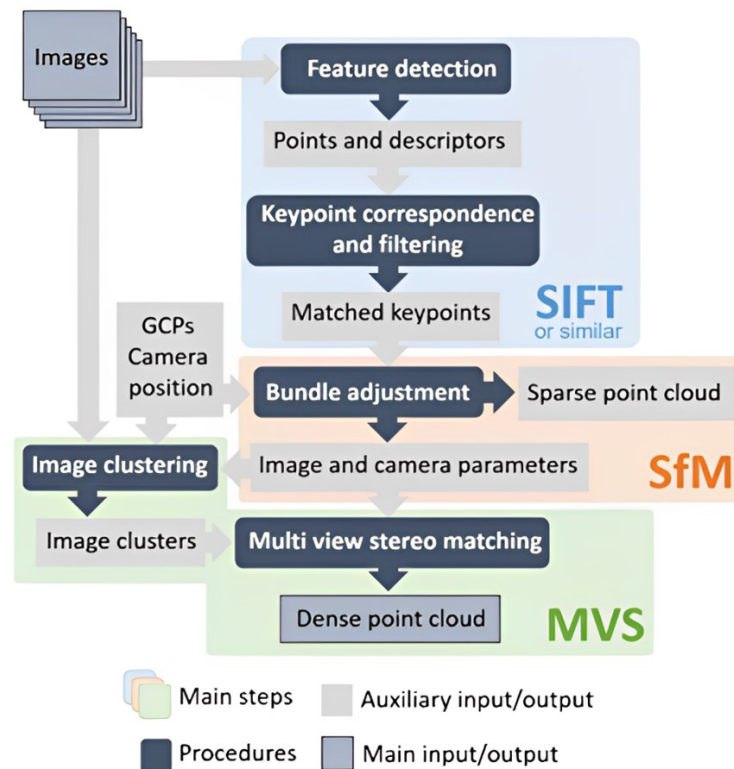


Figure 2-Photogrammetry framework (Iglhaut *et al.*, 2019)

SIFT is the process of matching points and creation of local descriptors. These descriptors are scale invariant and can be used to check the geometry and keypoints. After that, it is done a keypoint check that will validate the points and sweep others (to filter for SfM) and maintain only healthy and usable points (Iglhaut *et al.*, 2019), as shown in figure 3. The geometric verification uses estimation techniques as RANSAC (Random Sample Consensus) (Pepe, Fregonese e Crocetto, 2022).

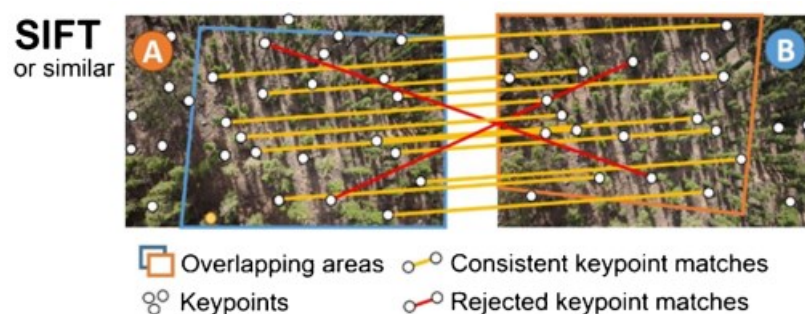


Figure 3 -SIFT example (Iglhaut *et al.*, 2019)

After SIFT, SfM basically creates a sparse point cloud. Afterwards, it is created a track of the points matched and these points are tied. To track, match and tie these points it is used a technique called bundle adjustment that optimizes the 3D coordinates of point of interest and refines camera poses. There are two types of bundle adjustment, iterative and global (Jiang et al., 2020). The main differences between iterative and global processes are the precision. The first one, presented in figure 4 is more precise than the global method, and iterative method can tolerate more outlier ratio than the global process (Jiang, Jiang e Jiang, 2020).

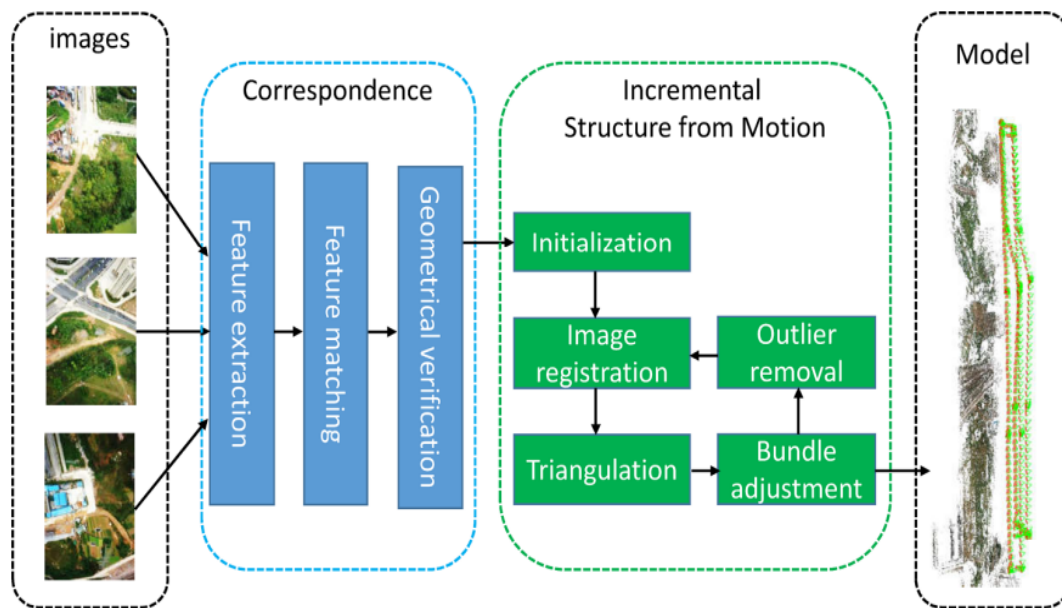


Figure 4-Iterative SfM (Jiang, Jiang e Jiang, 2020)

Finally, after bundle adjustment is created a sparse point cloud that may be densified with MVS or other method. An example of algorithm used for reconstruction of 3D models based on MVS and SfM data is PMVS (Patch Match Stereo). In reconstruction the MVS can give depth to the structure and texturize. As an example, at the figure 5, it is presented a workflow used for 3D reconstruction via software Meshroom (Chen & Rakha, 2021).

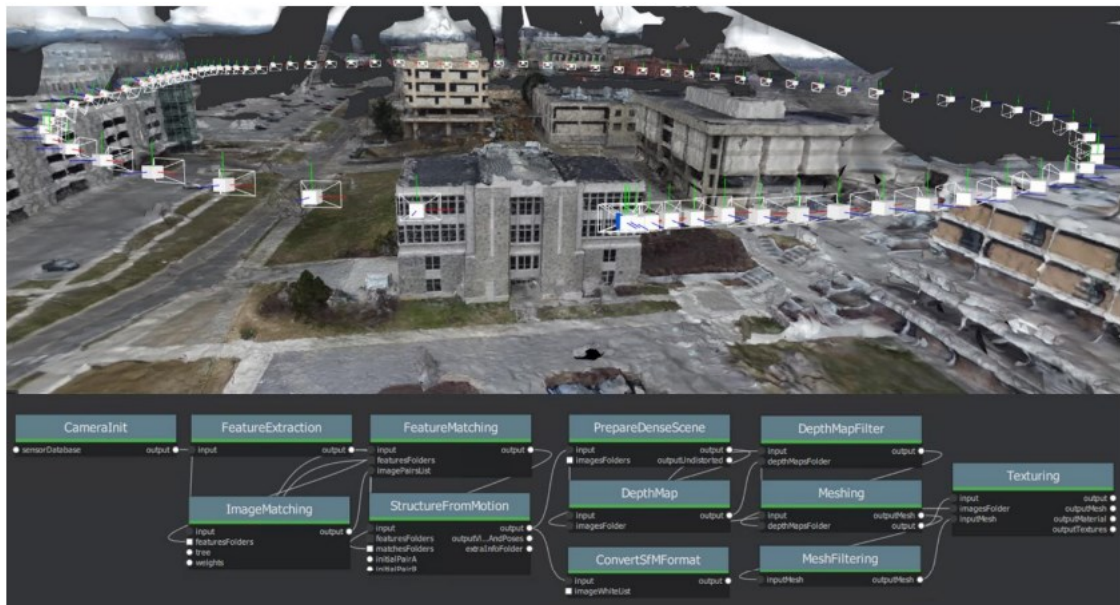


Figure 5 - 3D reconstruction Via Meshroom (Chen e Rakha, 2021)

## 2.2 LASER SCANNER

Laser scanners are the most precise alternative to the creation of as-built BIM models. Other traditional methods, such as, photography and total stations, involves more manual intervention and creates more errors and imprecision. Instead, laser scanners can offer a millimeter accuracy, are fast on data collection and can scan even the most excentric surfaces (Tang *et al.*, 2010).

The laser scanner working principle is based on the optical triangulation, that is obtained by projecting a collimated laser beam onto a target, and by acquiring the profile shape with an imaging device (a CCD) that must be placed at a certain, known, angle, as shown in figure 6 (Fontana *et al.*, 2003).

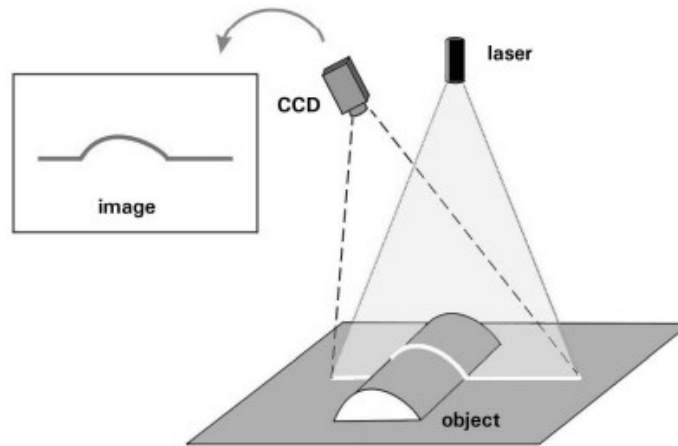


Figure 6- Laser Scanner and CCD example (Fontana *et al.*, 2003)

In order to obtain a point cloud, it is important to survey in various locations and understand that these equipment uses local and relative coordinates system, as shown in figure 7. Either way, as happens in photogrammetric surveys, it is important to have topographic targets as reference on the exterior of the building, to help in the post processing step.

After performing all the surveys, the alignment of all surveys and the transference of the local and relative coordinates for a global and common coordinates system is accomplished (OLIVEIRA, 2022). This step is called point cloud registration. Some equipment automatically performs the so-called pre-registration, i.e., a registration while the other surveys are in execution without the need of topographic targets on site. This procedure is only possible due to the Visual Inertial System (VIS) included in the equipment.

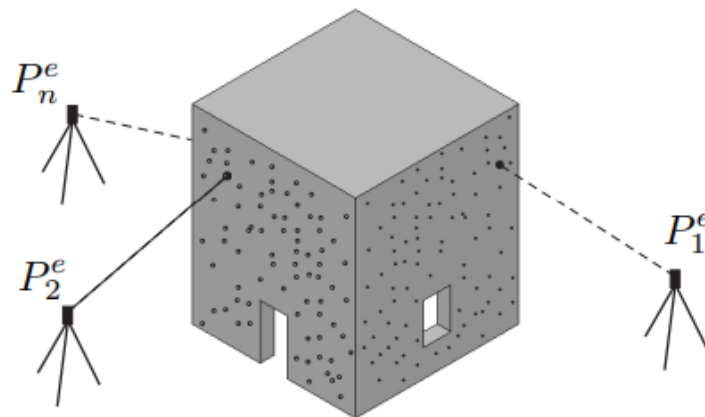


Figure 7-Laser scanner positioning for building survey example (Castellazzi *et al.*, 2015)

There are two main techniques that permits the success of laser scanners surveys. The first is Time of flight (ToF), illustrated in figure 8, that measures the distance from a point shooting a laser ray and calculating the time it comes back. The time is multiplied by the velocity of the light and divided by 2, this last factor is given by half the pulse length (Pfeifer e Briese, 2007).

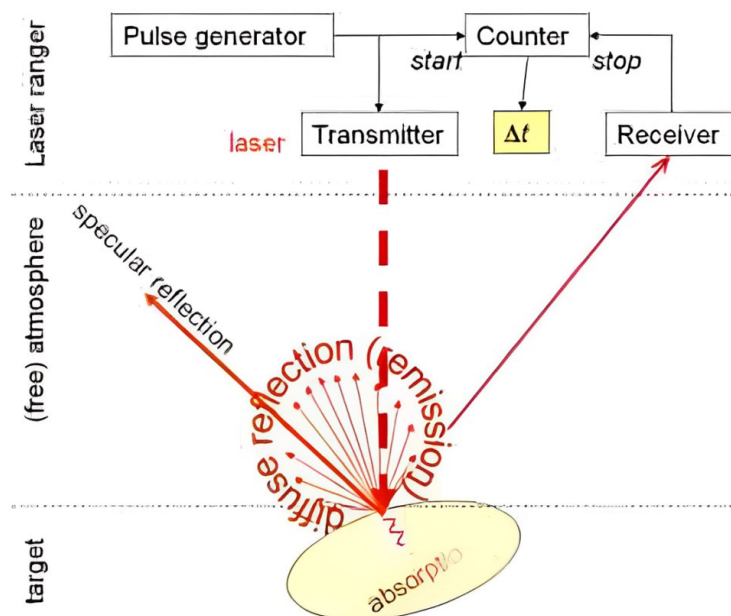


Figure 8-ToF schema (Pfeifer e Briese, 2007)

The second technique is the Phase Shift measurement. This technique requires that the laser scanner uses continuous wave laser, as presented in figure 9. Here, the main principle is the comparison between the emitted and received wave phases. As shown on figure 9, the long modulation wavelength will dictate the distance in the equation, the short modulation wavelength is related to the precision that can be obtained on that survey and the carrier wave that is a high frequency waveform that serves as a reference (Pfeifer & Briese, 2007).

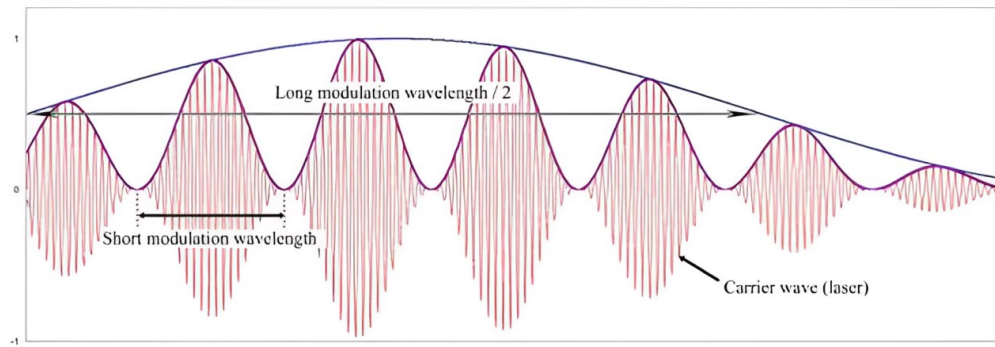


Figure 9-Phase shift waves schema (Pfeifer e Briese, 2007)

Besides, the study of Pfeifer e Briese (2007) refers that phase shift is more precise than time of flight. The study comparing both concluded that the performance of ToF equipment can successfully compete and even surpass the phase shift equipment (San José Alonso *et al.*, 2011). Therefore, even for terrestrial surveys the ToF is an accurate option, however, differently from PS, it can be used to measure larger ranges on airborne surveys.

## 2.3 PRACTICAL EXAMPLES

### 2.3.1 Photogrammetry case studies

The first example is a photogrammetry of an industrial facility reported by Zicarelli (1992). This study is about a conversion of a condenser unit and the replacement of a pressure vessel of an industrial facility (Figure 10). Even though the study is from 1992, a 3D model of the replacement condenser unit based on the existing one was created, according to figure 11.

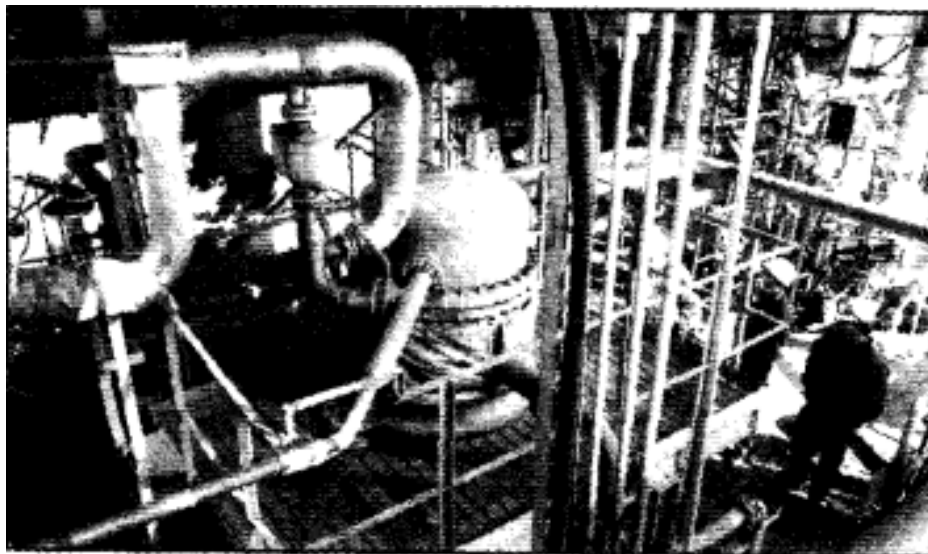


Figure 10-Existing condenser (Zicarelli, 1992)

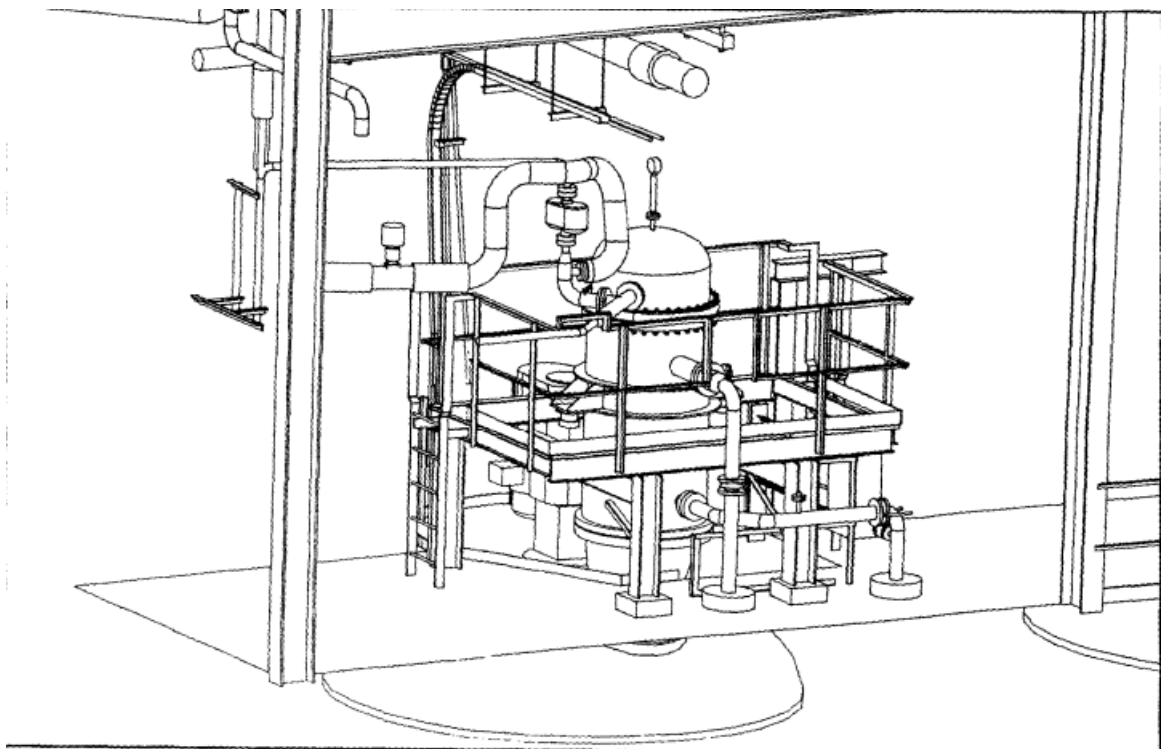


Figure 11- 3D CAD model of condenser replacement (Zicarelli, 1992)

An interesting fact is that, for computer processing, the data used were scans of photo negatives. This demonstrates that photogrammetry has been continuously improving for over 30 years. Even during that time, the benefits of photogrammetry were evident: high-quality control, cost-effectiveness, great accuracy, precise information, increased safety compared to traditional methods, and minimized field data acquisition and office analysis.



The second example explored the use of low-cost documentation of traditional agro-industrial buildings by close-range photogrammetry (Arias *et al.*, 2007). In this study the authors did not use drones to support the data acquisition, neither GCP's or topographical support, but they used targets placed on the wall of the building as reference. They also used low-cost standard digital cameras and for site references support colored adhesive tapes were adopted. The main objective of this study was to create a 3D models, plans and side views of different traditional agro-industrial buildings in Galicia, north of Spain, for documentation to help on conservation and reutilization of these type of buildings.

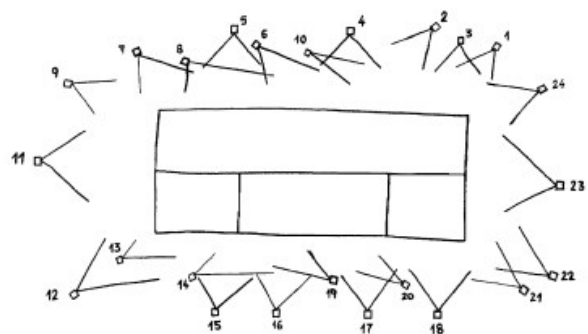


Figure 12- Example of traditional agro-industrial building and camera positions for data acquisition (Arias *et al.*, 2007).

At the end of the study, the objectives were accomplished, since the authors got the documentation, shown in figure 13 and figure 14, with low cost investment and without specialized knowledge of photogrammetry. This method saved money, time and the level of accuracy fulfilled the objectives. The con point cited is the limitation of the method using stationary cameras for tall buildings.

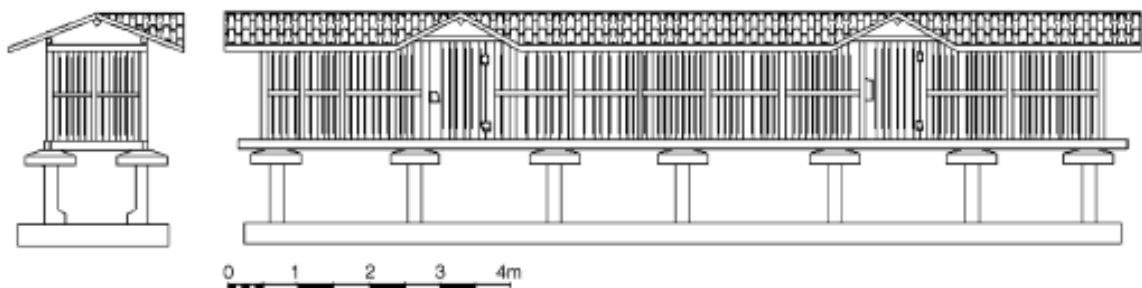


Figure 13- Side views of traditional agro-industrial building (Arias *et al.*, 2007)





Figure 14- 3D model of traditional agro-industrial building (Arias *et al.*, 2007)

The third example presented the uses of drones and photogrammetry in project monitoring for a hospital building (Jadon e Patil, 2020). The authors used drones to support volumetric estimations, progress reporting, structural integrity maintenance, safety, inventory management, quality assurance, taking fast decisions, advertisements, marketing and team communication. The hospital building progress monitorization is summarized in figure 15. The authors used the 3DF Zephyr software to convert the data into 3D model in .rvt format.

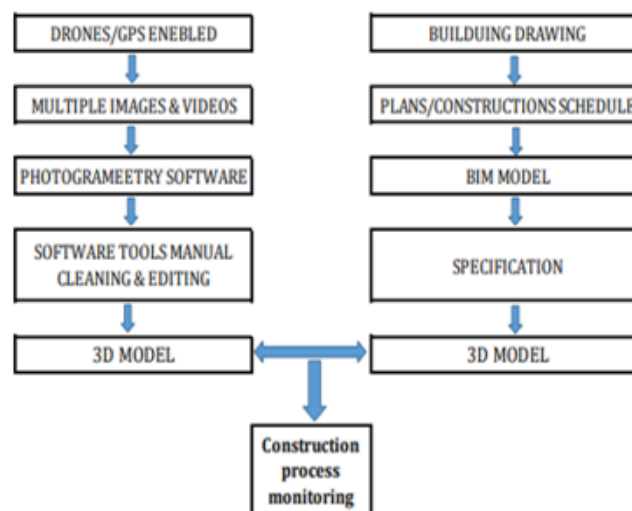


Figure 15-Hospital construction monitoring workflow (Jadon e Patil, 2020)

This workflow consists in continuously creating 3D models from photogrammetry and comparing to a 3D model based on construction drawings, as shown in figure 16.

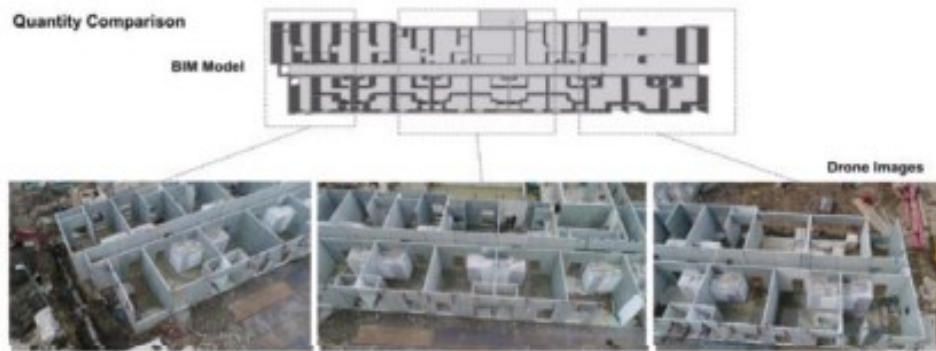


Figure 16- Quantity comparison (Jadon e Patil, 2020)

### 2.3.2 Laser scanner case studies

Badenko *et al.* (2019) proposed a methodology to create an as-built 3D model for clash test, structural and insulation analysis of an existing industrial building. To fulfill these objectives, the authors started defining the classifications of elements using the OmniClass standard. Subsequently, they determined the level of detail required for the final model. After, these two steps they perform a laser scanning to obtain a trustable point cloud, see figure 17. Laser scanning was performed using Leica BLK360 based on ten stations with medium resolution, the registration was automatically done in Leica software and the segmentation of the point cloud was done in Cloud Compare software.



Figure 17- SPbPU Future Factory Point cloud (Badenko *et al.*, 2019)

This study does not explain the modelling of the full building, but the authors did clash tests to predict future incompatibilities with the new equipment layout. At the end, they proposed the workflow presented in figure 18, concluding that this process needs to be improved. Therefore, this study demonstrated that the main difficulties for users are related to the lack of universal software for the creation of as-built BIM-models (Badenko *et al.*, 2019), since the authors faced difficulties on the modelling, anyway they see this workflow as something to be used more frequently in AEC industry.

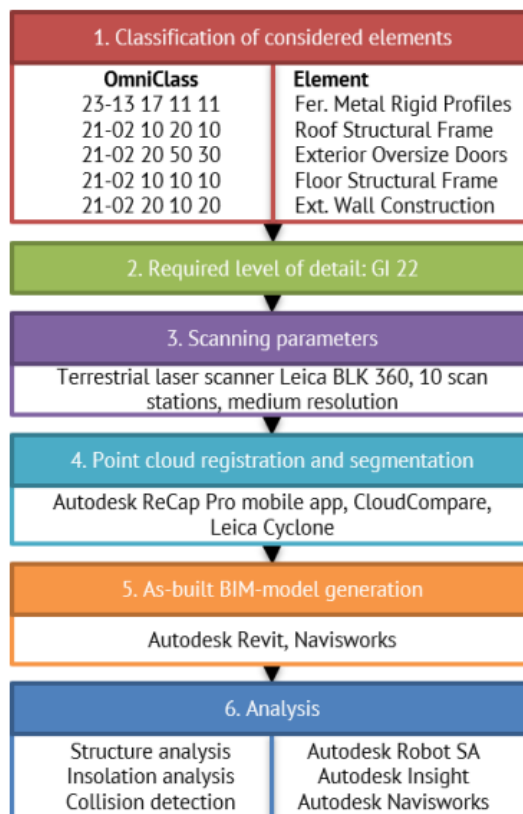


Figure 18- Proposed workflow (Badenko *et al.*, 2019)

The second practical example shows the full process, from the data acquisition till the final 3D model, as depicted in figure 19. This example is focused on The Headington Hill Building, a historic mansion located in Oxford (Almukhtar *et al.*, 2021).

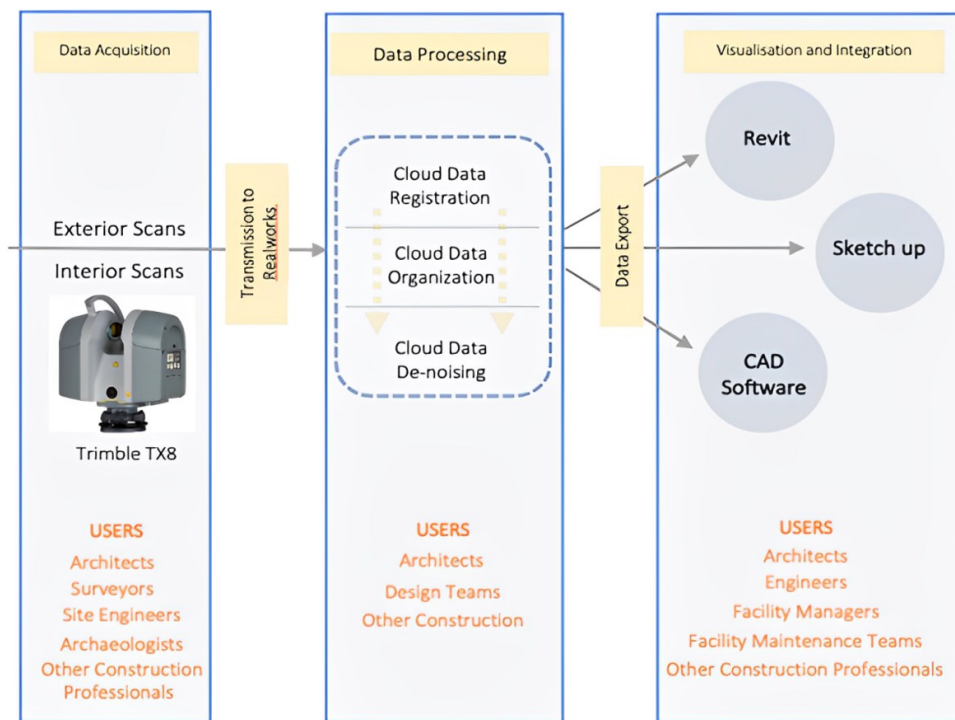


Figure 19- Framework using laser scanner (Almukhtar *et al.*, 2021)

For data acquisition, a Trimble TX8 laser scanner was used. The external scans involved five stations, including interior scans. As illustrated in the framework above, data processing follows data acquisition, beginning with registration. This process is divided into two parts: automatic registration (Figure 20), followed by manual registration based on the preliminary automatic registration.

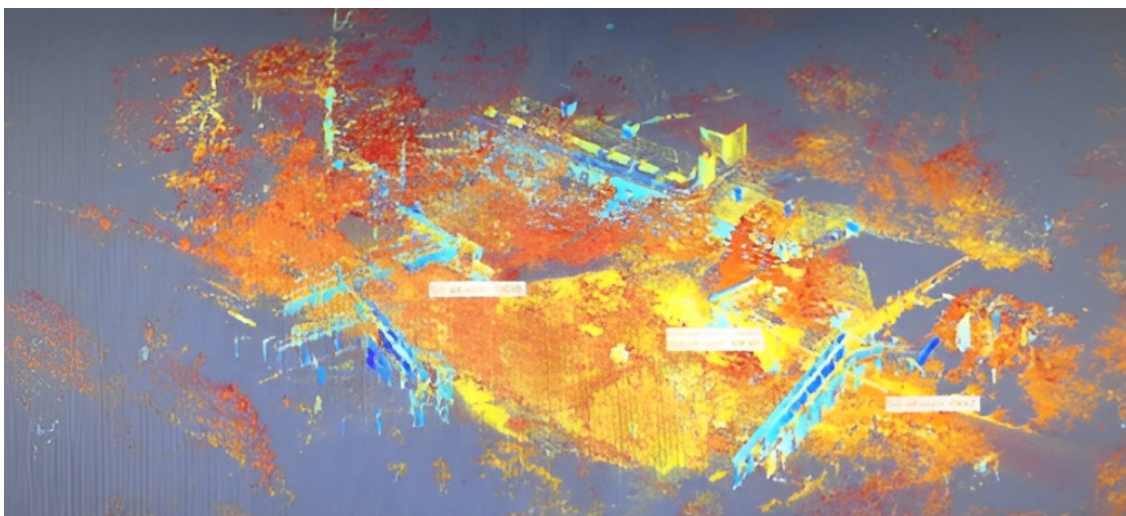


Figure 20- Automatic cloud registration (Almukhtar *et al.*, 2021)

After the registration, it was necessary to organize and clean the point cloud as shown in figure 21. With the data processing finalized the cloud model was integrated into a BIM process using the IFC format. As the software Trimble Realworks® used for data processing does not have the export option for IFC, the solution was exporting to DWG format and then importing in Revit to posteriorly export to IFC.

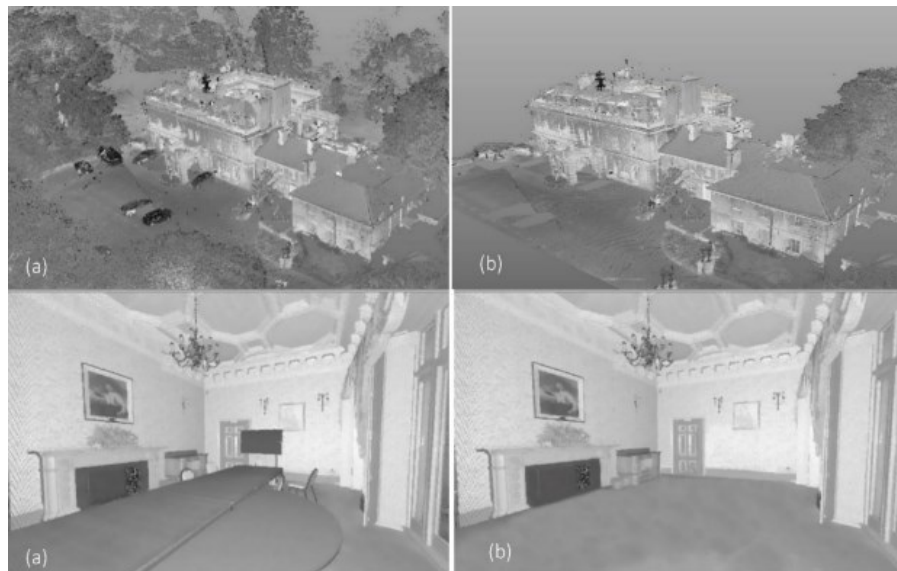


Figure 21- The Headington Hill Building: (a) Before cleaning (b) After cleaning (Almukhtar *et al.*, 2021)

The authors considered that the proposed framework is an added value for construction management and can be used for various purposes. The cloud model or even the 3D model can be used for documenting and oversee the impact of future changes, or even for maintenance support. Anyway, they see the integration into BIM process as something to be improved, since the dwg when imported to Revit becomes a family block that is not easily changed or managed (Figure 22).



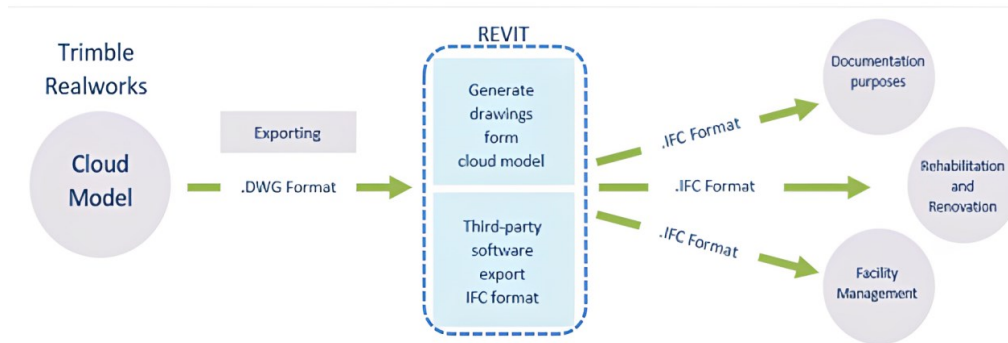


Figure 22-Integration with BIM process framework (Almukhtar *et al.*, 2021)

## 2.4 DATA FUSION

The point clouds fusion uses point clouds acquired from laser scanners and photogrammetry. Under these circumstances, it is important to have topographic support in the field survey for georeferencing. This georeferencing is based on control points that are crucial to the fusion as it is suggested in the research of Lee and Choi (2004). The same study proposes a framework for fusion, from the data acquisition stage until getting the final model, as depicted in figure 23.

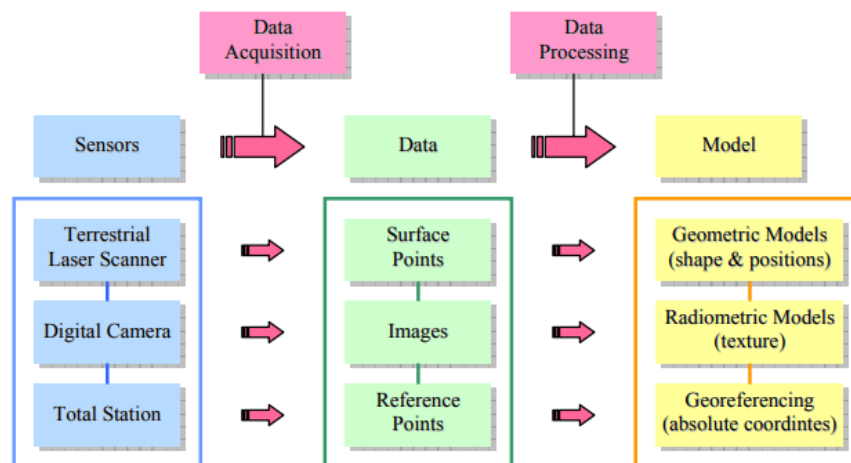


Figure 23- Proposed framework for data fusion (Lee and Choi, 2004)

To validate this framework, the process was applied to an existing building (Figure 24) and the results were compared to the original building project. To achieve this objective, it was used a TLS, digital camera (without drone support) and a total station. This study did not explain step-by-step the field survey but provided dedicated mathematical models for point clouds registration and other for images registration.



Figure 24-Building studied (Lee and Choi, 2004)

This study considered the final point cloud as a 3D model. For that reason, the authors proposed a workflow, figure 25, for building modelling that describes the necessary adjustment and refinement to get the final point cloud from TLS and images. It is possible to see that the refinement is done by the edges of the building and the patches that refers to the georeferenced control points. After this process all the information was grouped to obtain the final point cloud.

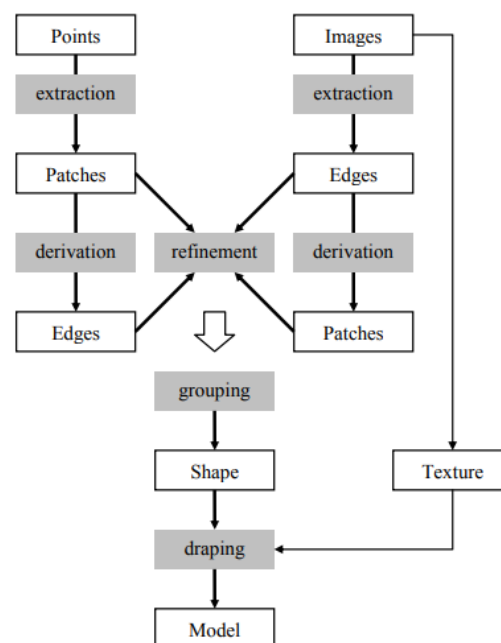


Figure 25- Proposed fusion workflow (Lee and Choi, 2004)

After obtaining the final point cloud, a plan view of the building was created (denominated derived model) and compared to the project plan view (designated as planning model), as can

be seen in figure 26, in which the red lines represent the derived model and the blue lines represent the planning model.

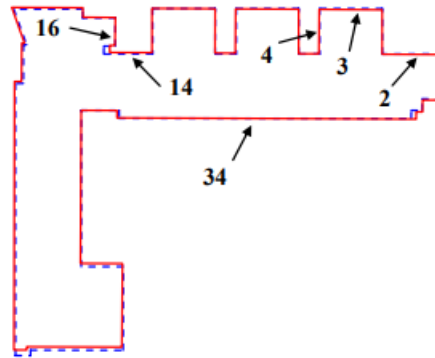


Figure 26- Comparison between derived model and planning model (Lee and Choi, 2004)

Furthermore, this study compared the surveyed building dimensions with the dimensions derived on total station, according to the results presented in table 1. It is possible to see that the total station results are more precise, but the derived model results are very similar to the total stations results. The only results that have big discrepancies are the ones from planning model, which the authors attribute to construction errors.

Table 1 - Linear dimensions comparison (Lee and Choi, 2004)

No.	Planning Model	Derived Model	Total Station
2	9,975	10,013	10,030
3	7,500	7,344	7,390
4	10,350	10,404	10,400

Another study, from OLIVEIRA (2022), applied the fusion process for a railway bridge, using a workflow like the one shown in figure 23. However, data acquisition was quite different since used drone support for photos.





Figure 27- Case study bridge of Aveiro railway bridge (OLIVEIRA, 2022)

After the field surveys, the software Leica Cyclone Register 360® was used for data processing of the laser scanner point clouds, and software Itwin® was used for marking the control points, tie points and creating a point cloud from the photos. With these two georeferenced point clouds, the Itwin® was used again to make the fusion to obtain an unified point cloud (with TLS and photos information). A comparison between the point clouds results and the design drawings bridge was performed according to figure 28 (OLIVEIRA, 2022).

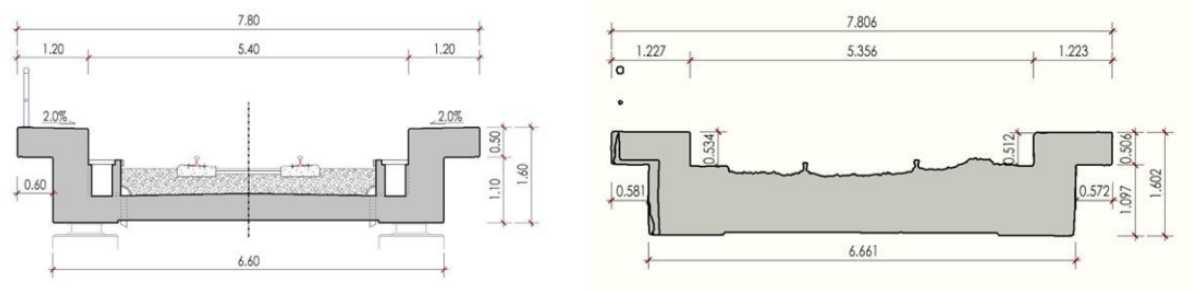


Figure 28- Comparison between bridge design solution and point clouds (OLIVEIRA, 2022)

The proposed fusion method is useful for geometric evaluation and stated that the part more prone to errors was the field survey in which the methodology needs to be improved (OLIVEIRA, 2022).

Summarily, the data fusion gets a balance between laser scanners and photogrammetry advantages and disadvantages. Even though, the laser scanners can be attached to drones however the cost for this technique application is still a challenge. Otherwise, photogrammetry comes specially as a cheaper alternative and provides a better texturized mesh (OLIVEIRA, 2022). Considering that information derived from laser scanners provide denser point clouds

and lower acquisition and processing time (Popescu *et al.*, 2019), the combination of both methods is the best solution to have balanced costs, acquisition and processing time and have dense point clouds with texture.

### 2.5 SEMI-AUTOMATIC MODELLING FROM POINT CLOUDS

The use of BIM processes for documentation and other purposes is rising. Regarding scan-to-BIM the already mentioned reasons presented in this chapter like safety, preservation, scheduled maintenance and facility management, increasingly require that BIM models are done faster and more accurately. To achieve these needs, and considering the lack of products that automatizes this process, the automation of modelling from point clouds is an ample field for research (Previtali *et al.*, 2014).

Typically, it is necessary to know on beforehand the classification system of the elements and the level of development that is needed. Here lies the first difficulty for automation modelling from point clouds. The level of development depends on the specification document selected to be followed and the working plan to be accomplished. The classification system does not seem to be an issue as it has a large variety of options and can be changed after or during modelling. The most used classification systems are Omniclass and Uniclass 2015 (Gavina, 2023).

Table 2 shows the UK LOD according to PAS 1192-2, US LOD according to American Institute of Architects (AIA). The descriptions follows the Royal Institute of British Architects (RIBA) work plan stages (Gavina, 2023). It is important to remember that LODs specifications and work plans

may vary depending on the country and specifications being followed (Gavina, 2023), therefore another description for each LOD content is shown in figure 29.

Table 2 - LOD and corresponding contents (Gavina, 2023)

UK LOD	US LOD	DESCRIPTION	CONTENT
1		Brief	A model communicating the performance requirements and site constraints. Building models would be block models only
2	LOD 100	Concept	Conceptual or massing model including basic areas and volumes, orientation and cost. In the RIBA Plan of Work, this is equivalent to stage 2
3	LOD 200	Developed design	A design development model, "generalized systems with approximate quantities, size, shape, location and orientation." Equivalent to RIBA stage 3
4	LOD 300	Production	Equivalent to RIBA stage 4. Production, or pre-construction, "design intent" model representing the end of the design stages. Modelled elements are accurate and coordinated, suitable for cost estimation and regulatory compliance checks.
5	LOD 400	Installation	Model suitable for fabrication and assembly, with accurate model of the construction requirements and specific components, including specialist sub-contract geometry and data.
6	LOD 500	As Built	An "as built" model showing the project as it has been constructed. The model and associated data is suitable for maintenance and operations of the facility.
7		In Use	Asset Information Model used for ongoing operations, maintenance and performance monitoring

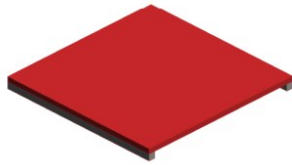
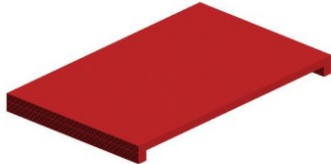
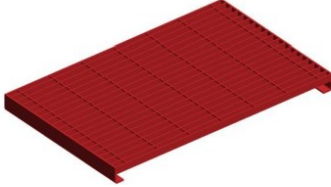
100	See B1080	
200	Inclusions: <ul style="list-style-type: none"> <li>• <b>Element envelope</b></li> </ul>	
300	Element modeling to include: <ul style="list-style-type: none"> <li>• Overall geometry.</li> <li>• Thickness</li> </ul>	
350	Inclusions <ul style="list-style-type: none"> <li>• Panel layout and grating deck edges.</li> <li>• Openings with any dimension greater than 6" (15 cm) or as noted</li> <li>• Indication of span direction</li> <li>• Configuration of grating elements</li> </ul>	

Figure 29 - Fundamental LOD examples (BIMFORUM, 2023)

Understanding the different requirements for each LOD and work plan helps to perceive one of the issues in automatizing the scan-to-BIM process. Anyway, automatic modelling from point

clouds have already had some achievements. One of them is the automatic shape extraction with dedicated algorithms, such as, RANSAC, MLESAC, MSAC and many others. In this work, RANSAC will be explored due to its large use for construction purposes and for being the algorithm most used in academic research on construction (Zhang, Li and Shan, 2021) (Nan and Wonka, 2017).

RANSAC extracts shapes from point clouds by randomly drawing minimal sets of points and constructing corresponding geometric primitives. A minimal set is the smallest number of points required to define a specific type of geometric primitive. After defining the minimal sets, the algorithm tests them against all the point cloud data, evaluating the corresponding score, that works like a scoring system where the most suitable minimal set for each geometric primitive is selected. In other words the score represents how many points in the data are well approximated by that primitive (Schnabel, Wahl and Klein, 2007).

The use of RANSAC diminishes the issues with bad segmentation and human errors, taking an important role in segmentation process, due to the fact that this algorithm can find planar, cylindrical, spherical, conical and toroidal shapes, as shown in Figure 30 for the original point cloud and the RANSAC approximation. Most of the buildings have most of its main elements with planar shapes and therefore RANSAC becomes a straight way to segment buildings point clouds in a faster way (Previtali *et al.*, 2014).



Figure 30 - RANSAC application: a) Point cloud; b) Geometries after RANSAC application (Schnabel, Wahl e Klein, 2007)

After the point clouds segmentation comes the modelling. This step can be done manually or semi automatically from the segmentation results. The semi-automatic strategy uses the segmentation results as input for a script that already does part of the modelling or parametrization, as shown in the study of Nan and Wonka (2017). Otherwise, the manual

strategy gets the segmented point cloud and began modelled from the beginning over the point cloud, or measuring it and modelling.

Xiong and Wang (2021) presents the segmentation and semi-automatic modelling processes for an office room and a conference room. For segmentation, the study uses an alternative approach, however, for modelling the authors used a visual programming language (VPL) that uses nodes connected to each other, following the script layout of figure 31.

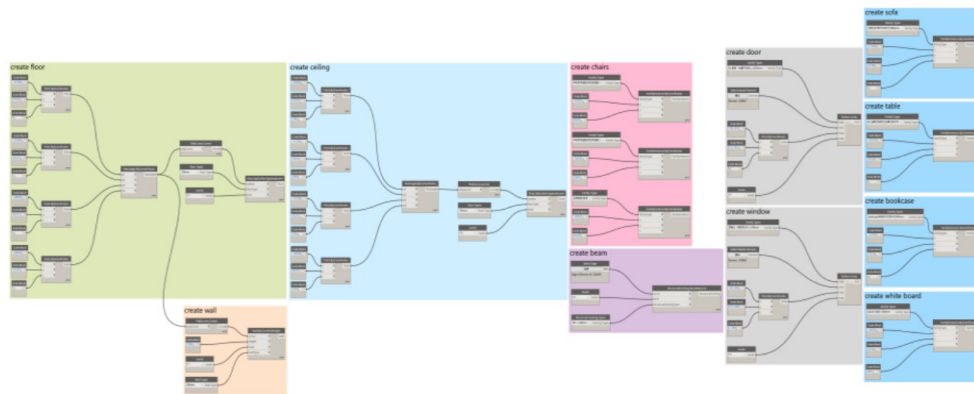


Figure 31 - Overview of VPL script (Xiong e Wang, 2021)

To generate the ground floor, the authors defined the elevation as zero and used the coordinates of four corner points. With these points it was possible to create lines, from lines create curves and from curves generate floors. The same technique was used for ceilings just changing the elevation from zero to 2,704m in their case.

Moving forward, to generate the walls the authors used the boundary lines of the floor as reference and ceiling height for the nodes input. The boundary lines created a reference of direction for the walls and the ceiling height was considered equal to the wall's height.

For other instance families, the authors used a dedicated Python script. They explained that if the family was host-based they needed to use their custom script, otherwise they could use standard scripts just using the coordinates as input for positioning.

The final model, presented in figure 32, has a good accuracy and reflects the point cloud, even with the modelling simplifications.

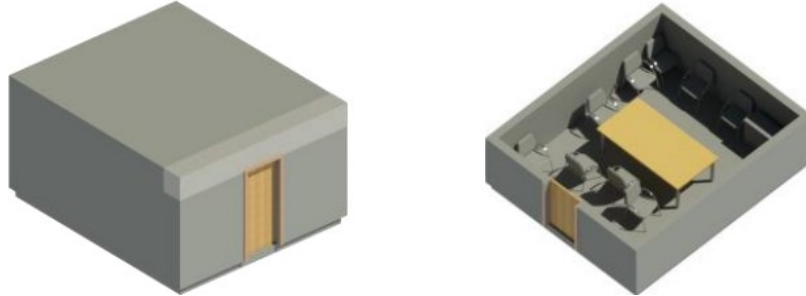


Figure 32 - Final model of the conference room (Xiong and Wang, 2021)

Another case study presented by Jung *et al.* (2014) follows a different methodology for semi-automatic modelling from point clouds. These authors developed the so-called geometric model that consists of shapes derived from a segmentation process. From this model they did a manual modelling to create an as-built model. The study framework is presented in figure 33 which were applied to an university building in South Korea, as presented in figure 34.

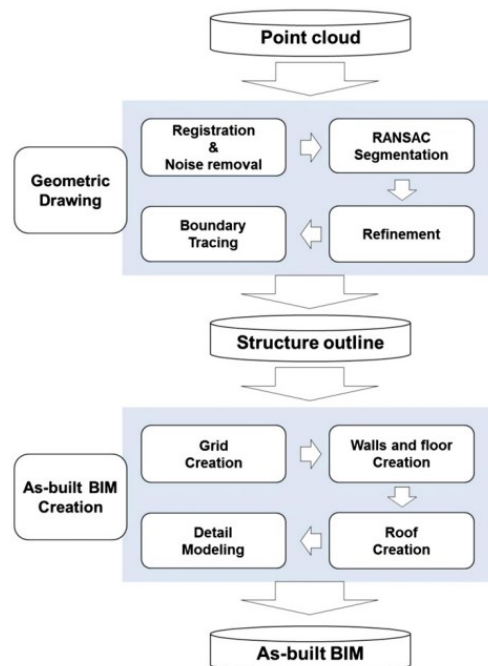


Figure 33 – Semi-automatic modelling framework (Jung *et al.*, 2014)





Figure 34 - South Korean university building (Jung *et al.*, 2014)

In order to create the geometric drawing, after doing the RANSAC segmentation, the refinement starts defining a refinement grid cell-size (RGC), that together with tracing grid cell-size (TGC) determines the connectivity of the points. This step prepares the boundary tracing that will substitute the point cloud, as shown in figure 35, to obtain a geometric drawing that is lighter than point cloud data (Jung *et al.*, 2014).

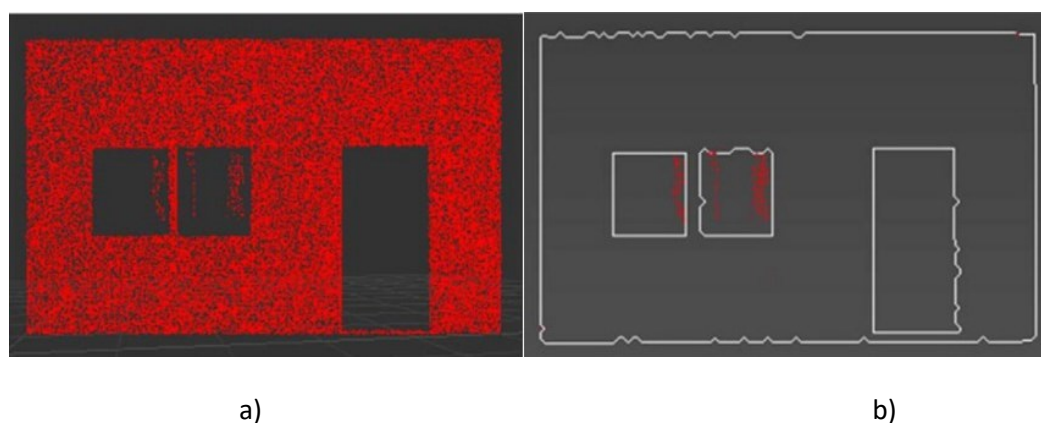


Figure 35 - Refinement example a) point cloud; b) refined and boundary traced (Jung *et al.*, 2014)

In this study, the second part of the framework presented in figure 33 was done entirely manually using a traditional design process, showing that by this way it is also possible to obtain

good results. Similarly to the semi-automated segmentation process, the authors stated that the major contributions of their research can be applied to huge point cloud data in complex structures (Jung et al., 2014). The final results of the study can be seen in figure 36.

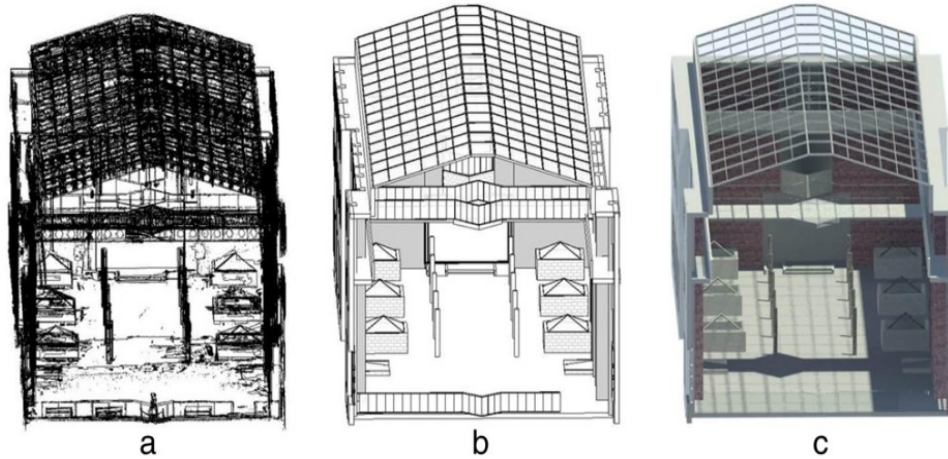


Figure 36 - Comparison between study phases a) geometric model; b) as-built model; c) 3D rendered model (Jung *et al.*, 2014)



### 3. METHODOLOGY

This chapter will address the research methodologies for field surveys, data processing and modelling. Based on literature review there will be proposed a framework of all these processes. Also, this chapter will describe the technologies used for this study, basically field survey equipment and software, with emphasis for the purposes, data sheet information and other relevant information. Finally, it will be addressed an explanation about the scripts and analytics involved in the process, with focus on the developed Dynamo script.

#### 3.1 GENERAL ASPECTS

For this study was developed a framework based on 2.Literature Review chapter. This framework can be divided into two parts. First aims defining LOD and other objectives besides the two strategies of performing field surveys, with and without topographic support. This first part of the framework is presented in figure 37.

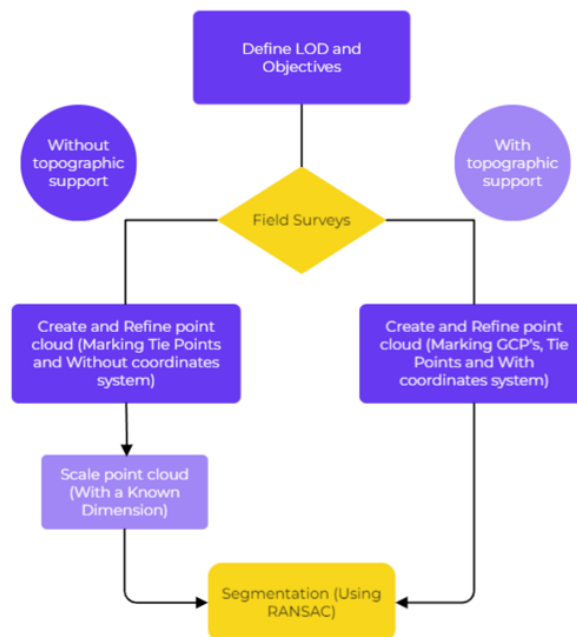


Figure 37 - Proposed framework - Part 1

Field surveys can be done with cameras or laser scanner. Depending on the case, it is recommended to have drone support, a plan of flight and topographic support. It is possible to perform a field survey without topographic support, which means that is not possible to associate the point cloud and the GCP's to a georeferenced system. To create the point cloud from photos the point cloud refinement is based on the tie points and fake GCPs (this last one was tested but not used in this study). Using aerial triangulation and reconstructing the cloud many times, adjusting the tie points and settings of the software, makes possible to reach a final point cloud that is relatable to reality. After, this cloud needs to be scaled with a known dimension as reference which can be a dimension taken on site or a project dimension. After scaling, the point cloud is ready to be segmented. It is important to refer that the scaling step is not necessary if only the laser scanner was used for the surveys.

The other alternative takes more time on field survey step but saves time on point cloud creation stage. The topographic support on site gives essential and precise information to create a more accurate point cloud in less time, since the points to be marked in photos to create the point will only be GCPs and a few tie points in specific zones. With topographic support it is easier to make the fusion process of point clouds from laser scanner and point clouds from photos, since they have the same GCP's and they follow the same reference system. Another important aspect is that a scale is not needed since it has already the real dimensions applied.

After the point cloud creation, following the framework, it is ready to be segmented. This step requires the use of RANSAC method explained in 2.Literature Review chapter. To find planar shapes in the structure, the RANSAC method can be adjusted depending on the density of the point cloud. Thus having the planar shapes of the structure it is possible to find the normal to each plan, that will define if the plan represents a roof, floors or walls.

The second part of the framework is focused on modelling and start right after the segmentation stage is completed, as can be seen in figure 38.



Figure 38 - Proposed framework - Part 2

Second part of the framework follow two different branches after the segmentation stage is concluded.

The 2D modelling branch follows a simple idea of drawing over the point cloud. To achieve that it is necessary to import the point cloud to a digital drawing environment. After, it is necessary to align the point cloud in the correct direction. This part of alignment can be done or partially executed in the segmentation step, using RANSAC and aligning all the point cloud to the plan. After having everything organized in the view, it is possible to draw polylines over the point cloud boundaries to get a 2D model.

The 3D modelling branch requires other approach after segmentation, particularly, to get the information of the normal of the planes organized in a csv file. This will be used as input for a Dynamo script that will create walls, roof and floor, based on the planes found in RANSAC. Also, it is needed to refine manually the walls heights and connections, floor and roof boundaries.

Finally, having all the model refined, it is possible to get a 3D model that is near to point cloud information using a semi-automatic strategy. The script created for this procedure will be explained in section 3.3.

3.2 COMPONENTS

Components can be divided in survey components and design components, this last one encompassing component used for point cloud creation and modelling.

Following the framework, and starting by the survey components, the equipment used in this study were drones, cameras mounted on drones, laser scanners and a software for flight planning.

Table 3 shows the differences between the aircrafts, while the table 4 presents the different systems, and table 5 compares the cameras attached to each drone. These three tables give a comparison and full information of DJI Mini, 1DJI M2EA and DJI Mavic M3 (DJI, 2024).

Table 3 - Aircrafts comparison










<div></div> <div>Aircraft</div>	DJI MINI 1	DJI M2EA	DJI Mavic 3M
 Max take-off Weight (g)	249	1100	1050
 Dimensions - Unfolded (LxWxH) (mm)	159x202x55	322x242x84	347,5x283x139,6
 Maximum take-off altitude above sea level (m)	3000	6000	6000
 Max Flight time Windless (min)	30	31	43
 GNSS	GPS+GLONASS	GPS+GLONASS	GPS+Galileo+BeiDou+GLONASS
 Option for RTK Module	No	Yes	Yes

Table 4 - Systems comparison





















   Gimball, Sensing System and Battery		DJI MINI 1	DJI M2EA	DJI Mavic 3M
	Stabilization	3-axis (tilt, roll, pan)	3-axis (tilt, roll, pan)	3-axis (tilt, roll, pan)
	Max control speed	120°/s	120°/s	100°/s
	Angular Vibration Range	±0,01°	±0,005°	±0,007°
	Sensing System Type	Infrared sensing system	Omnidirectional obstacle Sensing	Omnidirectional binocular vision system, with na infrared system at the bottom of the aircraft
	Battery Capacity	2400mAh	3850mAh	5000mAh
	Battery Voltage	7,2V	15,4V	15,4V
	Battery Type	Li-ion 2S	LiPo	LiPo 4S
	Battery Weight	100g	297g	335.5g


Table 5 - Cameras comparison










Cameras				
		DJI MINI 1	DJI M2EA	DJI Mavic 3M
	Sensor	1/2.3" CMOS	1/2" CMOS	4/3 CMOS
	Effective Pixels (MP)	12MP	48MP	20MP
	FOV	83°	84°	84°
	Aperture	f/2.8	f/2.8	f/2.8 to f/11
	Focus	1 m to ∞	1 m to ∞	1 m to ∞
	Photography Modes	Single shot Interval 2/3/5/7/10/15/0/3 0/60 s	Single shot Interval 2/3/5/7/10/15/0/3 0/60 s or Panorama:Spher e	Timelapse; JPEG+RAW; Panorama; JPEG: 0.7/1/2/3/5/7/10/1 5/20/30/60 s

DJI pilot is the software for flight planning used in this study. It is compatible with all drones from DJI enterprise series. It was used on the drone command control but can be also installed on other platforms.

There were used two different laser scanners for this study, BLK360 (Leica, [s.d.]) and NOVA MS50 (*Leica Nova MS50 Datasheet*, [s.d.]), which are presented and compared on table 6. More details about the measurement technology of laser technologies are explained in chapter 2.2. Phase shift and time of flight techniques when combined creates the Wave Form Digitizing (WFD) which gives better results than using the techniques separately (Maar and Zogg, 2021).

Table 6 - Laser scanners comparison



Laser Scanners		BLK 360	NOVA MS50
	Measurement Technology	High speed Time of Flight enhanced by WFD	Wave Form Digitising (WFD)
	Weight	1kg	7,6kg
	Accuracy (Any surface)	4mm at a distance of 10m and 7mm at a distance of 20m	2 mm + 2 parts per million (ppm)
	Battery	Li-ion, capacity for more than 40 setups	Li-ion, maximum operating time of 9 hours
	Memory	Internal Memory: Storage for more than 100 setups	Internal memory: 1GB / Memory card 1GB or 8GB
	Scanning Range	From 0,6 to 60m	Max range 1000m
	Rotation	360°	180°
	Imaging	Sensor: 15MP 3 camera system; 150 MP full dome capture	Sensor: 5MP CMOS; Up to 20 fps; FOV: 19,4°
	Points Measurement rate	360000 points/s	1000 points/s

On field survey another software used was Leica Cyclone Field 360 associated with laser scanners, This software provides a quality control on site, a scanner control and a pre-registration of the point cloud.

### 3.METHODOLOGY

Following the next step of the framework of figure 37, to create and segment point clouds, the software used in this study were Leica Cyclone Register 360, Itwin Capture Modeler, CloudCompare and Autodesk Recap.

With Leica Cyclone Register 360 it is possible to do the final register of the point clouds from the laser scanners, creating complete point clouds. The Itwin Capture Modeler software provides an environment for point cloud creation from photos and point cloud fusion, according to the method explained in section 2.4.

The CloudCompare and Autodesk Recap were used for point cloud management and segmentation, such as point cloud refinement, cleaning, scaling, change the reference axis, change format and the use of mathematical algorithms, as RANSAC.

Finalizing the segmentation step, it goes to the drawing production process detailed in figure 38. For 2D drawings, it was used the Autocad 2024 software. For 3D drawings, it was used Revit 2023 software that provides an environment for 3D drawings, and Dynamo, a native software for programming that uses Python language as basis. Figure 39 shows the system requirements for each software.



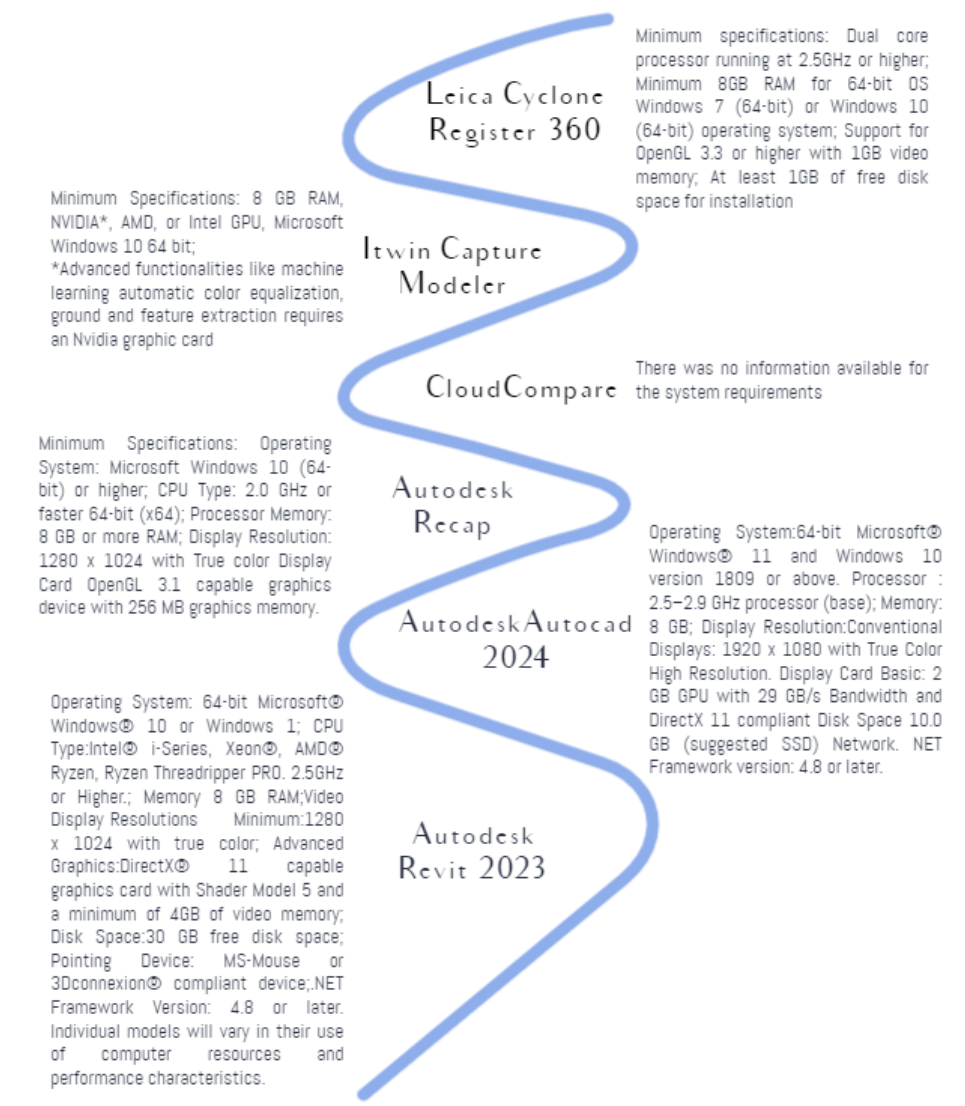


Figure 39 – Softwares system requirements

### 3.3 SEMI-AUTOMATIC 3D MODELLING SCRIPT

On figure 38, on the 3D modelling branch, it is cited a Dynamo script (Annex A). This section is focused on detailing the script step by step.

The csv file used as input for this script is organized in eleven columns and the number of rows depend on how many planes are recognized in RANSAC process. The columns are separated in Name, Width, Height, Cx, Cy, Cz, Nx, Ny, Nz, Dip and Dip dir. All items refer to plane's characteristics the C's fields refers to the center coordinates of the plane, the N's fields refer to the normal vector of the plane and Dip fields refers to the angular deviations of the plane.

### 3.METHODOLOGY

In Dynamo environment it is possible to import a csv data from a file path, but it comes with just one column with the information separated by “;”. Then, it is created a list with the csv data. However, this list needs to be flattened as it has too many levels. A node is used to split the information by “;” creating a list from csv file with columns, as presented in figure 40.

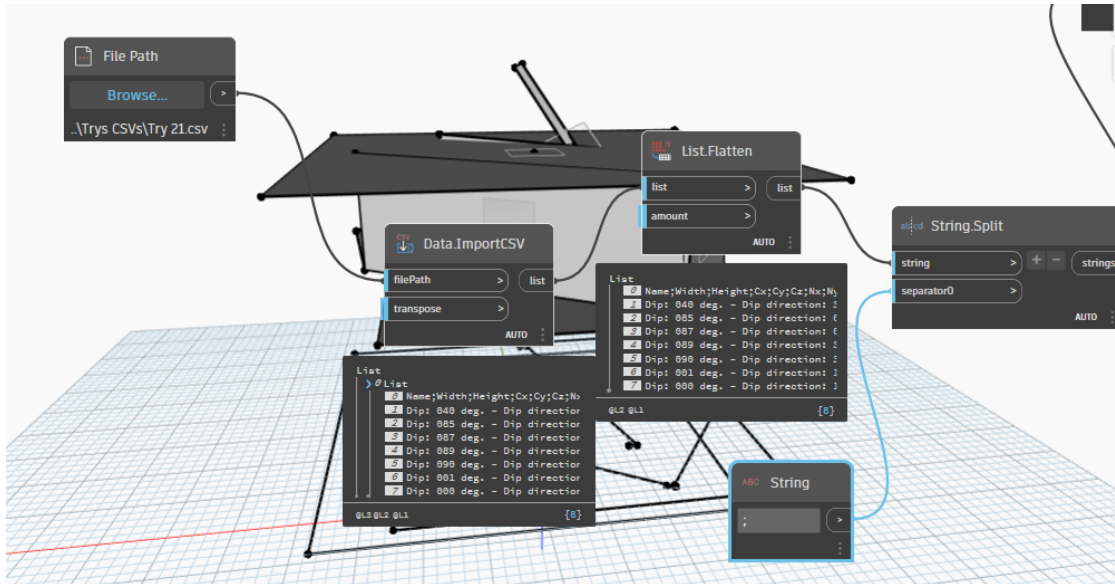


Figure 40 – Dynamo script - part 1

To create and organize the information, as well as start defining points and vectors, it is created a list of each row with exception of the first row that includes the description of each column. This strategy enable to create separated lists of each column and maintain the order of the planes, with a list for Cx, other for Cy and another list for Cz. These three lists are used as input of Point.ByCoordinates node. Following the same logic of coordinates lists, three lists for the normal are used as input of Vector.ByCoordinates node. This results in a list of normal vectors with x, y and z information. The same happens for Point.ByCoordinates, but in this case to get a list of points with x, y and z information, as shown in figure 41.

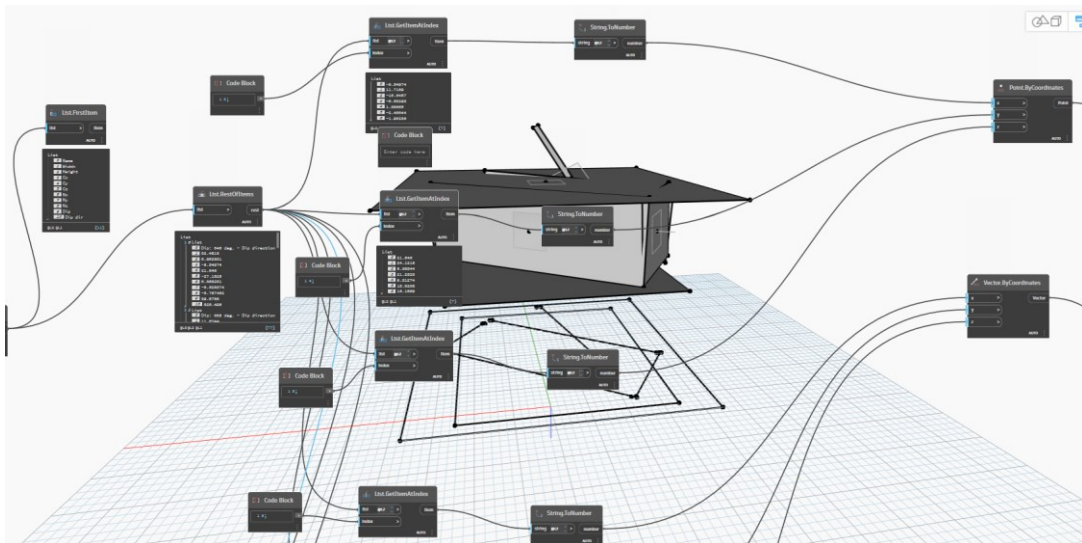


Figure 41 – Dynamo script - part 2

Based on the lists of normal vectors and points with x, y and z information, it is created a list of planes. This list of planes, merged with the lists of height and width, are used as input to create rectangles. From the list of rectangles, it is created a list of surfaces, and from that it is created a list of faces. After getting the faces it is possible to obtain the faces vertices, particularly with the Vertices.PointGeometry node which retrieve the x, y and z coordinates of the vertices points. The output list needs to be flattened to be used as input of a custom Python script, as shown in figure 42.

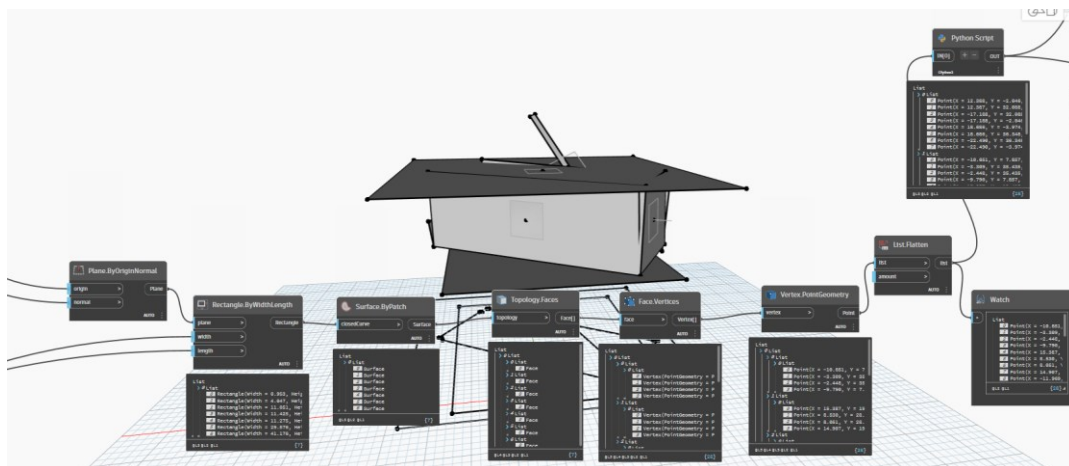


Figure 42 – Dynamo script - part 3

This custom Python script, figure 43 was written with the objective to separate the planes that will be modelled as walls, and planes that will be modelled as floors or roofs. To achieve that, the script calculates the difference between the maximum z value and the minimum z value of

### 3.METHODOLOGY

each rectangle. If the result is greater than 1 it will be considered a wall. Otherwise, if it is lower than 1 it will be considered a floor or roof. The output of this script are two lists, walls points and floors or roofs points, both with x, y and z coordinates.

```
1# Load the Python Standard and DesignScript Libraries
2import sys
3import clr
4clr.AddReference('ProtoGeometry')
5from Autodesk.DesignScript.Geometry import *
6import clr
7clr.AddReference('RevitAPI')
8from Autodesk.Revit.DB import *
9
10# Definir a classe Point para representar pontos com coordenadas X, Y e Z
11class Point:
12    def __init__(self, X, Y, Z):
13        self.X = X
14        self.Y = Y
15        self.Z = Z
16
17# Função para calcular a diferença entre o valor máximo e mínimo de Z para cada conjunto de 4 pontos
18def calculate_z_difference(points):
19    z_differences = []
20    less_than_one_list = []
21    greater_than_one_list = []
22
23    # Iterar pelos pontos em conjuntos de 4
24    for i in range(0, len(points), 4):
25        # Extrair valores de Z para o conjunto atual de pontos
26        z_values = [point.Z for point in points[i:i+4]]
27
28        # Calcular a diferença entre os valores máximo e mínimo de Z
29        z_diff = max(z_values) - min(z_values)
30        z_differences.append(z_diff)
31
32        # Categorizar pontos com base na condição de valor de Z
33        if z_diff < 1:
34            less_than_one_list.extend(points[i:i+4])
35        else:
36            greater_than_one_list.extend(points[i:i+4])
37
38    return less_than_one_list, greater_than_one_list
39
40# Input para a lista de pontos vinda do nó Dynamo
41points_input = IN[0]
42
43# Chamar a função para calcular diferenças de Z e categorizar pontos
44less_than_one, greater_than_one = calculate_z_difference(points_input)
45
46# Saída dos resultados (pode ser usada para criar ou modificar elementos no Revit)
47OUT = less_than_one, greater_than_one
```

Figure 43 – Python script for walls, floors and roofs separation

The List.GetItemAtIndex node gets the roofs and floors list as output. This list needs to be flattened to be used as input for other custom script (Figure 44). Therefore, this list is separated into two lists, roof list and floor list. Again, the List.GetItemAtIndex node needs to be used to get only the floors list. After that the points coordinates will be separated in x, y and z lists, as shown in figure 45.

```
1# Extrair a lista de pontos do nó Dynamo
2points_list = IN[0]
3
4# Ordenar a lista de pontos com base nos valores de Z
5sorted_points = sorted(points_list, key=lambda p: p.Z)
6
7# Separar a lista em duas partes
8first_part = sorted_points[:4]
9second_part = sorted_points[4:]
10
11# Saída dos resultados
12OUT = [first_part, second_part]
```

Figure 44 – Python script for roofs and floors points separation

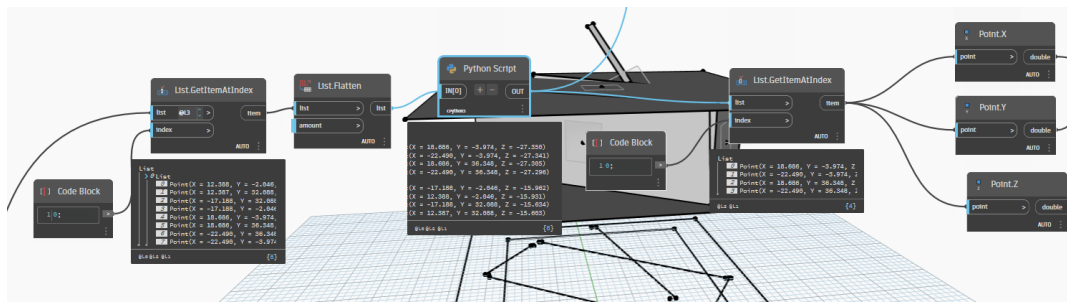


Figure 45 – Dynamo script - part 4

The x and y lists are used to create 2D points list. This list will be used as input for a custom Python script (Figure 46) to order the points and get a rectangle if the points are connected by the lists' order. Again, after this custom Python script, it is possible to get the x and y lists with the correct order and get once again the 2D points. From these points it is possible to get polycurves by points with the rectangle configuration and then get curves from these polycurves. These curves can be finally used as input for a node that models the floor. Other two inputs for this final node are the floor type, that is only a node where the user can select the floor type and the level, as presented in figure 47 .

To get the level defined, the average value of the Z's list is done to get an elevation result that is not a maximum or a minimum. The level is obtained by the node `Level.ByElevationAndName`.

```

1 # Extrair os quatro pontos vértices do retângulo do nó Dynamo
2 rectangle_vertices = IN[0]
3
4 # Calcular o centro do retângulo
5 center_x = sum([p.X for p in rectangle_vertices]) / 4
6 center_y = sum([p.Y for p in rectangle_vertices]) / 4
7
8 # Calcular a largura e a altura do retângulo
9 width = max([p.X for p in rectangle_vertices]) - min([p.X for p in
rectangle_vertices])
10 height = max([p.Y for p in rectangle_vertices]) - min([p.Y for p in
rectangle_vertices])
11
12 # Criar pontos para formar um retângulo com base nos vértices
13 rectangle_points = [
14     [center_x - width/2, center_y - height/2],
15     [center_x + width/2, center_y - height/2],
16     [center_x + width/2, center_y + height/2],
17     [center_x - width/2, center_y + height/2],
18 ]
19
20 # Saída dos resultados (pontos do retângulo)
21 OUT = rectangle_points

```

Figure 46 – Python script to order the 2D points

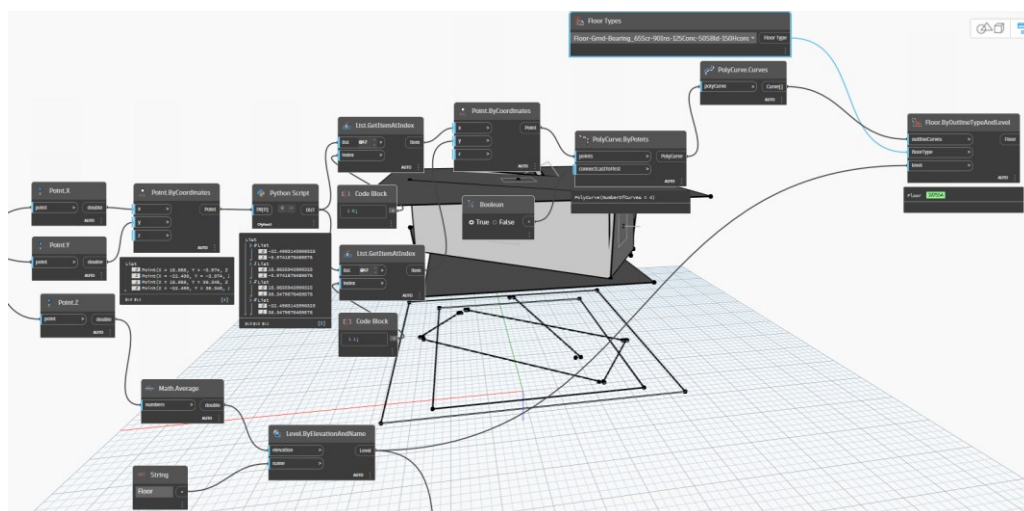


Figure 47 – Dynamo script - part 5

Walls modelling starts by getting the walls points list. This list needs to be flattened by dividing into three other lists, x, y and z lists. 2D points are created using x and y lists, and the list of these 2D points is used as input for a custom Python script (Figure 48). This script creates a list of every first two items from every four items of the list. In this way it is possible to get two points to create a reference line for wall creation. After, the Python script node, the output points list is divided into lengths of 2 to create the polycurves. From the list of polycurves, a list of curves is created, and this list needs to be flattened before being used as input for a wall modelling node. Besides the curves list, it is needed as input, the level, wall type, and heights, as shown in figure 49.

The heights list is obtained from the Z's points list, that is used as input for another custom Python script (Figure 50). This script, for every four listed items it calculates the averages of the two maximum z values and two minimum values. Based on this result, it calculates the difference between them and gives as output the absolute values. This provides a list of heights as an output which are ready to be used as input for the wall modelling node.



```

1# Extrair a lista de pontos do nó Dynamo
2points_list = IN[0]
3
4# Função para obter apenas os dois primeiros itens a cada quatro itens da
  lista
5def get_first_two_items(points_list):
6    result = []
7
8    # Iterar pelos elementos da lista em conjuntos de 4
9    for i in range(0, len(points_list), 4):
10        # Adicionar os dois primeiros itens de cada conjunto de 4 à lista
        de resultados
11        result.extend(points_list[i:i+2])
12
13    return result
14
15# Chamar a função para obter apenas os dois primeiros itens a cada quatro
  itens
16output_result = get_first_two_items(points_list)
17
18# Saída dos resultados
19OUT = output_result

```

Figure 48 – Python script get first two items from every four items

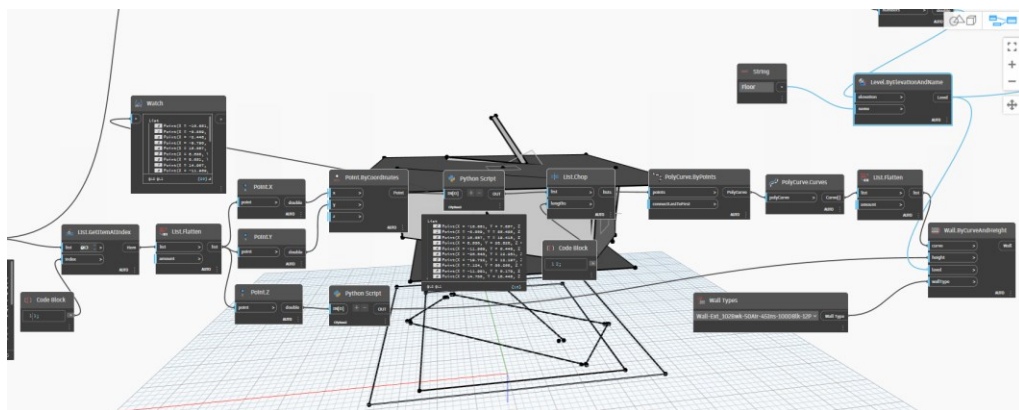


Figure 49 – Dynamo script - part 6

```

1# Importar namespaces necessários para Dynamo
2import clr
3clr.AddReference('RevitAPI')
4from Autodesk.Revit.DB import *
5
6# Input para a lista de valores
7input_list = IN[0]
8
9# Função para calcular a média dos dois valores mínimos e a média dos dois valores máximos em conjuntos de 4 itens,
10# em seguida, calcula a diferença absoluta entre essas médias
11def calculate_min_max_averages_and_absolute_difference(input_list):
12    min_averages = []
13    max_averages = []
14
15    # Iterar pelos elementos da lista em conjuntos de 4
16    for i in range(0, len(input_list), 4):
17        # Pegar os dois valores mínimos
18        min_values = sorted(input_list[i:i+4]):[:2]
19        min_average = sum(min_values) / len(min_values) if min_values else 0.0
20        min_averages.append(min_average)
21
22        # Pegar os dois valores máximos
23        max_values = sorted(input_list[i:i+4], reverse=True):[:2]
24        max_average = sum(max_values) / len(max_values) if max_values else 0.0
25        max_averages.append(max_average)
26
27    # Calcular a diferença absoluta entre as médias dos dois valores mínimos e dos dois valores máximos
28    absolute_difference = [abs(max_avg - min_avg) for max_avg, min_avg in zip(max_averages, min_averages)]
29
30    return absolute_difference
31
32# Chamar a função para calcular as médias e a diferença absoluta
33absolute_difference_output = calculate_min_max_averages_and_absolute_difference(input_list)
34
35# Saída dos resultados (diferença absoluta entre as médias)
36OUT = absolute_difference_output
37

```

Figure 50 – Python script for heights calculation

### 3.METHODOLOGY

To model the roof (Figure 51) it is necessary to get the roof's coordinates list from the Python script of figure 44. After that, it is essential to break this list in three lists of x, y and z coordinates. The process is similar to floors modeling process, it is created a list of points, these points are ordered using the same Python script of the floors (Figure 46). After, all points are ordered to get a rectangle, a polycurve list is created, and then a curve list is defined that will serve as input for Roof.ByOutlineTypeAndLevel node. After defining the roof type, the level is obtained calculating the average z value and creating the level using the node Level.ByElevationAnd Name.

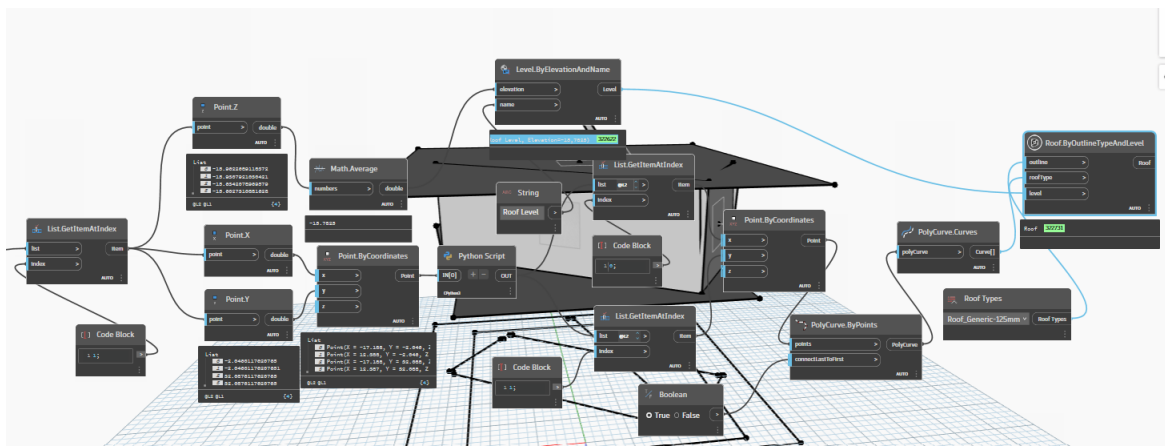


Figure 51 – Dynamo script - part 7



## **4. CASE STUDIES**

This chapter is focused on detailing two case studies where the proposed workflow integrating digital surveys and BIM modelling, detailed on chapter 3 was applied. In the first case study, a railway bridge, the methodology was performed without topographic support and 2D modeling. In the second case study, an industrial warehouse, the methodology was performed with topographic support and 3D modeling.

### **4.1 GOUSSET PLATE FROM GDAŃSKI RAILWAY BRIDGE (POLAND)**

#### **4.1.1 General description**

This case study was executed in collaboration with Warsaw University of Technology and the main objective was to compare the design dimensions of a gousset plate with the real dimensions obtained from laser scanner and photogrammetry.

This Gousset plate is part of the metallic structure of Gdański railway bridge, that is located in Warsaw, Poland. The Gdański bridge, is composed of 6 spans, total length of 406,5 m and 17 m of width. The span studied is marked in red in figure 52 and the gousset plate detail is highlighted in figure 53.

#### 4. CASE STUDY



Figure 52 – Gdański bridge: span location



Figure 53 – Gusset plate location

The design dimensions of bridge's structural elements were provided by the Warsaw University of Technology. The distance between the lower and upper horizontal chord is 5,97 m. The distance between the vertical posts of the truss, that are perpendicular to the horizontal chords, is 5,50 m, as shown in figure 54.

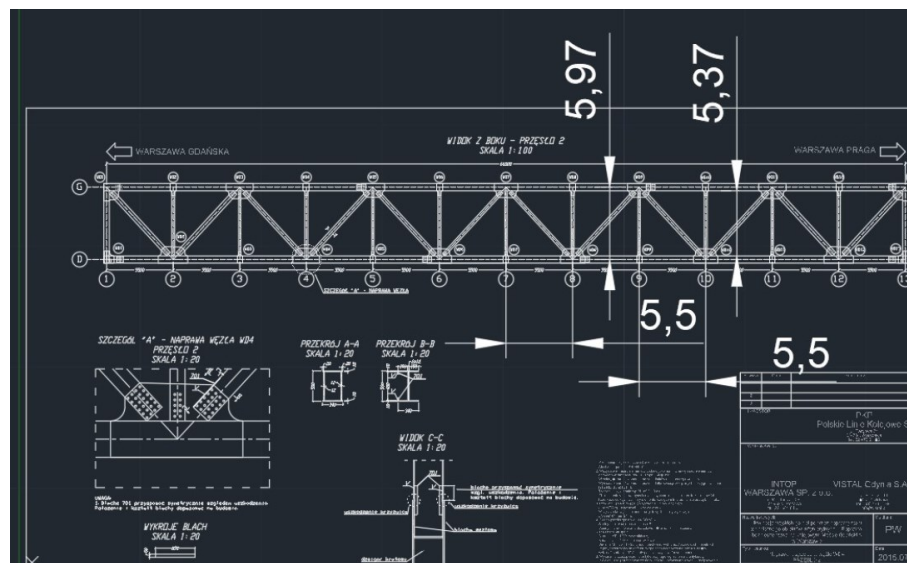


Figure 54 – Gdański bridge: structural frames distances

#### 4.1.2 Framework implementation

Following the framework, figure 37, without topographic support, the field survey was done with a drone DJI Mini 1, without GNSS. In total were taken 1297 photos, including frontal, top and bottom views of the span, besides different angles and distances from the structure, as shown in figure 55.



Figure 55 - Bottom, top and front bridge's photos

#### 4. CASE STUDY

To create the point cloud from the field survey photos, the first step involved filtering the photos, from which 646 photos remained. To aero triangulate this set, it was used 149 tie points to adjust manually the photos. These points do not have topographic information associated. The process was performed iteratively until achieve good results. After the aero triangulation, the reconstruction of the model, shown in figure 56, needs to be done to finalize the point cloud creation.

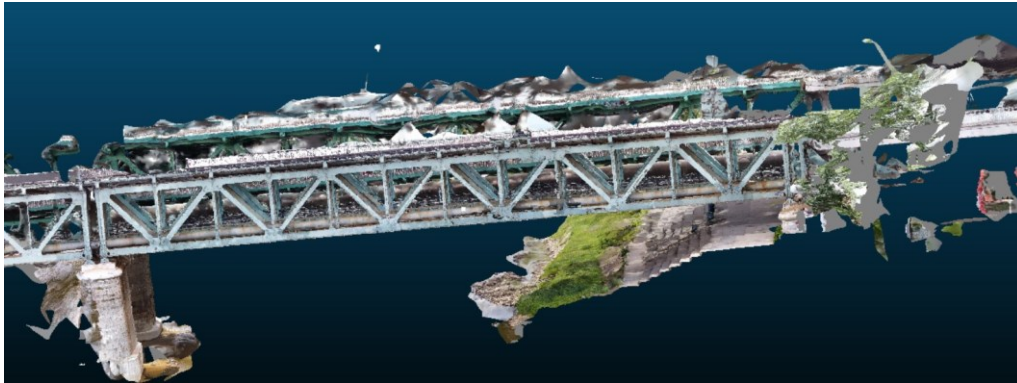


Figure 56 – Gdański bridge point cloud

To achieve the study objectives, it was needed to clean the point cloud and isolate the gousset plate. With that it is possible to scale the point cloud, comparing the measurements between the point cloud and the design, detailed in figure 54. After scaling the point cloud, it is necessary to go through the segmentation step, according to figure 37. Segmentation was done using RANSAC method to find the main plane of the model, see figure 57, and orientate the structure forcing the plane to be aligned to X, Y and Z axis. This makes the point cloud ready to the modeling stage, despite the holes on the structure caused by insufficient overlap of the photos and blurred images.

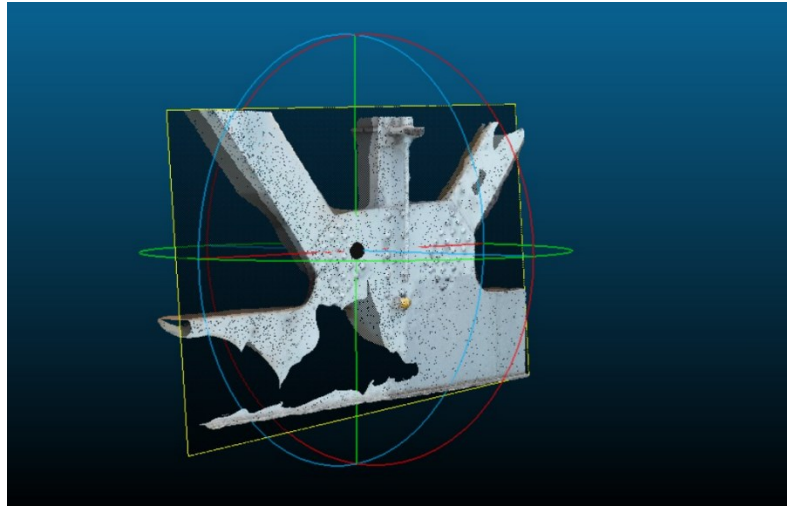


Figure 57 - Gousset plate point cloud after applying RANSAC method

#### 4.1.3 2D Modeling

For the 2D modeling, the hole on gousset plate seen in figure 58 is not an issue, since it does not affect any boundaries or rivets. In this way, to model the gousset plate, it was necessary to use a CAD software and import the point cloud. In this part it is relevant to verify the measurement system and units to guarantee that the point cloud shows correct dimensions.

Inside the CAD software environment and with the point cloud imported, it may be necessary to align to the pretended plan view. For that it was necessary to rotate the point cloud on both directions of the plane, aligning the plan view of the point cloud with the view of the gousset plate model defined by design, and design drawings, as shown in figure 58.

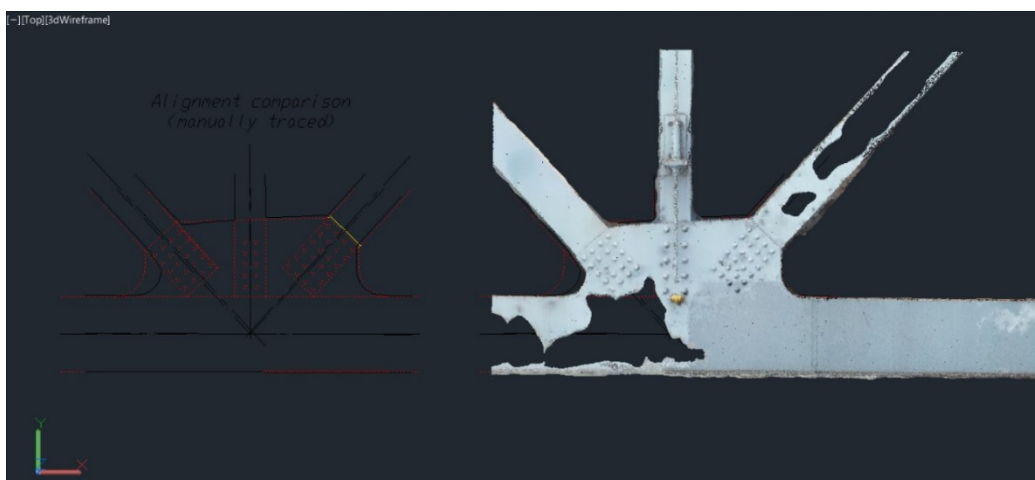


Figure 58 – Point cloud in CAD software aligned

After, polylines were traced following the boundaries and circles defined on the rivets, as presented in figure 59. After finishing the model, it was possible to overlap all three different models, as depicted in figure 60.

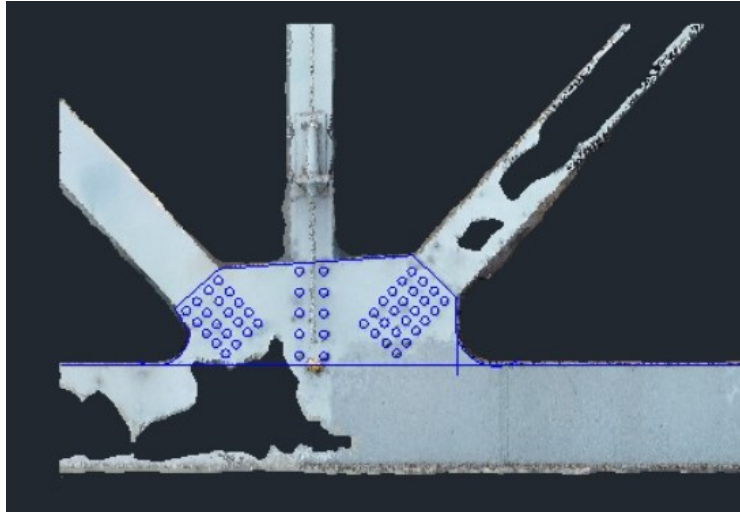


Figure 59 – 2D modelling with polylines and circles

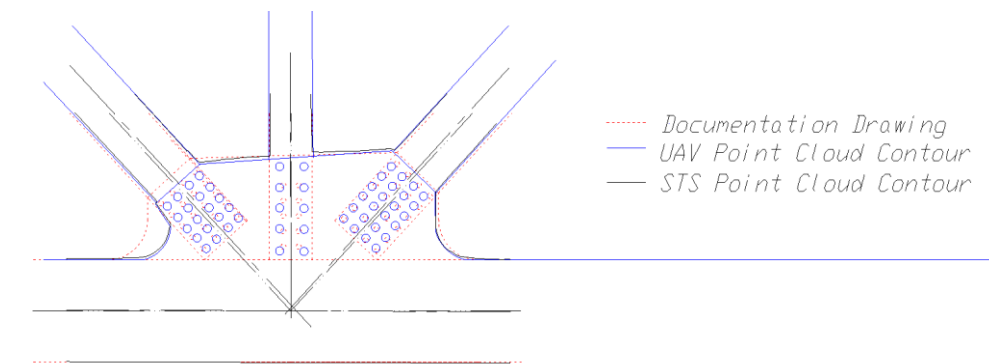


Figure 60 – Comparison of three models of the Gousset plate

## 4.2 INDUSTRIAL WAREHOUSE (PORTUGAL)

### 4.2.1 General description

The second case study is an industrial warehouse, figure 61 located in Valongo, within Porto metropolitan area. This case study was done in collaboration with the contractor company Garcia Garcia, which pretended to have the building point cloud and a 3D model to get structural dimensions. This information is relevant since the warehouse is under expansion and the documentation would serve to preserve the interventions' building historic.



For this study the LOD 200 was defined. figure 29 states that LOD 200 representation is approximated in terms of dimensions, elements, location and orientation and it is used as placeholder. This specific LOD was defined because there was no open-source, tested script available for the semi-automation of 3D modeling using point cloud data as input. As shown in section 3.3, previous studies developed scripts and workflows that required much more from the user for input and modelling, therefore, the LOD 200 was a challenge in terms of creating a more automatized script that requires less from the user. On the other hand, achieving a higher and more complex LOD was unnecessary, as the approximate main dimensions would be accurately represented in the 3D model.



Figure 61 - Warehouse overview

#### 4.2.2 Framework implementation

Following the proposed workflow of figure 37, this case study is performed with topographic support using a total station, and also the laser scanner and drone. Starting by the total station and topographic support, there were not used tags or marks on the building façades to serve

#### 4. CASE STUDY

as reference points. Instead of that, the building corners and anti-plague stickers, that were already installed in situ, were used, as shown in figure 62.



Figure 62 – References for topographic survey

The topographic survey data used the European terrestrial reference system 89 (ETRS89) used for Portugal on shore surveys, based on 26 control points with known coordinates, as shown in figure 63.

```
100, -30051.1572, 176806.1562, 128.4520,  
101, -30043.7214, 176782.3486, 128.4640,  
102, -30048.5450, 176780.8333, 124.4107,  
103, -30053.2252, 176795.6972, 124.3638,  
104, -30051.1474, 176806.1382, 121.0579,  
105, -30051.1001, 176806.0332, 121.1382,  
106, -30048.3188, 176797.1059, 121.1070,  
107, -30043.8507, 176782.3554, 118.6599,  
108, -30036.7828, 176814.4022, 123.5766,  
200, -30035.4972, 176811.1802, 118.6521,  
201, -30010.8209, 176818.8988, 118.7220,  
202, -29990.2102, 176825.1769, 119.9462,  
203, -29990.2027, 176825.2192, 128.4598,  
204, -29994.5842, 176827.6263, 123.5997,  
205, -30005.4587, 176820.0741, 118.8773,  
300, -29986.4406, 176800.1149, 118.6813,  
301, -29984.9549, 176796.9327, 123.6139,  
302, -29985.3729, 176800.6104, 128.4970,  
303, -30043.5283, 176782.3684, 128.4613,  
304, -30033.2005, 176785.6229, 127.5252,  
305, -30027.0572, 176783.7446, 123.5659,  
306, -30048.3379, 176780.8572, 124.4148,  
307, -30027.7196, 176787.2887, 119.2357,  
308, -30020.0073, 176782.0691, 118.0878,  
309, -29994.2290, 176791.2501, 118.2078,  
310, -29995.6151, 176777.4004, 128.4389,
```

Figure 63 - Control points coordinates

The laser scanner survey needed 23 setups around the building to be completed and had a bundle error of 0.007 m, as shown in annex B. It should be emphasized that this survey did not



cover the roofs, considering the considerable time and effort required. To perform the field survey, an Ipad Pro 11 (2<sup>nd</sup> Generation)® was used to do the laser scanner point cloud pre-registration and correct eventual on site errors, as seen in figure 64. At the end, the survey was successful accomplished (more information is available in Annex B) and the model was ready to be registered. On this step the control points with topographic data were pointed in the model and the point cloud was in the correct scale and global reference system, as depicted in figure 65.



Figure 64 - Laser scanner survey of the warehouse



Figure 65 – Marking control points on laser scanner point cloud

The photographs survey used two drones retrieving 2001 photos. For the roof survey it was used a flight plan software, as shown in figure 66. However, the drones survey was not limited to roof photos, the façades were captured too, as shown in figure 67. For the survey

#### 4. CASE STUDY

preparation, there was the need to ask for an authorization of National Civil Aviation Authority (ANAC) and drones' pilots had to be certified by the same authority.



Figure 66 - Flight plan software in use



Figure 67 - Drone surveys

After the field survey, the control points were marked on the photos and an aerial triangulation was performed 17 times to improve the model by adjusting settings and tie points. To get the final model it was necessary to filter the photos original getting a total of 1855 photos. For aerial triangulation the laser scanner point cloud was already included in the fusion process. The final aerial triangulation can be seen in figure 68 and more details are provided in annex C.

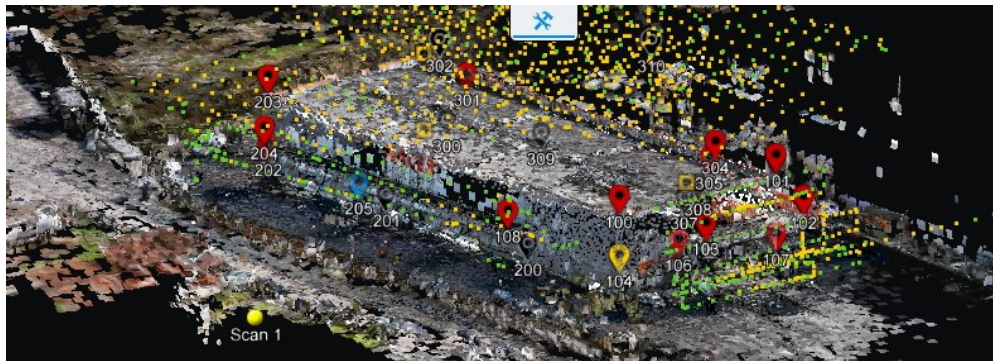


Figure 68 – Final aerial triangulation

It is important to emphasize that not all control points were marked in points clouds. Some of them could not be found on photos and others were repeated. At the end from the initial 26 control points, shown in figure 63, only 17 control points were marked.

After the aerial triangulation, a reconstruction of the model was done to conclude and texturize the point cloud, depicted in figure 69. After, it was necessary to fill some holes on walls and roof, clean the noise on point cloud and subsample, as the noisy version was so dense that was hard to work with. The final version of the model is presented in figure 70.

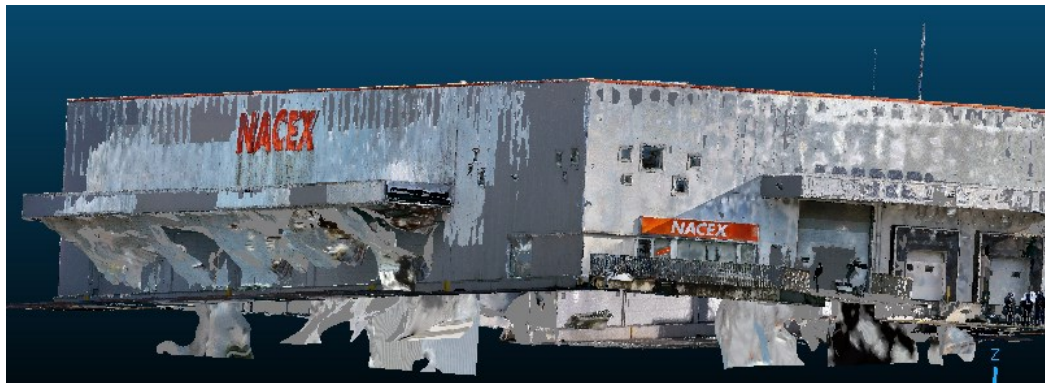


Figure 69 - Model reconstruction with noisy data



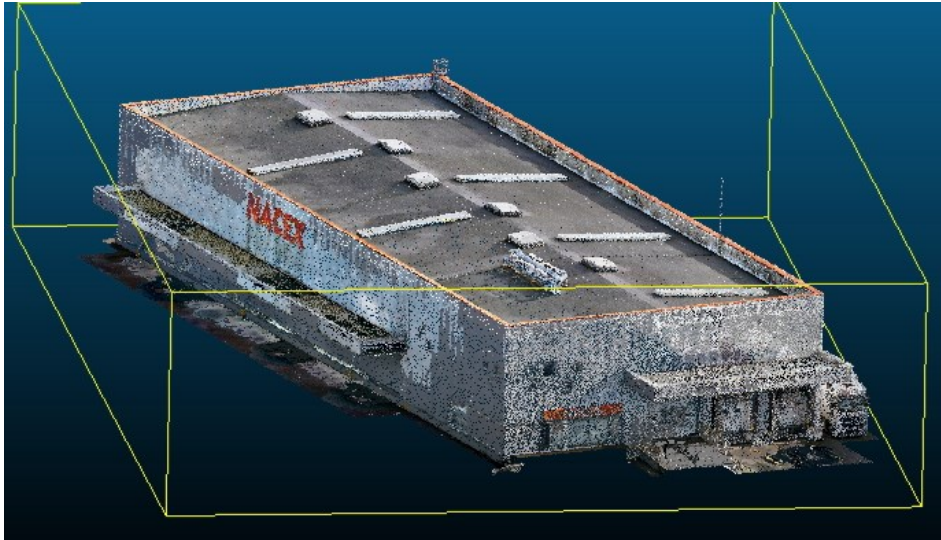


Figure 70 - Warehouse point cloud final version

Following the proposed framework of figure 37, the segmentation encompasses the RANSAC method to find planes on the point cloud. This requires refining the settings, leveraging the minimum number of points to support a primitive and choosing to find only planes (Figure 71). This refinement is important to do not find more planes than necessary, because having more than necessary can mean that it will be generated in model fictional walls, floors or roof and the final 3D model will lose its trustable and accuracy.

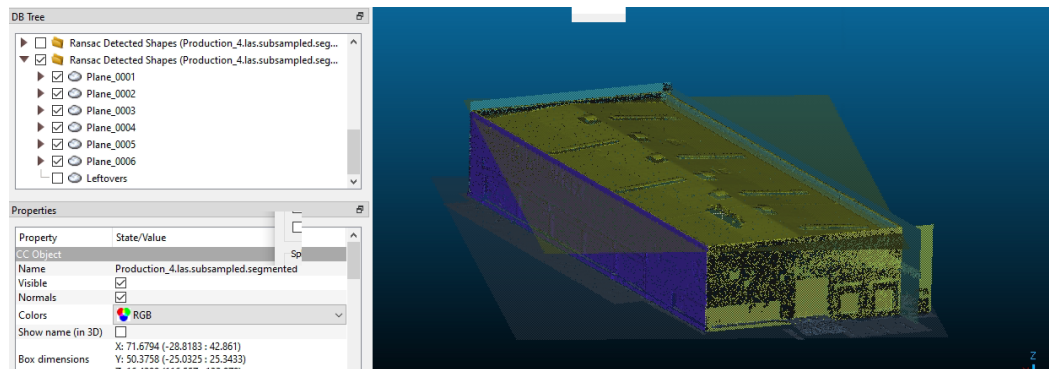


Figure 71 - RANSAC method applied to the warehouse point cloud

### 4.2.3 3D Modeling

The next step, after finalizing the segmentation, is to develop a concise and reliable 3D model using the framework proposed in figure 38. In that way, it was created a script to semi-automatize the process according to the details of section 3.3. The data to be used as input for that script is derived from planes acquired by RANSAC method. This input needs to be in csv

format and the order of the columns needs to be as defined in table 7, otherwise the script will not work.

Table 7 - Columns order

Name	Width	Height	Cx	Cy	Cz	Nx	Ny	Nz	Dip	Dip dir
Dip: 000 deg. - Dip direction: 325 deg.	681.197	425.749	817.215	0.593395	127.836	-0.000763	0.0010867	0.999999	0.0740187	324.908
Dip: 089 deg. - Dip direction: 343 deg.	69.146	116.592	962.699	-118.742	123.605	-0.299669	0.954002	0.0088408	894.934	342.562
Dip: 090 deg. - Dip direction: 163 deg.	639.908	10.178	455.072	123.829	123.373	-0.297817	0.954615	-0.003973	897.723	162.673
Dip: 089 deg. - Dip direction: 253 deg.	254.406	130.125	386.524	987.129	123.053	0.954859	0.296429	-0.019351	888.912	252.753
Dip: 000 deg. - Dip direction: 197 deg.	716.798	503.773	70.212	0.153851	118.273	-0.001655	-0.005553	0.999983	0.332202	196.602
Dip: 089 deg. - Dip direction: 073 deg.	287.817	106.399	-217.237	-107.543	123.19	0.955908	0.293503	0.0097611	894.407	729.314

The script used in this case study is pretended to be generic. For the script development was necessary to learn VPL and Python language from scratch. The result of the script output for this case study is shown in figure 72.

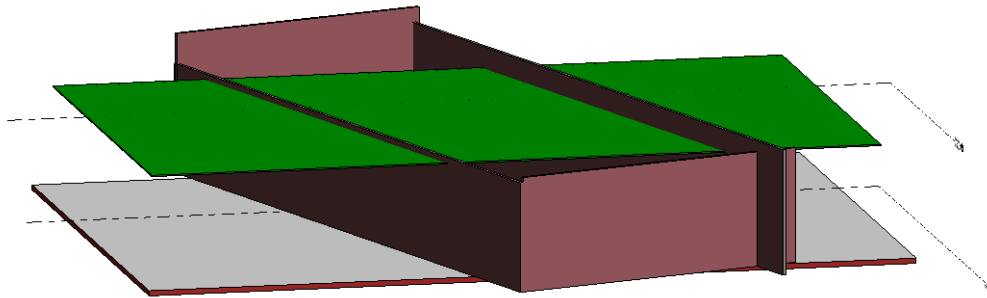


Figure 72 – Script output

The last step to finalize the model was adjusting the walls heights and connections, adjust the floors and roofs boundaries. This adjustment is simple and, depending on the software used for modeling, can be done very quickly with minimal effort. The finalized warehouse 3D model can be seen in figure 73.

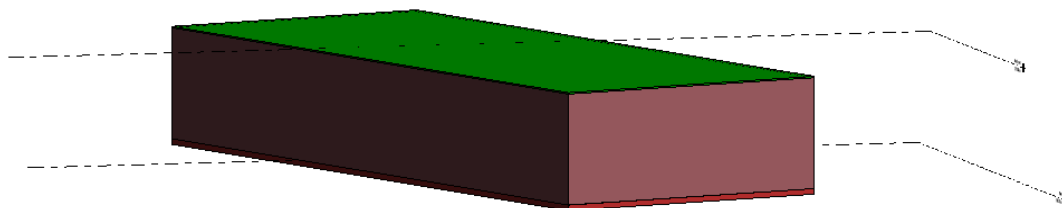


Figure 73 - Warehouse final 3D model



## 5.DISCUSSION

The first case study allowed to achieve great results. The final comparison between the designed gousset plate and the digital surveys results show a difference between them, and this may result from construction changes or renovations. Another comparison was also studied, particularly, between the laser scanner results and the photogrammetry results. This analysis revealed that the horizontal spacing between rivets connecting the vertical member do not differ by 39% and 31%, while the vertical spacing do not differ by 63% and 59%, respectively, for the UAV and laser scan compared to the design model.

The results for the second case study were as expected. The point cloud creation was successfully done, considering the photogrammetry, laser scanner and their fusion. This was confirmed by the low error between control points in final model and the topographic coordinates. The script allowed the semi-automatization of the process and allowed to reach a LOD 200 model, as the generic example presented in figure 74.

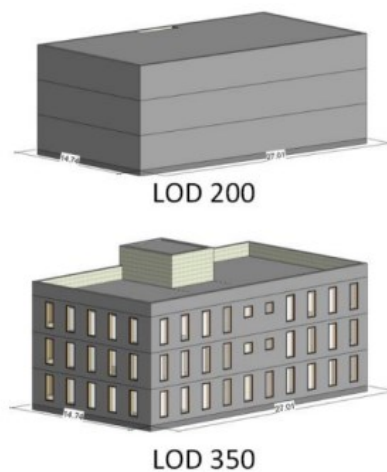


Figure 74 – Example of different LOD's applied to buildings (Abualdenien and Borrmann, 2022)

Both case studies accomplished the proposed goals, including the framework proposal that was tested, validated and can be improved in future studies with more automatization and reducing the tasks' time and manual decisions. It was clear that for both case studies, the use of laser scanner and photography's assisted by drones brought more efficiency to the process, decreasing the time spent on site and excluding the need of scaffold and specialized inspectors. This technology is a safer, faster and more precise method than the traditional way of doing these reality capture activities. It was observed that the step that took more time was the point cloud creation, aerial triangulation and reconstruction. Another task that took considerable time was the segmentation, not because of the RANSAC method, but also due to the fact that point clouds were so dense that computer could not support. Even the subsample exigence is very high for the computer.

It was noticed, during this study, that the field surveys with digitalization and using a well-established workflow are more efficient. Also, this study applied recent resources of flight planning, which is very valuable and promising to enhance the automatization. Following the automatization concept, the effort to create the script on VPL and Python open ways to the 3D modelling semi-automation from point clouds.

Aiming for future developments that seek to continue evolving the proposed framework and process automation, the aerial triangulation, reconstruction, and segmentation can take less time and demand less from the computer with technological advancements. As computers become more powerful in terms of data processing and memory, and as software continues to develop its BIM interface, technologies like Neural Radiance Fields (NeRFs) (Mildenhall et al., 2020) have the potential to become routine in the construction industry, much like laser scanners and drones.

For modeling, future studies may focus on automating 2D modeling, and the script for 3D modeling can be improved to achieve higher LOD levels, more precise segmentation results, and greater generality, especially for floors and roofs.

Field surveys can be enhanced by optimizing flight planning to capture all drone-supported photos. While the laser scanner already has a solid and fast workflow, future studies should implement the VIS technology cited in chapter 2.2 to further improve this workflow. Additionally, staying informed about emerging technologies and studying their applications will be crucial.



## **6.FINAL REMARKS**

The engineering is evolving and needs to incorporate the technology advances of society to improve itself, diminishing the workforce needed and reducing the time needed to deliver the tasks. This study was a contribution to this improvement and as cited in this work opens ways for more development in all proposed workflow steps, meaning that they need to be updated too.

This study, allied the proven and tested work methods, surveys and point cloud creation, with the new, new resources application and automation, incorporating this proposal in a framework. In this thesis, the created script was thoroughly explained so that future work can continue to automate this workflow, consequently leading to greater productivity in the construction sector.



## REFERENCES

ABUALDENIEN, Jimmy; BORRMANN, André - Levels of detail, development, definition, and information need: a critical literature review. **Journal of Information Technology in Construction**. . ISSN 1874-4753. 27:2022) 363–392. doi: 10.36680/j.itcon.2022.018.

ALMUKHTAR, Avar *et al.* - Reality Capture of Buildings Using 3D Laser Scanners. **CivilEng**. . ISSN 2673-4109. 2:1 (2021) 214–235. doi: 10.3390/civileng2010012.

ANAMIKA S. JADON; DAMINI A. PATIL - Uses of Drones and Photogrammetry in Project Monitoring . **International Research Journal of Engineering and Technology (IRJET)**. 07:12 (2020) 1765–1771.

ARIAS, P. *et al.* - Low-cost documentation of traditional agro-industrial buildings by close-range photogrammetry. **Building and Environment**. . ISSN 03601323. 42:4 (2007) 1817–1827. doi: 10.1016/j.buildenv.2006.02.002.

AUTODESK - **System requirements for Revit 2023 products** [Em linha], atual. out. 2023. [Consult. 3 fev. 2024]. Disponível em  
WWW:<URL:<https://www.autodesk.com/support/technical/article/caas/sfdcarticles/sfdcarticles/System-requirements-for-Autodesk-Revit-2023-products.html>>.

AUTODESK - **System requirements for Autodesk ReCap Pro and ReCap Photo** [Em linha], atual. 2024. [Consult. 3 fev. 2024]. Disponível em  
WWW:<URL:<https://www.autodesk.com/support/technical/article/caas/sfdcarticles/sfdcarticles/System-requirements-for-Autodesk-ReCap-Pro-and-ReCap-Photo.html>>.

AUTODESK - **System requirements for AutoCAD 2024 including Specialized Toolsets** [Em linha], atual. jan. 2024. [Consult. 3 fev. 2024]. Disponível em  
WWW:<URL:<https://www.autodesk.com/support/technical/article/caas/sfdcarticles/sfdcarticles/System-requirements-for-AutoCAD-2024-including-Specialized-Toolsets.html>>.

- BADENKO, V. *et al.* - SCAN-TO-BIM METHODOLOGY ADAPTED FOR DIFFERENT APPLICATION. **The International Archives of the Photogrammetry, Remote Sensing and Spatial Information Sciences**. . ISSN 2194-9034. XLII-5/W2:2019) 1–7. doi: 10.5194/isprs-archives-XLII-5-W2-1-2019.
- BENTLEY - ContextCapture | Guide for photo acquisition. 2017).
- BIMFORUM - Level of Development (LOD) Specification - Part I. 2023).
- LEICA - **blk360\_spec\_sheet\_2\_0** [Em linha] [Consult. 29 abr. 2024]. Disponível em WWW:<URL:<https://shop.leica-geosystems.com/>>.
- CASTELLAZZI, Giovanni *et al.* - From Laser Scanning to Finite Element Analysis of Complex Buildings by Using a Semi-Automatic Procedure. **Sensors**. . ISSN 1424-8220. 15:8 (2015) 18360–18380. doi: 10.3390/s150818360.
- CHEN, Kaiwen; RAKHA, Tarek - CV-based Registration of UAV-captured Façade Inspection Images to 3D Building Point Cloud Models. **SimAUD 2021**. 2021).
- DJI - **Mavic Mini - Suporte do Produto** [Em linha], atual. mai. 2024. [Consult. 15 abr. 2024]. Disponível em WWW:<URL:<https://www.dji.com/pt/support/product/mavic-mini>>.
- DJI - **Mavic 2 Enterprise Advanced - Specifications** [Em linha], atual. mai. 2024. [Consult. 15 abr. 2024]. Disponível em WWW:<URL:<https://enterprise.dji.com/mavic-2-enterprise-advanced/specs>>.
- DJI - **Mavic 3 - Specifications** [Em linha], atual. mai. 2024. [Consult. 15 abr. 2024]. Disponível em WWW:<URL:<https://ag.dji.com/mavic-3-m/specs>>.
- FONTANA, Raffaella *et al.* - High-resolution 3D digital models of artworks. Em SALIMBENI, RENZO (Ed.) - [Em linha] Disponível em WWW:<URL:<http://proceedings.spiedigitallibrary.org/proceeding.aspx?articleid=767706>>.
- GAVINA, Rui - Fundamentos da Metodologia BIM - Aula 2. Porto. 2023).
- HE, Shaohua *et al.* - Investigation of Measurement Accuracy of Bridge Deformation Using UAV-Based Oblique Photography Technique. **Sensors**. . ISSN 1424-8220. 22:18 (2022) 6822. doi: 10.3390/s22186822.
- IGLHAUT, Jakob *et al.* - Structure from Motion Photogrammetry in Forestry: a Review. **Current Forestry Reports**. . ISSN 2198-6436. 5:3 (2019) 155–168. doi: 10.1007/s40725-019-00094-3.

**iTwin® Capture Modeler Product Data Sheet -**

JIANG, San; JIANG, Cheng; JIANG, Wanshou - Efficient structure from motion for large-scale UAV images: A review and a comparison of SfM tools. **ISPRS Journal of Photogrammetry and Remote Sensing**. . ISSN 09242716. 167:2020) 230–251. doi: 10.1016/j.isprsjprs.2020.04.016.

JUNG, Jaehoon *et al.* - Productive modeling for development of as-built BIM of existing indoor structures. **Automation in Construction**. . ISSN 09265805. 42:2014) 68–77. doi: 10.1016/j.autcon.2014.02.021.

LEE, Impyeong; CHOI, Yunsoo - FUSION OF TERRESTRIAL LASER SCANNER DATA AND IMAGES FOR BUILDING RECONSTRUCTION . Seoul. 2004).

**Leica Cyclone Technical Specifications** - [Em linha] Disponível em WWW:<URL:URL:www.leica-geosystems.com>.

**Leica Nova MS50 Datasheet** - [Em linha] Disponível em WWW:<URL:www.leica-geosystems.com>.

Leica-Cyclone-FIELD-360-DS-1219-LR - [s.d.]).

MAAR, Hannes; ZOGG, Hans-Martin - **WFD Technology Optimised measuring meets individual demands** [Em linha] Disponível em WWW:<URL:www.leica-geosystems.com>.

MILDENHALL, Ben *et al.* - NeRF: Representing Scenes as Neural Radiance Fields for View Synthesis. 2020).

NADHIM, Evan *et al.* - Falls from Height in the Construction Industry: A Critical Review of the Scientific Literature. **International Journal of Environmental Research and Public Health**. . ISSN 1660-4601. 13:7 (2016) 638. doi: 10.3390/ijerph13070638.

NAN, Liangliang; WONKA, Peter - PolyFit: Polygonal Surface Reconstruction from Point Clouds. Em **2017 IEEE International Conference on Computer Vision (ICCV)**. [S.l.] : IEEE, Out. 2017. ISBN 978-1-5386-1032-9

**National BIM Report 2020** - [Em linha] [Consult. 10 jun. 2024]. Disponível em WWW:<URL:https://www.thenbs.com/knowledge/reports>.

OLIVEIRA, ROGÉRIO LOPES - **Modelos Digitais de Ponte Ferroviárias: Tecnologias de Reality Capture e Modelação BIM**. Porto : Instituto Politécnico do Porto, Out. 2022

## REFERENCES

- PEPE, Massimiliano; FREGONESE, Luigi; CROCETTO, Nicola - Use of SfM-MVS approach to nadir and oblique images generated through aerial cameras to build 2.5D map and 3D models in urban areas. **Geocarto International**. . ISSN 1010-6049. 37:1 (2022) 120–141. doi: 10.1080/10106049.2019.1700558.
- PFEIFER, N.; BRIESE, C. - Laser scanning – principles and applications. Em **GeoSiberia 2007 - International Exhibition and Scientific Congress**. [S.l.] : European Association of Geoscientists & Engineers, 2007. ISBN 978-94-6282-090-6
- POPESCU, Cosmin *et al.* - 3D reconstruction of existing concrete bridges using optical methods. **Structure and Infrastructure Engineering**. . ISSN 1573-2479. 15:7 (2019) 912–924. doi: 10.1080/15732479.2019.1594315.
- PREVITALI, M. *et al.* - Towards automatic indoor reconstruction of cluttered building rooms from point clouds. **ISPRS Annals of the Photogrammetry, Remote Sensing and Spatial Information Sciences**. . ISSN 2194-9050. II–5:2014) 281–288. doi: 10.5194/isprsannals-II-5-281-2014.
- RUAN, Guangchen *et al.* - High Performance Photogrammetry for Academic Research. Em **Proceedings of the Practice and Experience on Advanced Research Computing**. New York, NY, USA : ACM, 22 Jul. 2018. ISBN 9781450364461
- SAN JOSÉ ALONSO, J. I. *et al.* - COMPARING TIME-OF-FLIGHT AND PHASE-SHIFT. THE SURVEY OF THE ROYAL PANTHEON IN THE BASILICA OF SAN ISIDORO (LEÓN) . **International Archives of the Photogrammetry, Remote Sensing and Spatial Information Sciences, Volume XXXVIII-5/W16, 2011 ISPRS Trento 2011 Workshop, 2-4 March 2011**. Trento, Italy. 2011).
- SCHNABEL, R.; WAHL, R.; KLEIN, R. - Efficient RANSAC for Point-Cloud Shape Detection. **Computer Graphics Forum**. . ISSN 0167-7055. 26:2 (2007) 214–226. doi: 10.1111/j.1467-8659.2007.01016.x.
- TANG, Pingbo *et al.* - Automatic reconstruction of as-built building information models from laser-scanned point clouds: A review of related techniques. **Automation in Construction**. . ISSN 09265805. 19:7 (2010) 829–843. doi: 10.1016/j.autcon.2010.06.007.
- XIONG, Zhaoyang; WANG, Ting - Research on BIM Reconstruction Method Using Semantic Segmentation Point Cloud Data Based on PointNet. **IOP Conference Series: Earth and Environmental Science**. . ISSN 1755-1307. 719:2 (2021) 022042. doi: 10.1088/1755-1315/719/2/022042.

ZHANG, Wenyan; LI, Zhixin; SHAN, Jie - Optimal Model Fitting for Building Reconstruction From Point Clouds. **IEEE Journal of Selected Topics in Applied Earth Observations and Remote Sensing**. . ISSN 1939-1404. 14:2021) 9636–9650. doi: 10.1109/JSTARS.2021.3110429.

ZICARELLI, Philip - Industrial photogrammetry: a cost-effective solution for an «as-built» world. **Tappi Journal**. 1992) 75–78.





## **ANNEX A**

File Path

Browse...

..\..\Documents\DIPRE.csv

CSV Data.ImportCSV

filePath

list

transpose

AUTO

List.Flatten

list

list

amount

AUTO

String

:

String.Split

string

separator0

strings

AUTO

List.FirstItem

list

item

AUTO

List.RestOfItems

list

rest

AUTO



Library ↓



[ ] Code Block

1|3;

>

⋮

List.GetItemAtIndex

list @L2 >

Index >

item

AUTO ⋮

String.ToNumber

string @L2 >

number

AUTO ⋮

[ ] Code Block

Enter code here

⋮

List.RestOfItems

list >

rest

AUTO ⋮

List.GetItemAtIndex

list @L2 >

Index >

item

AUTO ⋮

String.ToNumber

string @L2 >

number

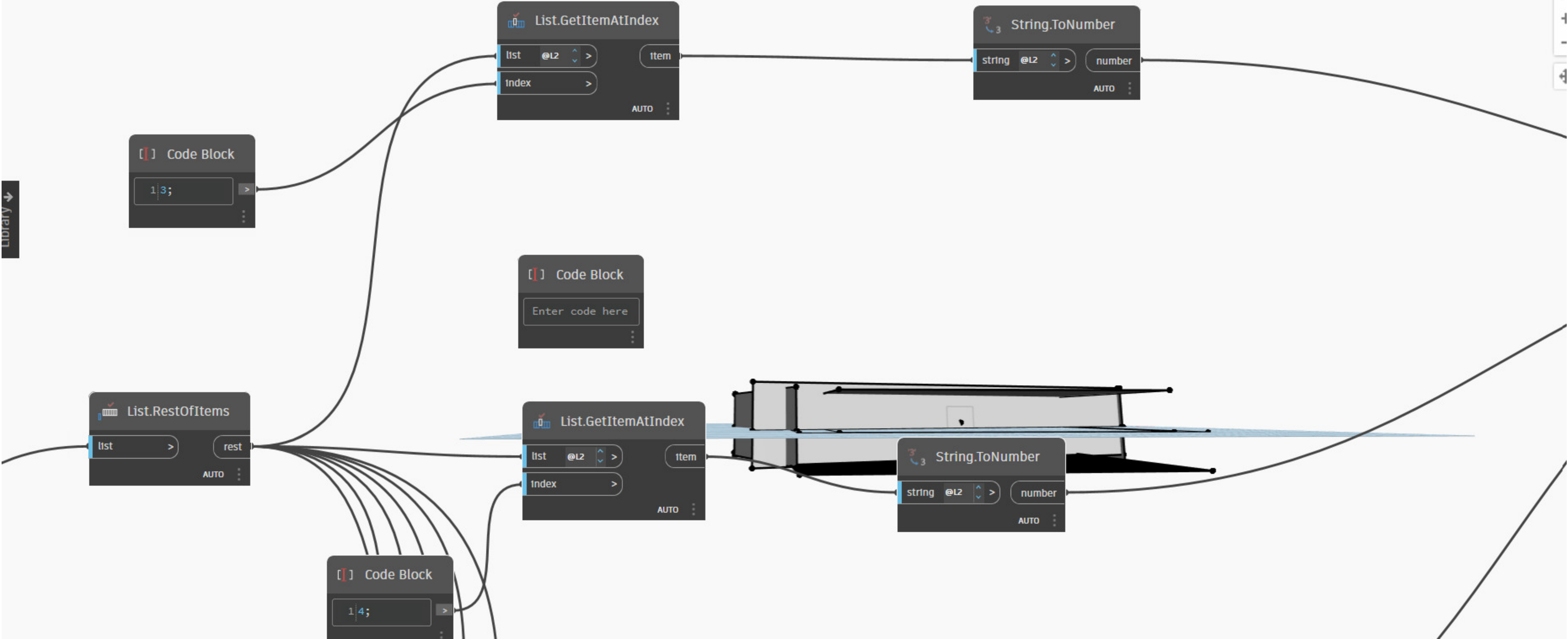
AUTO ⋮

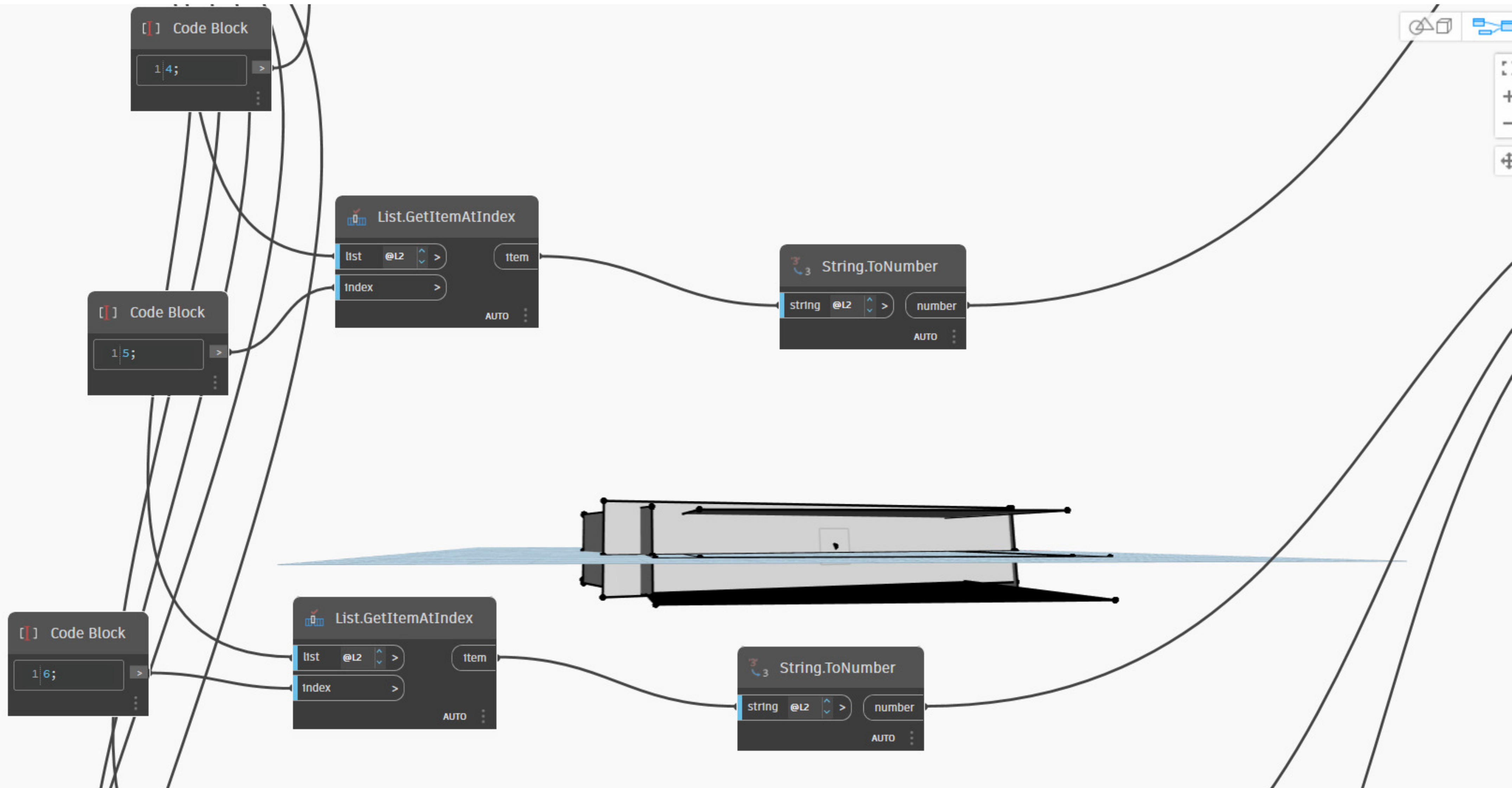
[ ] Code Block

1|4;

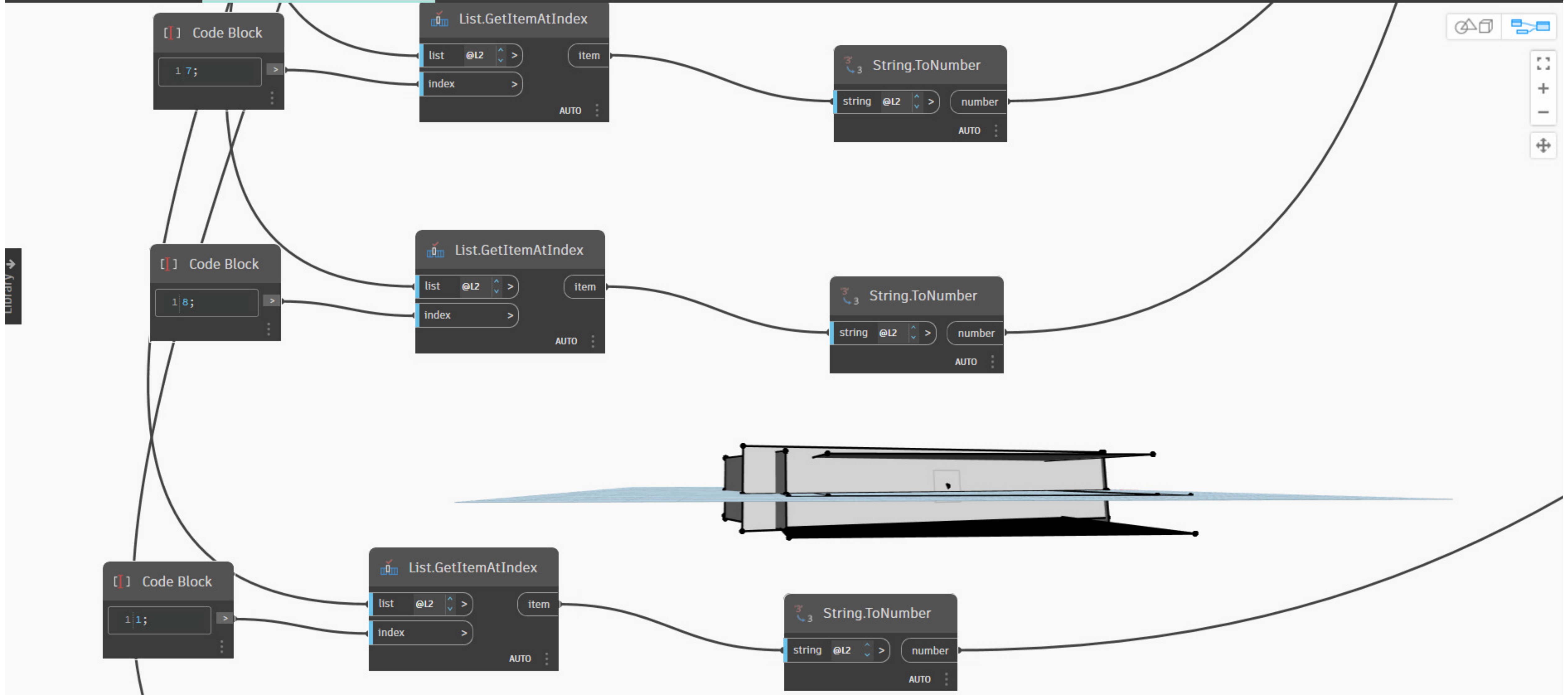
>

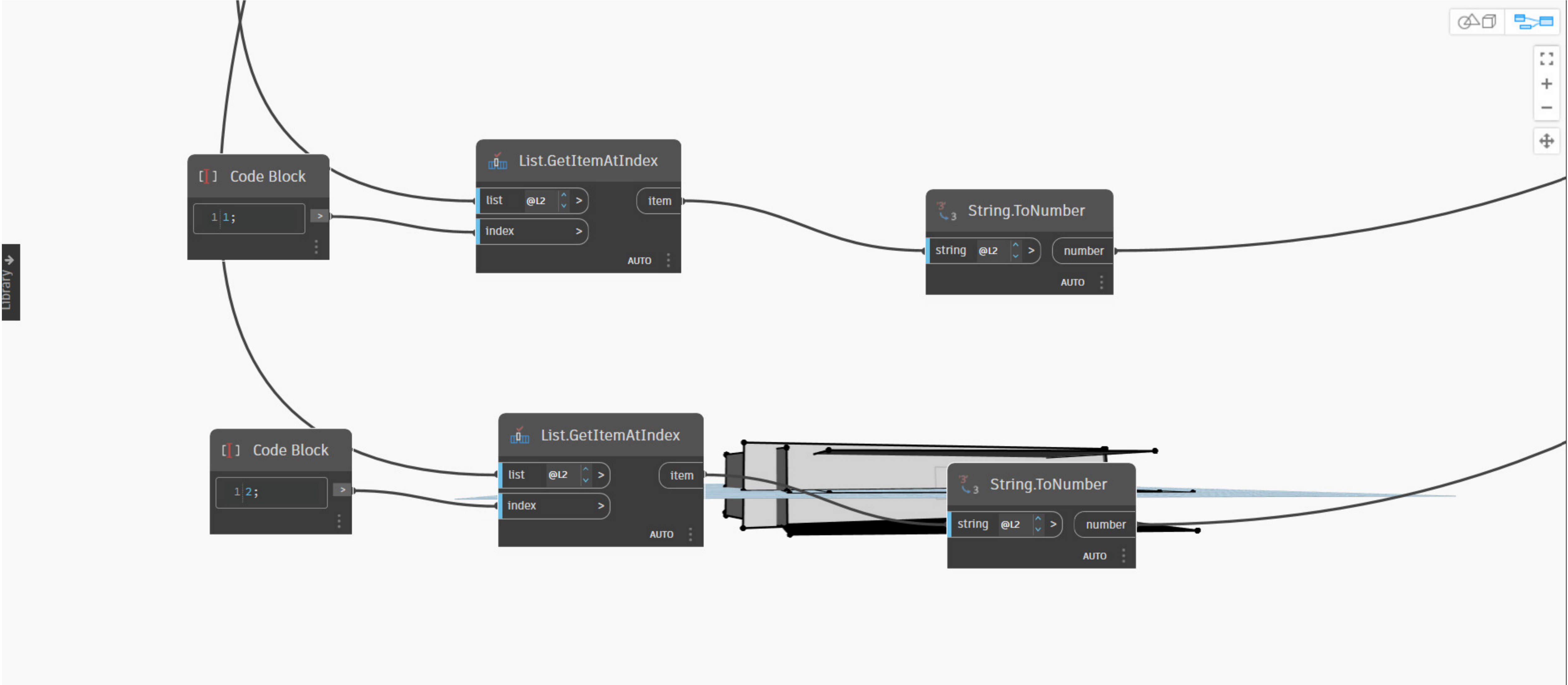
⋮

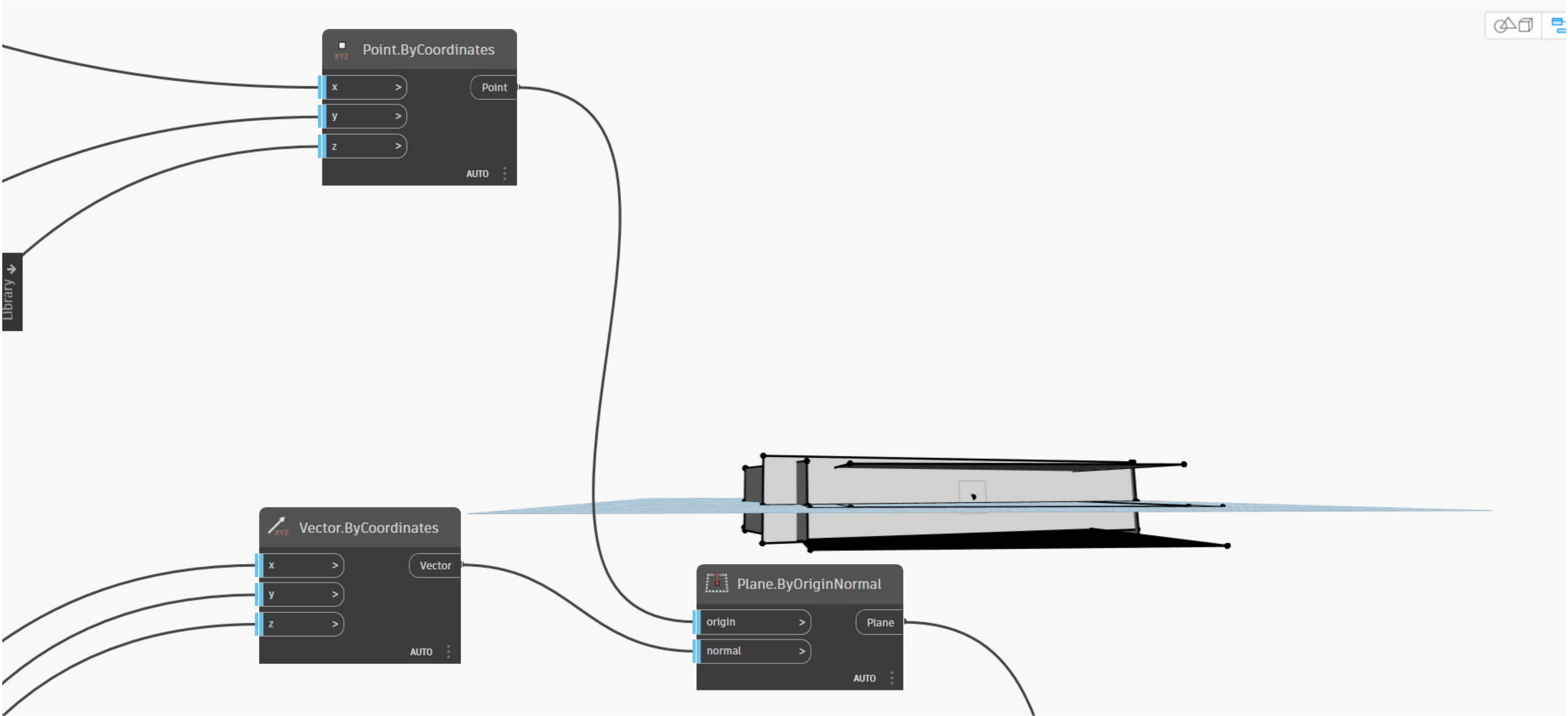




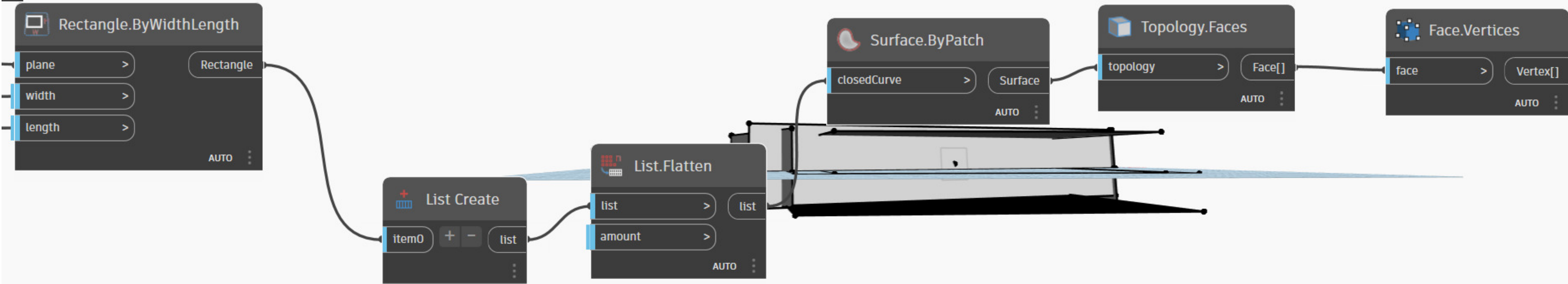
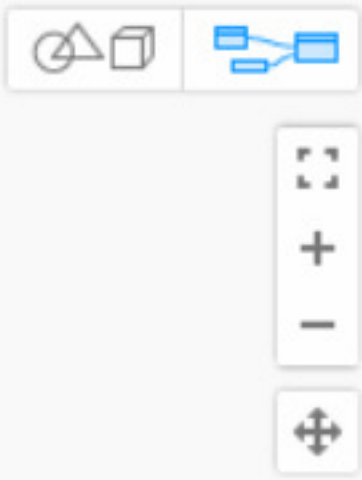




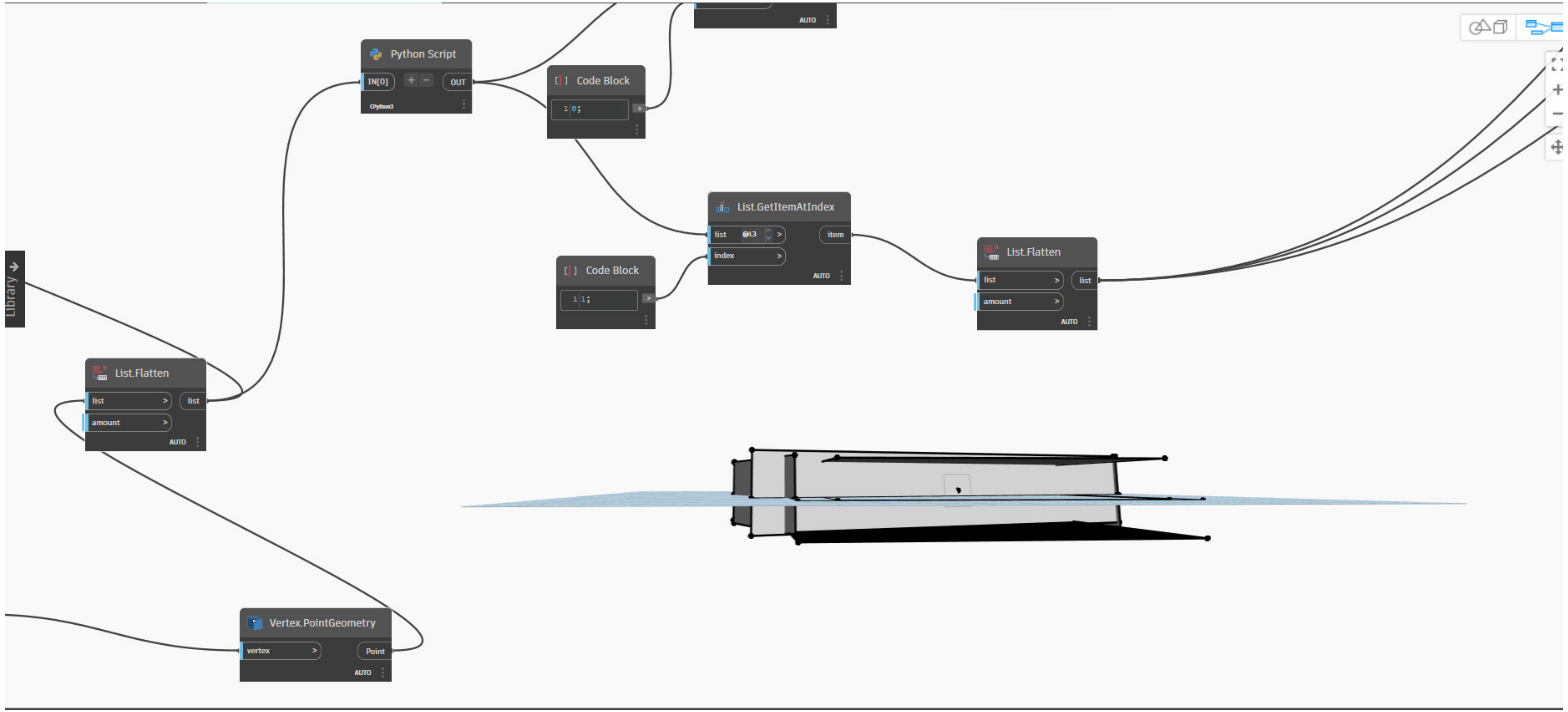




Library ↓

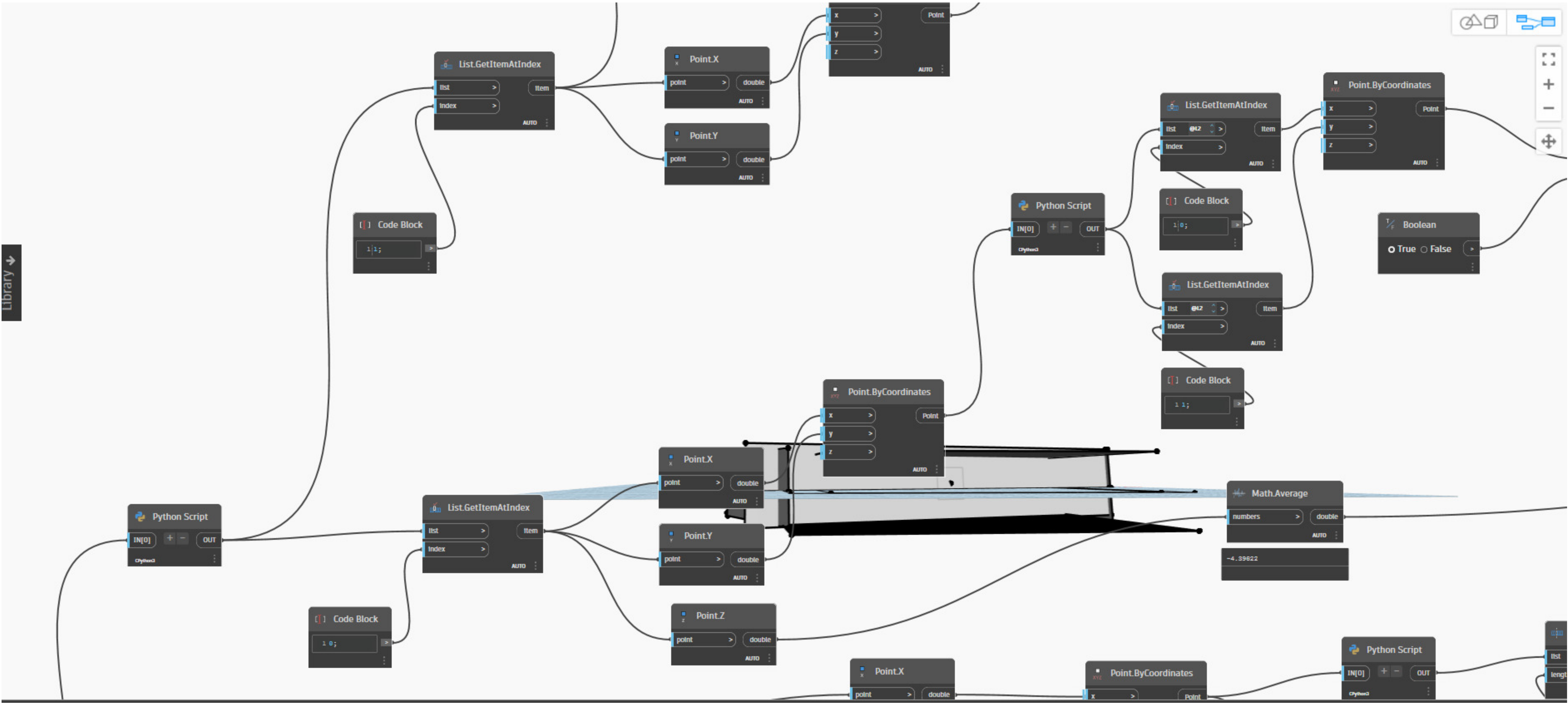






```
1 # Load the Python Standard and DesignScript Libraries
2 import sys
3 import clr
4 clr.AddReference('ProtoGeometry')
5 from Autodesk.DesignScript.Geometry import *
6 import clr
7 clr.AddReference('RevitAPI')
8 from Autodesk.Revit.DB import *
9
10 # Definir a classe Point para representar pontos com coordenadas X, Y e Z
11 class Point:
12     def __init__(self, X, Y, Z):
13         self.X = X
14         self.Y = Y
15         self.Z = Z
16
17 # Função para calcular a diferença entre o valor máximo e mínimo de Z para cada conjunto de 4 pontos
18 def calculate_z_difference(points):
19     z_differences = []
20     less_than_one_list = []
21     greater_than_one_list = []
22
23     # Iterar pelos pontos em conjuntos de 4
24     for i in range(0, len(points), 4):
25         # Extrair valores de Z para o conjunto atual de pontos
26         z_values = [point.Z for point in points[i:i+4]]
27
28         # Calcular a diferença entre os valores máximo e mínimo de Z
29         z_diff = max(z_values) - min(z_values)
30         z_differences.append(z_diff)
31
32         # Categorizar pontos com base na condição de valor de Z
33         if z_diff < 1:
34             less_than_one_list.extend(points[i:i+4])
35         else:
36             greater_than_one_list.extend(points[i:i+4])
37
38     return less_than_one_list, greater_than_one_list
39
40 # Input para a lista de pontos vinda do nó Dynamo
41 points_input = IN[0]
42
43 # Chamar a função para calcular diferenças de Z e categorizar pontos
44 less_than_one, greater_than_one = calculate_z_difference(points_input)
45
46 # Saída dos resultados (pode ser usada para criar ou modificar elementos no Revit)
47 OUT = less_than_one, greater_than_one
```







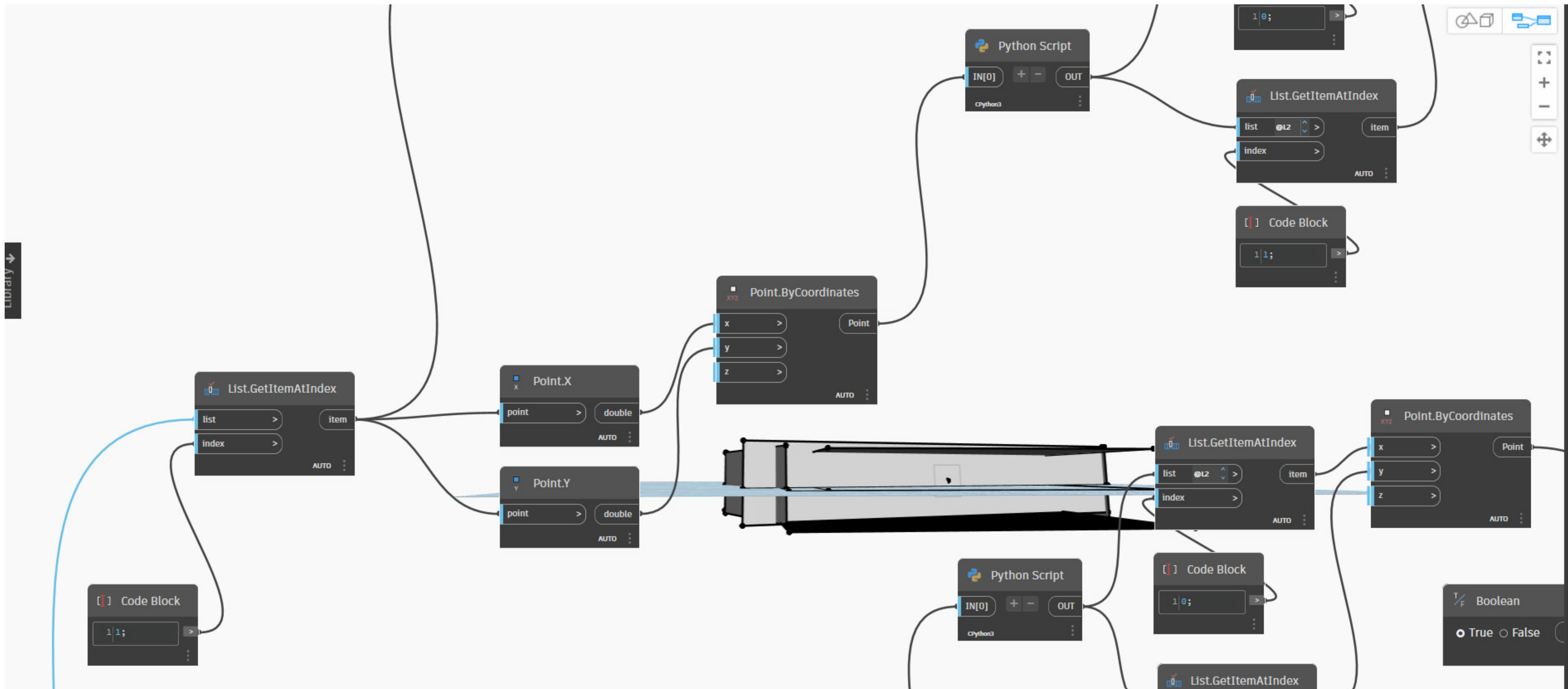
```
1 # Extrair a lista de pontos do nó Dynamo
2 points_list = IN[0]
3
4 # Ordenar a lista de pontos com base nos valores de Z
5 sorted_points = sorted(points_list, key=lambda p: p.Z)
6
7 # Separar a lista em duas partes
8 first_part = sorted_points[:4]
9 second_part = sorted_points[4:]
10
11 # Saída dos resultados
12 OUT = [first_part, second_part]
```



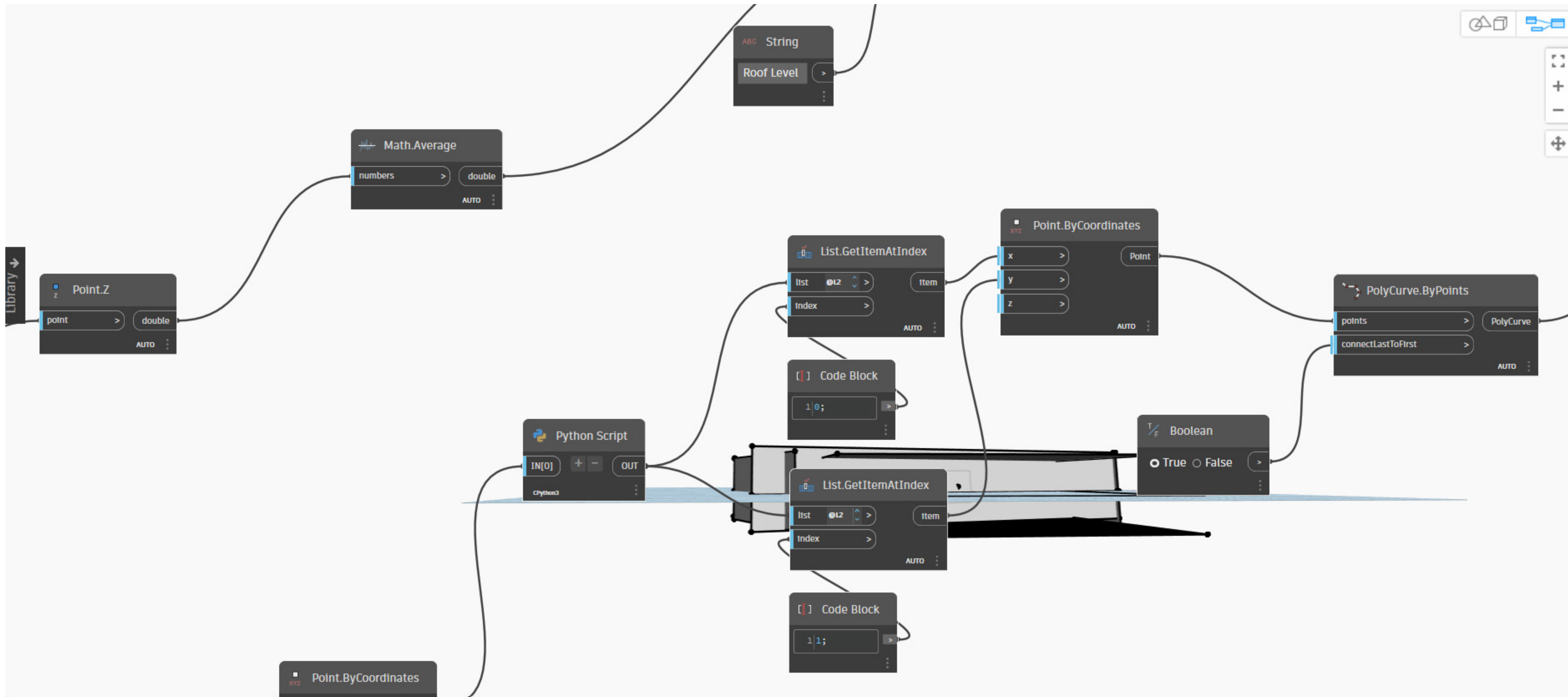
Run

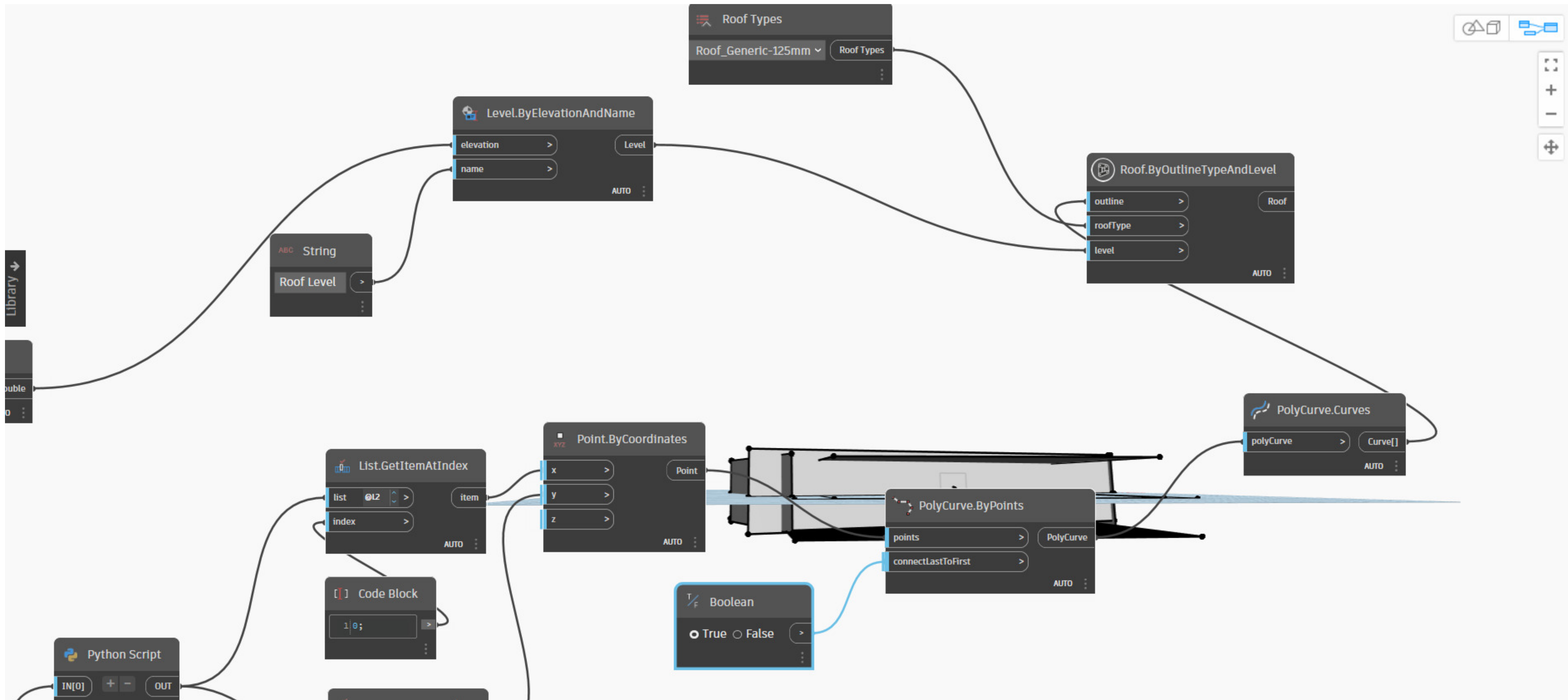
CPython3



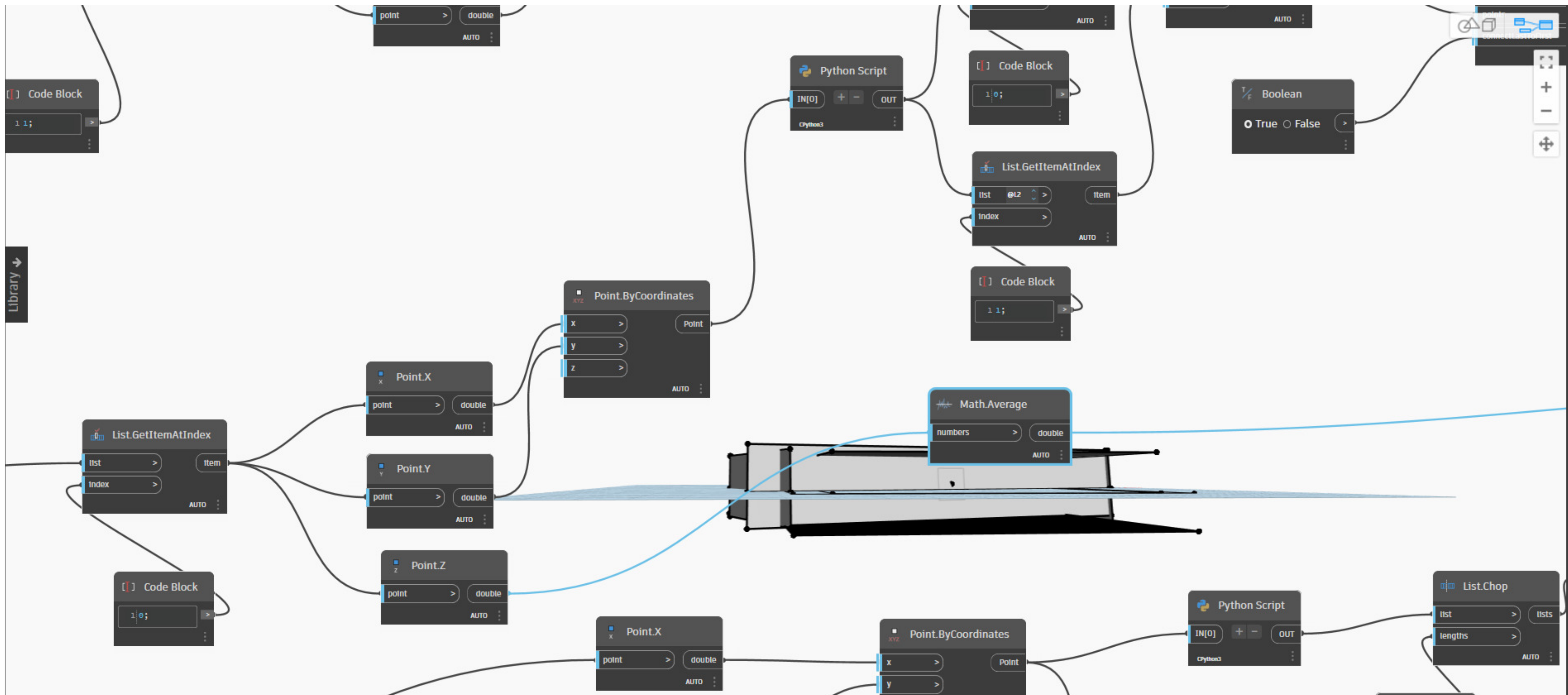
















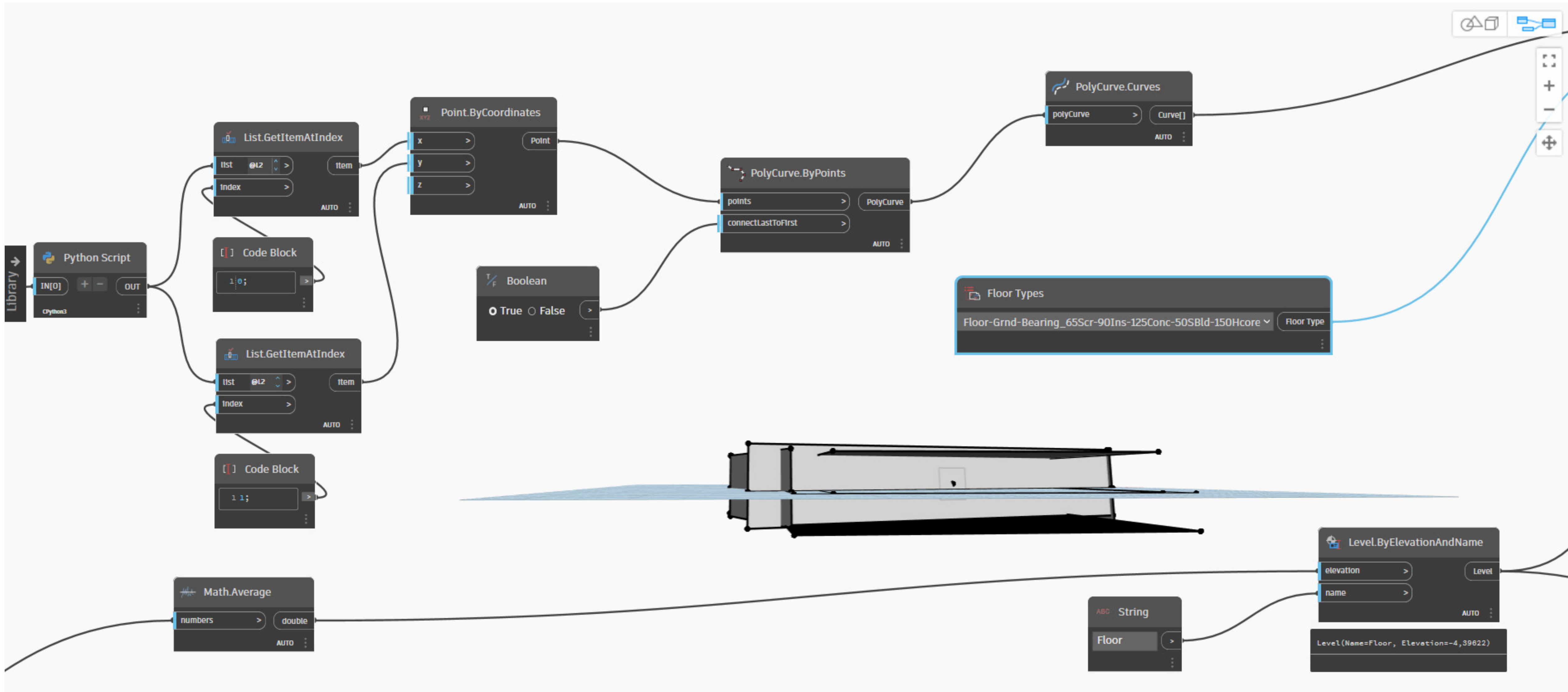
```
1 # Extrair os quatro pontos vértices do retângulo do nó Dynamo
2 rectangle_vertices = IN[0]
3
4 # Calcular o centro do retângulo
5 center_x = sum([p.X for p in rectangle_vertices]) / 4
6 center_y = sum([p.Y for p in rectangle_vertices]) / 4
7
8 # Calcular a largura e a altura do retângulo
9 width = max([p.X for p in rectangle_vertices]) - min([p.X for p in
rectangle_vertices])
10 height = max([p.Y for p in rectangle_vertices]) - min([p.Y for p in
rectangle_vertices])
11
12 # Criar pontos para formar um retângulo com base nos vértices
13 rectangle_points = [
14     [center_x - width/2, center_y - height/2],
15     [center_x + width/2, center_y - height/2],
16     [center_x + width/2, center_y + height/2],
17     [center_x - width/2, center_y + height/2],
18 ]
19
20 # Saída dos resultados (pontos do retângulo)
21 OUT = rectangle_points
```

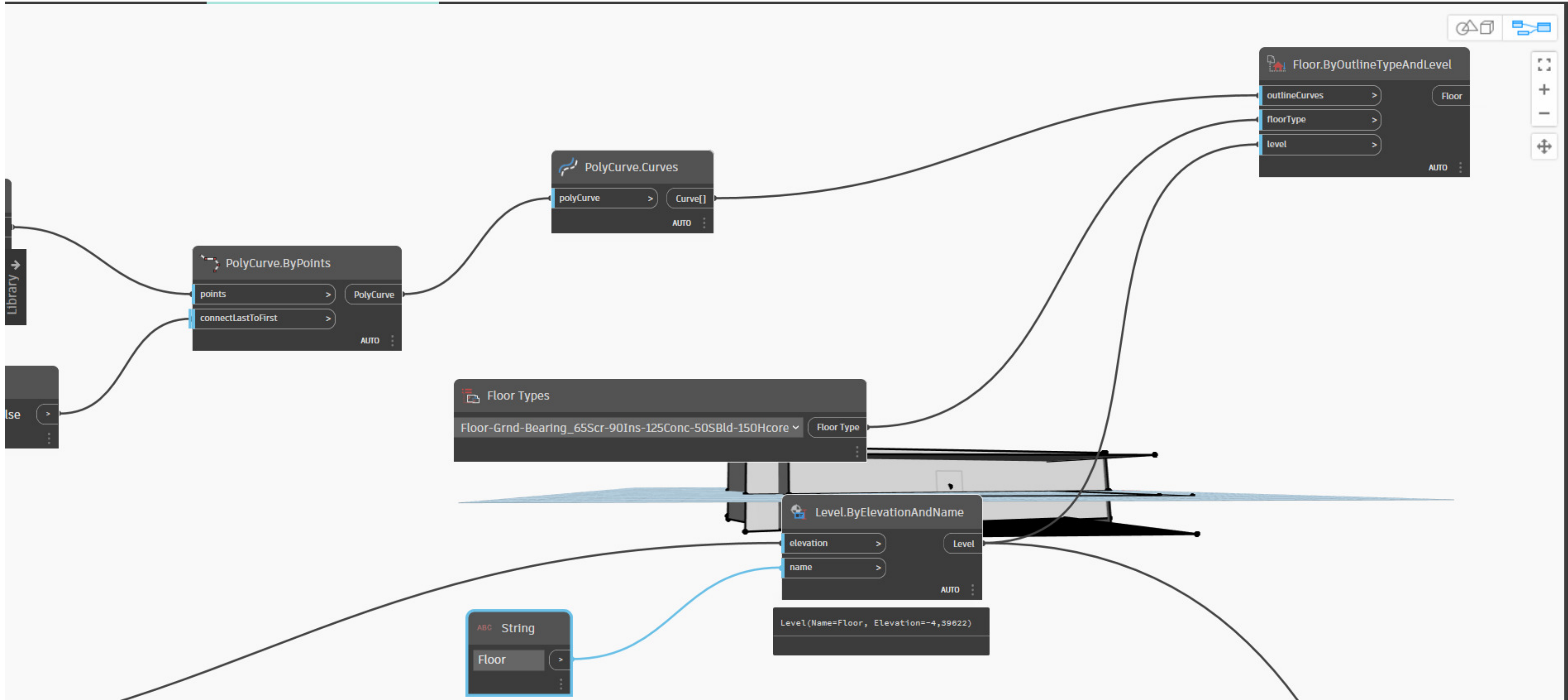


Run

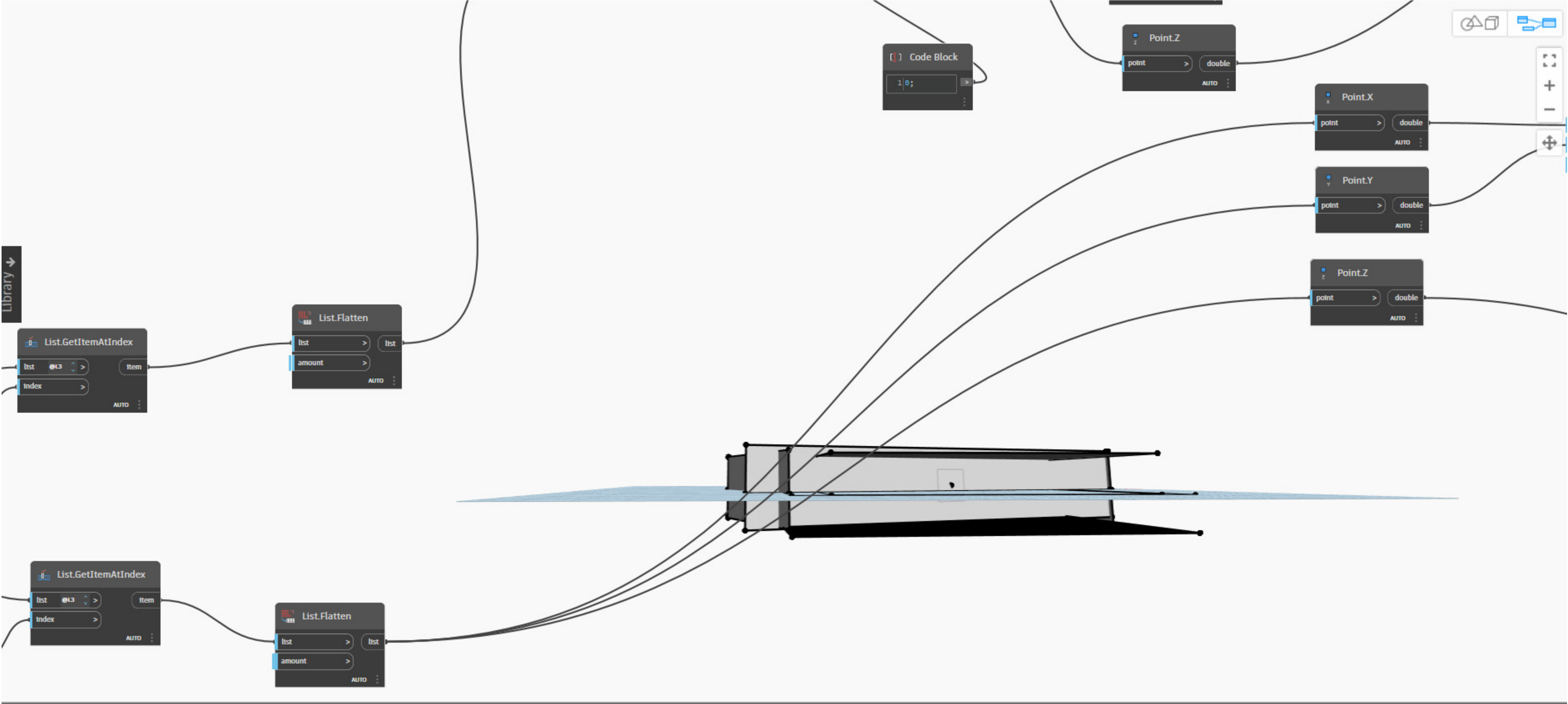
CPython3

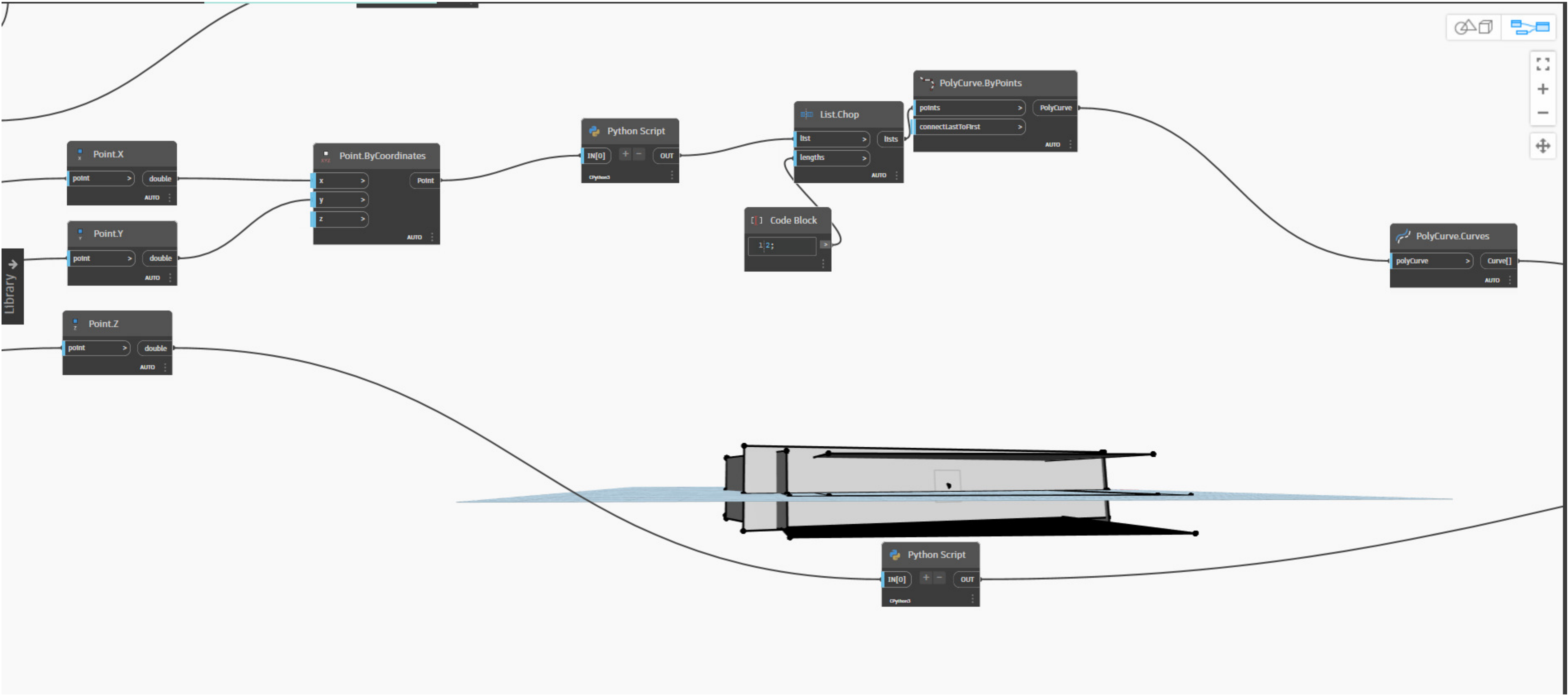












```
1 # Extrair a lista de pontos do nó Dynamo
2 points_list = IN[0]
3
4 # Função para obter apenas os dois primeiros itens a cada quatro itens da
  lista
5 def get_first_two_items(points_list):
6     result = []
7
8     # Iterar pelos elementos da lista em conjuntos de 4
9     for i in range(0, len(points_list), 4):
10         # Adicionar os dois primeiros itens de cada conjunto de 4 à lista
          de resultados
11         result.extend(points_list[i:i+2])
12
13     return result
14
15 # Chamar a função para obter apenas os dois primeiros itens a cada quatro
  itens
16 output_result = get_first_two_items(points_list)
17
18 # Saída dos resultados
19 OUT = output_result
```



Run

CPython3





```
1 # Importar namespaces necessários para Dynamo
2 import clr
3 clr.AddReference('RevitAPI')
4 from Autodesk.Revit.DB import *
5
6 # Input para a lista de valores
7 input_list = IN[0]
8
9 # Função para calcular a média dos dois valores mínimos e a média dos dois valores máximos em
  conjuntos de 4 itens,
10 # em seguida, calcula a diferença absoluta entre essas médias
11 def calculate_min_max_averages_and_absolute_difference(input_list):
12     min_averages = []
13     max_averages = []
14
15     # Iterar pelos elementos da lista em conjuntos de 4
16     for i in range(0, len(input_list), 4):
17         # Pegar os dois valores mínimos
18         min_values = sorted(input_list[i:i+4])[:2]
19         min_average = sum(min_values) / len(min_values) if min_values else 0.0
20         min_averages.append(min_average)
21
22         # Pegar os dois valores máximos
23         max_values = sorted(input_list[i:i+4], reverse=True)[:2]
24         max_average = sum(max_values) / len(max_values) if max_values else 0.0
25         max_averages.append(max_average)
26
27     # Calcular a diferença absoluta entre as médias dos dois valores mínimos e dos dois valores
  máximos
28     absolute_difference = [abs(max_avg - min_avg) for max_avg, min_avg in zip(max_averages,
  min_averages)]
29
30     return absolute_difference
31
32 # Chamar a função para calcular as médias e a diferença absoluta
33 absolute_difference_output = calculate_min_max_averages_and_absolute_difference(input_list)
34
35 # Saída dos resultados (diferença absoluta entre as médias)
36 OUT = absolute_difference_output
37
```



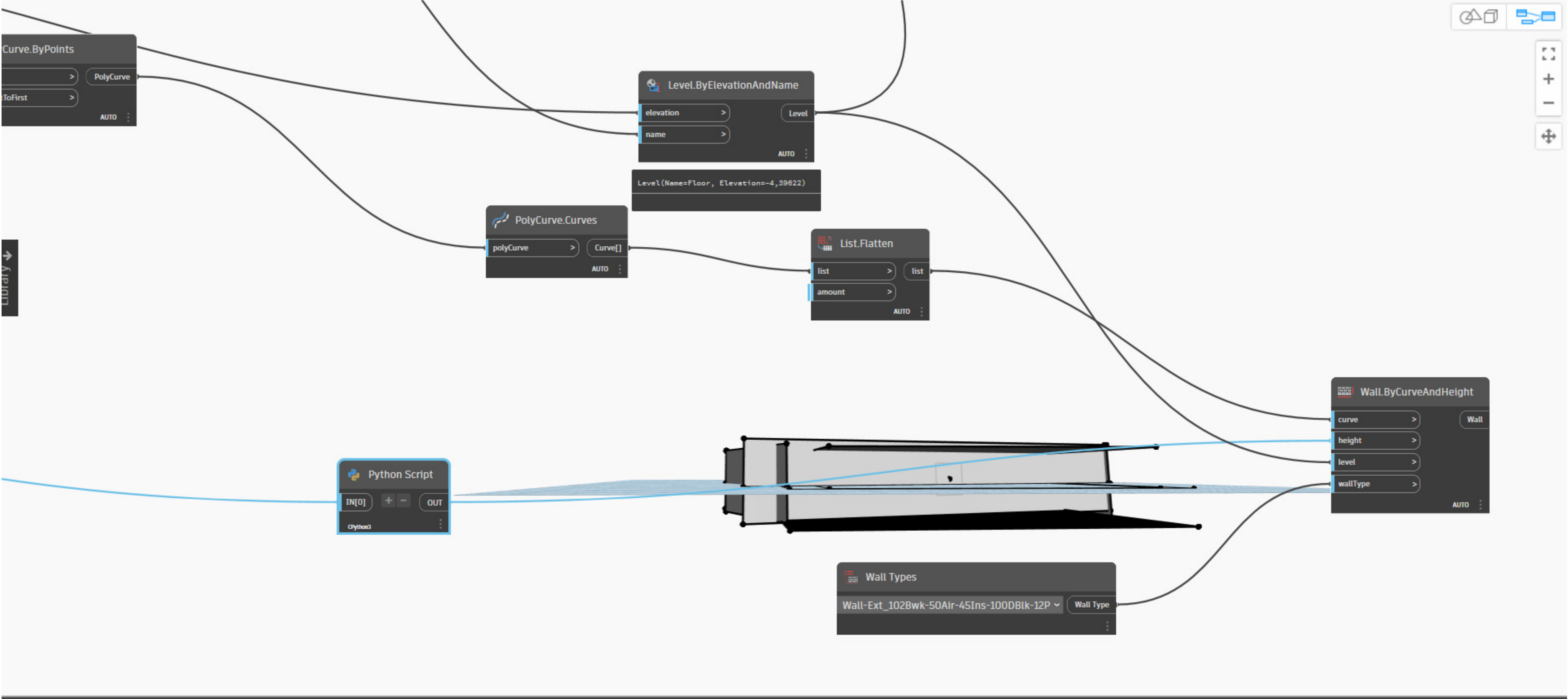
Run

CPython3



2 3









## **ANNEX B**

# Cyclone REGISTER 360

## Registration Report



### NACEX TLS CloudPoint

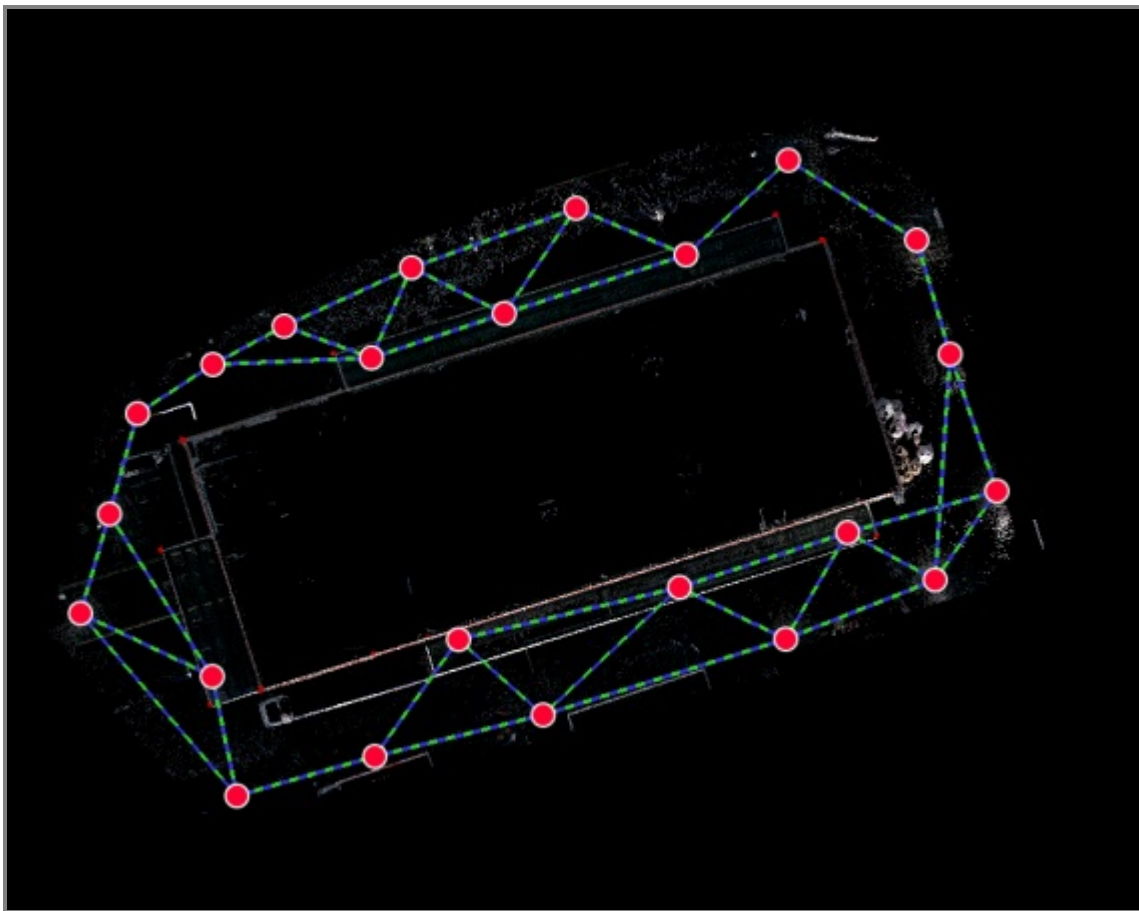
Feb 9, 2024

*Certified by:*

João Ventura, Pedro Oliveira, Ricardo Santos, Vinícius Ferreira

NACEX TLS CloudPoint

ISEP



Nacex 20231213

### Overall Quality

#### Error Results for Bundle 1

Setup Count: 23  
Link Count: 37  
  
Strength: 71 %  
Overlap: 55 %

Bundle Error  
0.007 m ✓

Overlap  
55 % ✓

Strength  
71 % ✓

0.007 m ✓

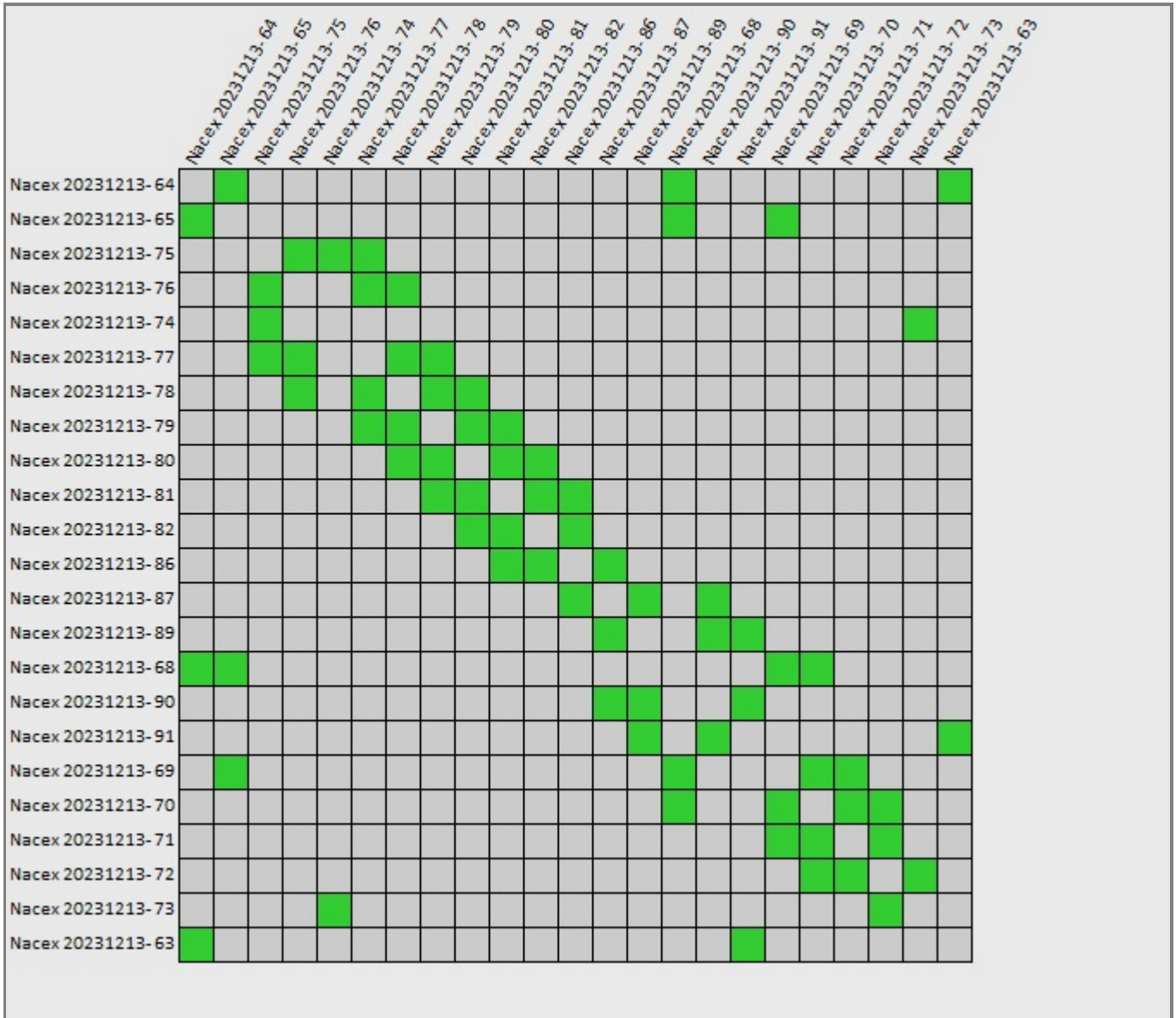
—

100

100

1

## Link-Quality Matrix #1 -



# Survey Report

Abs. Mean Error of Control to 'Bundle 1': **0.061 m**

Bundle Name	Setup	Label	Error
Bundle 1	Nacex 20231213- 65	100	0.010 m
	Nacex 20231213- 90	100	0.021 m
	Nacex 20231213- 63	100	0.061 m
	Nacex 20231213- 91	100	0.028 m
	Nacex 20231213- 64	100	0.022 m
	Nacex 20231213- 63	108	0.017 m
	Nacex 20231213- 64	108	0.019 m
	Nacex 20231213- 65	108	0.011 m
	Nacex 20231213- 81	303	0.070 m
	Nacex 20231213- 86	303	0.039 m
	Nacex 20231213- 87	303	0.045 m
	Nacex 20231213- 90	303	0.032 m
	Nacex 20231213- 63	104	0.074 m
	Nacex 20231213- 64	104	0.019 m
	Nacex 20231213- 65	104	0.025 m
	Nacex 20231213- 90	104	0.037 m
	Nacex 20231213- 91	104	0.014 m
	Nacex 20231213- 68	104	0.042 m
	Nacex 20231213- 75	203	0.124 m
	Nacex 20231213- 73	203	0.030 m
	Nacex 20231213- 74	203	0.072 m
	Nacex 20231213- 76	301	0.078 m
	Nacex 20231213- 77	301	0.070 m
	Nacex 20231213- 79	301	0.068 m
	Nacex 20231213- 73	204	0.047 m
	Nacex 20231213- 74	204	0.029 m
	Nacex 20231213- 71	204	0.115 m
	Nacex 20231213- 77	300	0.078 m
	Nacex 20231213- 78	300	0.075 m
	Nacex 20231213- 79	300	0.066 m
	Nacex 20231213- 81	304	0.191 m
	Nacex 20231213- 86	304	0.239 m

	Nacex 20231213- 87	304	0.249 m
	Nacex 20231213- 86	306	0.016 m
	Nacex 20231213- 87	306	0.011 m
	Nacex 20231213- 81	306	0.069 m
	Nacex 20231213- 82	307	0.043 m
	Nacex 20231213- 87	305	0.159 m
	Nacex 20231213- 86	305	0.189 m
	Nacex 20231213- 89	107	0.037 m
	Nacex 20231213- 90	107	0.038 m
	Nacex 20231213- 63	103	0.020 m
	Nacex 20231213- 91	103	0.019 m
	Nacex 20231213- 90	103	0.025 m
	Nacex 20231213- 63	105	0.028 m
	Nacex 20231213- 91	105	0.014 m
	Nacex 20231213- 73	202	0.069 m

# Link Error Results

## 1 Overview

Link Name	Setup 1	Setup 2	Overlap	Abs. Mean Error
Link 2	Nacex 20231213- 64	Nacex 20231213- 65	57 %	0.004 m
Link 3	Nacex 20231213- 75	Nacex 20231213- 76	59 %	0.005 m
Link 4	Nacex 20231213- 75	Nacex 20231213- 74	66 %	0.008 m
Link 5	Nacex 20231213- 76	Nacex 20231213- 77	63 %	0.012 m
Link 6	Nacex 20231213- 77	Nacex 20231213- 78	66 %	0.004 m
Link 7	Nacex 20231213- 78	Nacex 20231213- 79	66 %	0.005 m
Link 8	Nacex 20231213- 79	Nacex 20231213- 80	65 %	0.004 m
Link 9	Nacex 20231213- 80	Nacex 20231213- 81	47 %	0.005 m
Link 10	Nacex 20231213- 81	Nacex 20231213- 82	58 %	0.004 m
Link 11	Nacex 20231213- 82	Nacex 20231213- 86	37 %	0.005 m
Link 12	Nacex 20231213- 87	Nacex 20231213- 89	68 %	0.005 m
Link 13	Nacex 20231213- 65	Nacex 20231213- 68	59 %	0.009 m
Link 14	Nacex 20231213- 89	Nacex 20231213- 90	73 %	0.007 m
Link 15	Nacex 20231213- 90	Nacex 20231213- 91	74 %	0.005 m
Link 16	Nacex 20231213- 68	Nacex 20231213- 69	64 %	0.009 m
Link 17	Nacex 20231213- 69	Nacex 20231213- 70	65 %	0.012 m
Link 18	Nacex 20231213- 70	Nacex 20231213- 71	59 %	0.011 m
Link 19	Nacex 20231213- 71	Nacex 20231213- 72	62 %	0.009 m
Link 20	Nacex 20231213- 72	Nacex 20231213- 73	58 %	0.008 m
Link 21	Nacex 20231213- 73	Nacex 20231213- 74	25 %	0.004 m
Link 22	Nacex 20231213- 87	Nacex 20231213- 86	40 %	0.006 m
Link 23	Nacex 20231213- 63	Nacex 20231213- 91	49 %	0.007 m
Link 27	Nacex 20231213- 78	Nacex 20231213- 80	57 %	0.005 m
Link 29	Nacex 20231213- 87	Nacex 20231213- 90	57 %	0.005 m
Link 31	Nacex 20231213- 65	Nacex 20231213- 69	57 %	0.010 m
Link 34	Nacex 20231213- 89	Nacex 20231213- 91	50 %	0.008 m
Link 35	Nacex 20231213- 68	Nacex 20231213- 70	48 %	0.008 m
Link 36	Nacex 20231213- 69	Nacex 20231213- 71	57 %	0.011 m
Link 37	Nacex 20231213- 72	Nacex 20231213- 70	37 %	0.010 m
Link 39	Nacex 20231213- 64	Nacex 20231213- 63	51 %	0.005 m
Link 41	Nacex 20231213- 77	Nacex 20231213- 79	62 %	0.006 m
Link 42	Nacex 20231213- 81	Nacex 20231213- 86	68 %	0.006 m
Link 43	Nacex 20231213- 79	Nacex 20231213- 81	42 %	0.009 m
Link 44	Nacex 20231213- 76	Nacex 20231213- 78	51 %	0.006 m
Link 45	Nacex 20231213- 75	Nacex 20231213- 77	25 %	0.006 m
Link 47	Nacex 20231213- 68	Nacex 20231213- 64	44 %	0.007 m
Link 48	Nacex 20231213- 80	Nacex 20231213- 82	32 %	0.011 m

## 2 Details

Link Name	Setup 1	Setup 2	Overlap	Abs. Mean Error
Link 2	Nacex 20231213-64	Nacex 20231213-65	57 %	0.004 m
		Cloud to Cloud Target	Mean Target Error:	0.004 m --

Link Name	Setup 1	Setup 2	Overlap	Abs. Mean Error
Link 3	Nacex 20231213-75	Nacex 20231213-76	59 %	0.005 m
		Cloud to Cloud Target	Mean Target Error:	0.005 m --

Link Name	Setup 1	Setup 2	Overlap	Abs. Mean Error
Link 4	Nacex 20231213-75	Nacex 20231213-74	66 %	0.008 m
		Cloud to Cloud Target	Mean Target Error:	0.008 m --

Link Name	Setup 1	Setup 2	Overlap	Abs. Mean Error
Link 5	Nacex 20231213-76	Nacex 20231213-77	63 %	0.012 m
		Cloud to Cloud Target	Mean Target Error:	0.012 m --



Link Name	Setup 1	Setup 2	Overlap	Abs. Mean Error
Link 6	Nacex 20231213-77	Nacex 20231213-78	66 %	0.004 m
		Cloud to Cloud Target	Mean Target Error:	0.004 m --

Link Name	Setup 1	Setup 2	Overlap	Abs. Mean Error
Link 7	Nacex 20231213-78	Nacex 20231213-79	66 %	0.005 m
		Cloud to Cloud Target	Mean Target Error:	0.005 m --

Link Name	Setup 1	Setup 2	Overlap	Abs. Mean Error
Link 8	Nacex 20231213-79	Nacex 20231213-80	65 %	0.004 m
		Cloud to Cloud Target	Mean Target Error:	0.004 m --

Link Name	Setup 1	Setup 2	Overlap	Abs. Mean Error
Link 9	Nacex 20231213-80	Nacex 20231213-81	47 %	0.005 m
		Cloud to Cloud Target	Mean Target Error:	0.005 m --

Link Name	Setup 1	Setup 2	Overlap	Abs. Mean Error
Link 10	Nacex 20231213-81	Nacex 20231213-82	58 %	0.004 m
		Cloud to Cloud Target	Mean Target Error:	0.004 m --

Link Name	Setup 1	Setup 2	Overlap	Abs. Mean Error
Link 11	Nacex 20231213-82	Nacex 20231213-86	37 %	0.005 m
		Cloud to Cloud Target	Mean Target Error:	0.005 m --

Link Name	Setup 1	Setup 2	Overlap	Abs. Mean Error
Link 12	Nacex 20231213-87	Nacex 20231213-89	68 %	0.005 m
		Cloud to Cloud Target	Mean Target Error:	0.005 m --

Link Name	Setup 1	Setup 2	Overlap	Abs. Mean Error
Link 13	Nacex 20231213-65	Nacex 20231213-68	59 %	0.009 m
		Cloud to Cloud Target	Mean Target Error:	0.009 m --

Link Name	Setup 1	Setup 2	Overlap	Abs. Mean Error
Link 14	Nacex 20231213-89	Nacex 20231213-90	73 %	0.007 m
		Cloud to Cloud Target	Mean Target Error:	0.007 m --

Link Name	Setup 1	Setup 2	Overlap	Abs. Mean Error
Link 15	Nacex 20231213-90	Nacex 20231213-91	74 %	0.005 m
		Cloud to Cloud Target	Mean Target Error:	0.005 m --

Link Name	Setup 1	Setup 2	Overlap	Abs. Mean Error
Link 16	Nacex 20231213-68	Nacex 20231213-69	64 %	0.009 m
		Cloud to Cloud Target	Mean Target Error:	0.009 m --

Link Name	Setup 1	Setup 2	Overlap	Abs. Mean Error
Link 17	Nacex 20231213-69	Nacex 20231213-70	65 %	0.012 m
		Cloud to Cloud Target	Mean Target Error:	0.012 m --

Link Name	Setup 1	Setup 2	Overlap	Abs. Mean Error
Link 18	Nacex 20231213-70	Nacex 20231213-71	59 %	0.011 m
		Cloud to Cloud Target	Mean Target Error:	0.011 m --

Link Name	Setup 1	Setup 2	Overlap	Abs. Mean Error
Link 19	Nacex 20231213-71	Nacex 20231213-72	62 %	0.009 m
		Cloud to Cloud Target	Mean Target Error:	0.009 m --

Link Name	Setup 1	Setup 2	Overlap	Abs. Mean Error
Link 20	Nacex 20231213-72	Nacex 20231213-73	58 %	0.008 m
		Cloud to Cloud Target	Mean Target Error:	0.008 m --

Link Name	Setup 1	Setup 2	Overlap	Abs. Mean Error
Link 21	Nacex 20231213-73	Nacex 20231213-74	25 %	0.004 m
		Cloud to Cloud Target	Mean Target Error:	0.004 m --

Link Name	Setup 1	Setup 2	Overlap	Abs. Mean Error
Link 22	Nacex 20231213-87	Nacex 20231213-86	40 %	0.006 m
		Cloud to Cloud Target	Mean Target Error:	0.006 m --

Link Name	Setup 1	Setup 2	Overlap	Abs. Mean Error
Link 23	Nacex 20231213-63	Nacex 20231213-91	49 %	0.007 m
		Cloud to Cloud Target	Mean Target Error:	0.007 m --

Link Name	Setup 1	Setup 2	Overlap	Abs. Mean Error
Link 27	Nacex 20231213-78	Nacex 20231213-80	57 %	0.005 m
		Cloud to Cloud Target	Mean Target Error:	0.005 m --

Link Name	Setup 1	Setup 2	Overlap	Abs. Mean Error
Link 29	Nacex 20231213-87	Nacex 20231213-90	57 %	0.005 m
		Cloud to Cloud Target	Mean Target Error:	0.005 m --

Link Name	Setup 1	Setup 2	Overlap	Abs. Mean Error
Link 31	Nacex 20231213-65	Nacex 20231213-69	57 %	0.010 m
		Cloud to Cloud		0.010 m
		Target	Mean Target Error:	--

Link Name	Setup 1	Setup 2	Overlap	Abs. Mean Error
Link 34	Nacex 20231213-89	Nacex 20231213-91	50 %	0.008 m
		Cloud to Cloud		0.008 m
		Target	Mean Target Error:	--

Link Name	Setup 1	Setup 2	Overlap	Abs. Mean Error
Link 35	Nacex 20231213-68	Nacex 20231213-70	48 %	0.008 m
		Cloud to Cloud		0.008 m
		Target	Mean Target Error:	--

Link Name	Setup 1	Setup 2	Overlap	Abs. Mean Error
Link 36	Nacex 20231213-69	Nacex 20231213-71	57 %	0.011 m
		Cloud to Cloud		0.011 m
		Target	Mean Target Error:	--

Link Name	Setup 1	Setup 2	Overlap	Abs. Mean Error
Link 37	Nacex 20231213-72	Nacex 20231213-70	37 %	0.010 m
		Cloud to Cloud		0.010 m
		Target	Mean Target Error:	--

Link Name	Setup 1	Setup 2	Overlap	Abs. Mean Error
Link 39	Nacex 20231213-64	Nacex 20231213-63	51 %	0.005 m
		Cloud to Cloud		0.005 m
		Target	Mean Target Error:	--

Link Name	Setup 1	Setup 2	Overlap	Abs. Mean Error
Link 41	Nacex 20231213-77	Nacex 20231213-79	62 %	0.006 m
		Cloud to Cloud		0.006 m
		Target	Mean Target Error:	--

Link Name	Setup 1	Setup 2	Overlap	Abs. Mean Error
Link 42	Nacex 20231213-81	Nacex 20231213-86	68 %	0.006 m
		Cloud to Cloud		0.006 m
		Target	Mean Target Error:	--

Link Name	Setup 1	Setup 2	Overlap	Abs. Mean Error
Link 43	Nacex 20231213-79	Nacex 20231213-81	42 %	0.009 m
		Cloud to Cloud Target	Mean Target Error:	0.009 m --

Link Name	Setup 1	Setup 2	Overlap	Abs. Mean Error
Link 44	Nacex 20231213-76	Nacex 20231213-78	51 %	0.006 m
		Cloud to Cloud Target	Mean Target Error:	0.006 m --

Link Name	Setup 1	Setup 2	Overlap	Abs. Mean Error
Link 45	Nacex 20231213-75	Nacex 20231213-77	25 %	0.006 m
		Cloud to Cloud Target	Mean Target Error:	0.006 m --

Link Name	Setup 1	Setup 2	Overlap	Abs. Mean Error
Link 47	Nacex 20231213-68	Nacex 20231213-64	44 %	0.007 m
		Cloud to Cloud Target	Mean Target Error:	0.007 m --



Link Name	Setup 1	Setup 2	Overlap	Abs. Mean Error
Link 48	Nacex 20231213-80	Nacex 20231213-82	32 %	0.011 m
		Cloud to Cloud		0.011 m
		Target	Mean Target Error:	--



Nacex 20231213-3



ProjectIcon



## **ANNEX C**

Contents

[Project Summary](#)  
[Camera Calibration](#)  
[Photo Positions](#)  
[Photo Matching](#)  
[Surveys](#)  
[Control Points](#)  
[User Tie Points](#)

For more information, please see our [online manual](#).

Project Summary

Project:	DIPRE - NACEX - VF_backup
Number of photos:	1855
Ground coverage:	28158.9 square meters
Average ground resolution:	3.50224 mm/pixel
Scale:	1 : 11
Camera model(s):	DJI M3M, DJI MAVIC2-ENTERPRISE-ADVANCED
Processing date:	3/24/2024 6:17 PM
Processing time:	5h 26min

Quality Overview

Dataset:	1575 of 1855 photos calibrated (85%)
Keypoints:	Median of 11457 keypoints per image
Tie points:	306199 points, with a median of 841 points per photo.
Reprojection error (RMS):	1.14 pixels
Positioning / scaling:	Georeferenced using point clouds, not using control point

Camera Calibration

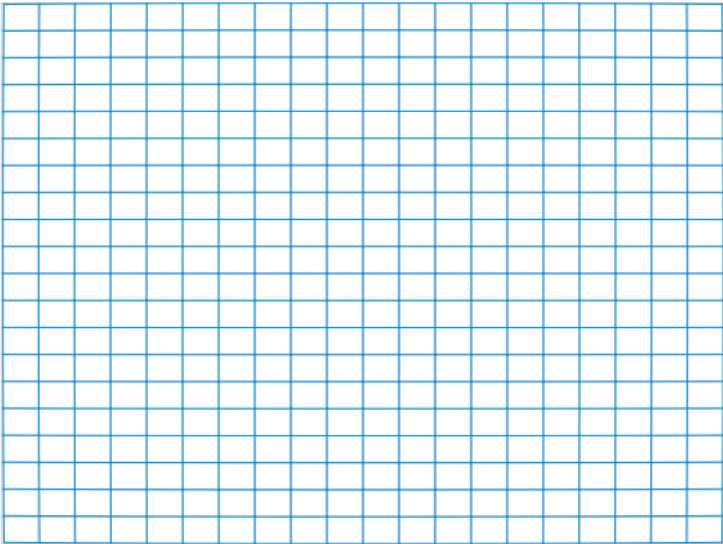
DJI MAVIC2-ENTERPRISE-ADVANCED 4.5mm 8000x6000

Name:	DJI MAVIC2-ENTERPRISE-ADVANCED
Model type:	Perspective
Image dimensions:	8000x6000 pixels
Sensor size:	6.4 mm
Number of photos:	547

Calibration Results

	Focal Length [mm]	Focal Length Equivalent 35 mm [mm]	Principal Point X [pixels]	Principal Point Y [pixels]	K1	K2	K3	P1	P2
Previous Values	4.99698	28.108	3926.75	2974.82	-0.012517	0.0217949	-0.0427171	-0.000250741	0.00042248
Optimized Values	4.7545	26.7441	3984.70	2985.45	-0.000509332	-0.0181153	0.0045242	7.34701e-05	-0.000193
Difference Previous / Optimized	-0.24248	-1.3639	57.95	10.63	0.0120077	-0.0399102	0.0472413	0.000324211	-0.00061548

Distortion Grid



Camera Lens Distortion: Gray lines represent the zero distortion grid, and blue lines represent the real camera values.

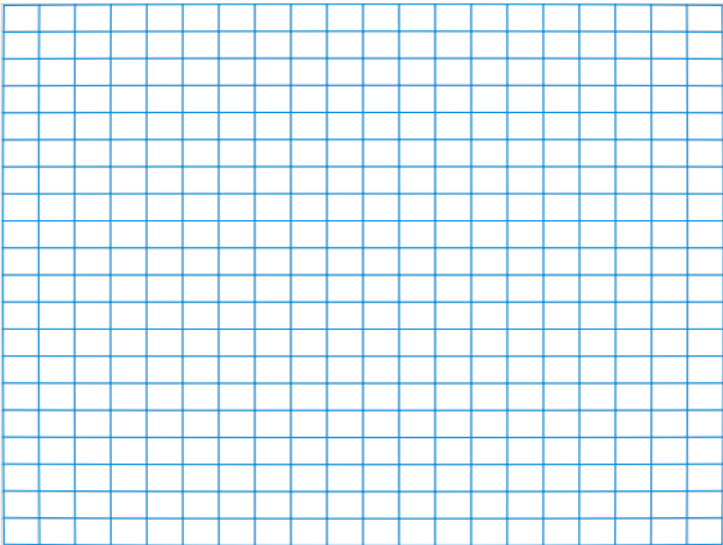
DJI MAVIC2-ENTERPRISE-ADVANCED 4.5mm 8000x6000

Name:	DJI MAVIC2-ENTERPRISE-ADVANCED
Model type:	Perspective
Image dimensions:	8000x6000 pixels
Sensor size:	6.4 mm
Number of photos:	728

Calibration Results

	Focal Length [mm]	Focal Length Equivalent 35 mm [mm]	Principal Point X [pixels]	Principal Point Y [pixels]	K1	K2	K3	P1	P2
Previous Values	4.99698	28.108	3926.75	2974.82	-0.012517	0.0217949	-0.0427171	-0.000250741	0.00042248
Optimized Values	4.7481	26.7081	3982.18	2987.98	-0.00100058	-0.0157486	0.00217666	0.000165954	-0.000153369
Difference Previous / Optimized	-0.24888	-1.3999	55.43	13.16	0.0115164	-0.0375435	0.0448938	0.000416695	-0.000575849

Distortion Grid



Camera Lens Distortion: Gray lines represent the zero distortion grid, and blue lines represent the real camera values.

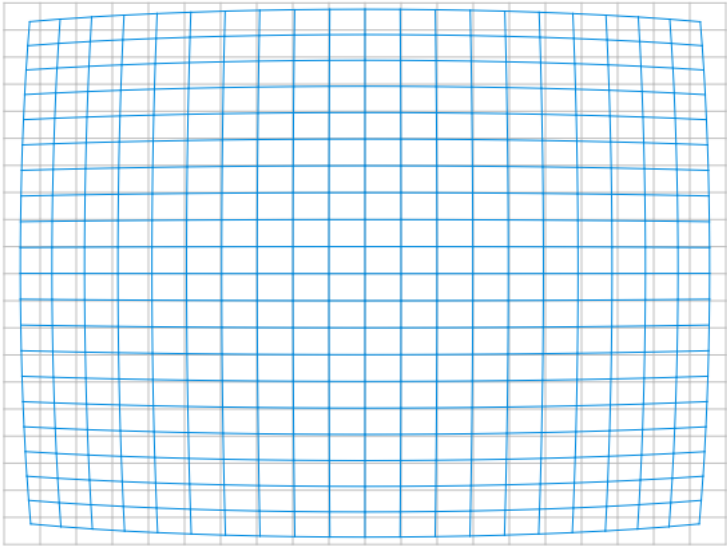
DJI M3M 12.29mm 5280x3956

Name:	DJI M3M
Model type:	Perspective
Image dimensions:	5280x3956 pixels
Sensor size:	18 mm
Number of photos:	184

Calibration Results

	Focal Length [mm]	Focal Length Equivalent 35 mm [mm]	Principal Point X [pixels]	Principal Point Y [pixels]	K1	K2	K3	P1	P2
Previous Values	12.6589	25.3179	2646.52	1968.78	-0.112575	0.0148744	-0.0270641	-8.572e-05	1e-07
Optimized Values	12.6277	25.2554	2641.84	1951.19	-0.110713	0.0147229	-0.0276113	-7.15084e-05	-0.00047157
Difference Previous / Optimized	-0.0312	-0.0625	-4.68	-17.59	0.001862	-0.0001515	-0.0005472	1.42116e-05	-0.00047167

Distortion Grid



Camera Lens Distortion: Gray lines represent the zero distortion grid, and blue lines represent the real camera values.

DJI M3M 12.29mm 5280x3956

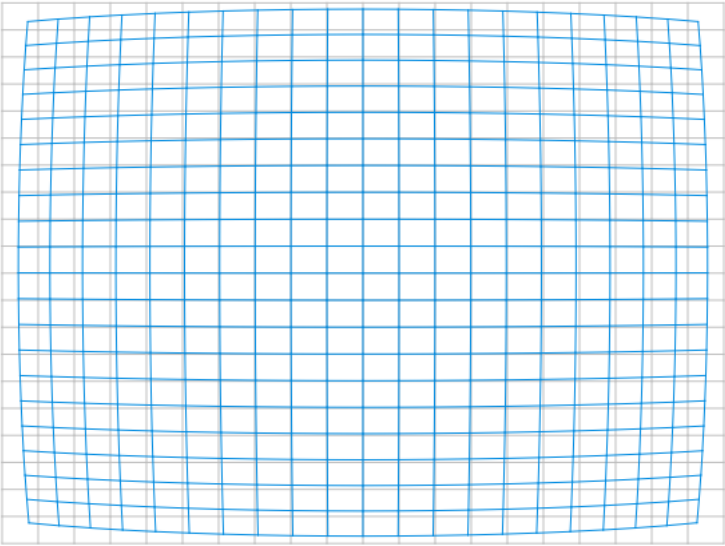
Name:	DJI M3M
Model type:	Perspective
Image dimensions:	5280x3956 pixels
Sensor size:	18 mm
Number of photos:	144

Calibration Results

	Focal Length [mm]	Focal Length Equivalent 35 mm [mm]	Principal Point X [pixels]	Principal Point Y [pixels]	K1	K2	K3	P1	P2
Previous Values	12.6589	25.3179	2646.52	1968.78	-0.112575	0.0148744	-0.0270641	-8.572e-05	1e-07
Optimized Values	12.6616	25.3232	2640.45	1949.39	-0.109997	0.00937542	-0.0239735	-6.81566e-05	-0.000541984
Difference Previous / Optimized	0.0027	0.0053	-6.07	-19.39	0.002578	-0.00549898	0.0030906	1.75634e-05	-0.000542084

Distortion Grid





Camera Lens Distortion: Gray lines represent the zero distortion grid, and blue lines represent the real camera values.

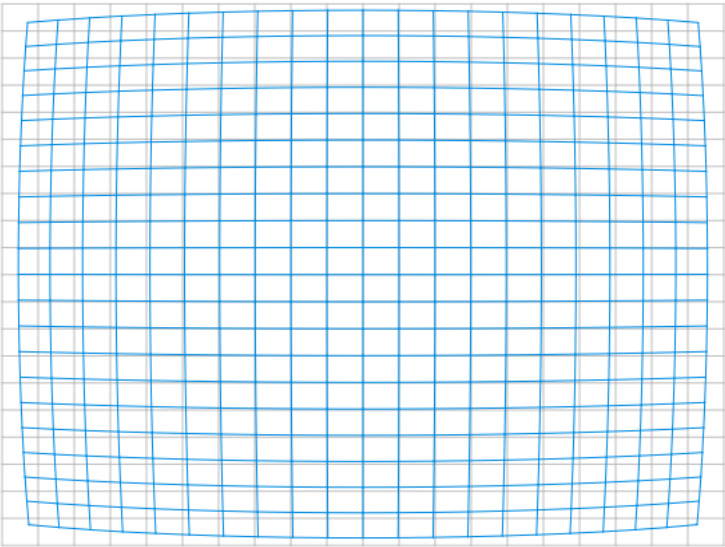
DJI M3M 12.29mm 5280x3956

Name:	DJI M3M
Model type:	Perspective
Image dimensions:	5280x3956 pixels
Sensor size:	18 mm
Number of photos:	110

Calibration Results

	Focal Length [mm]	Focal Length Equivalent 35 mm [mm]	Principal Point X [pixels]	Principal Point Y [pixels]	K1	K2	K3	P1	P2
Previous Values	12.6589	25.3179	2646.52	1968.78	-0.112575	0.0148744	-0.0270641	-8.572e-05	1e-07
Optimized Values	12.6553	25.3107	2641.17	1951.57	-0.113371	0.0190626	-0.0301729	-0.000138354	-0.000756097
Difference Previous / Optimized	-0.0036	-0.0072	-5.35	-17.21	-0.000796	0.0041882	-0.0031088	-5.2634e-05	-0.000756197

Distortion Grid



Camera Lens Distortion: Gray lines represent the zero distortion grid, and blue lines represent the real camera values.

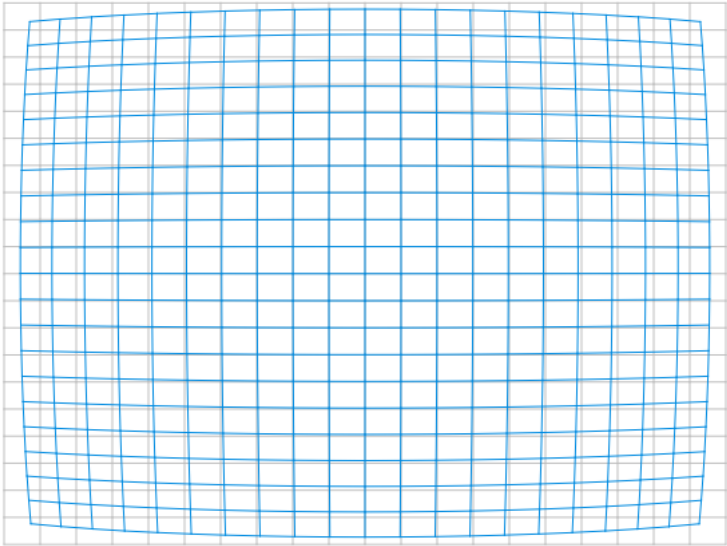
DJI M3M 12.29mm 5280x3956

Name:	DJI M3M
Model type:	Perspective
Image dimensions:	5280x3956 pixels
Sensor size:	18 mm
Number of photos:	67

Calibration Results

	Focal Length [mm]	Focal Length Equivalent 35 mm [mm]	Principal Point X [pixels]	Principal Point Y [pixels]	K1	K2	K3	P1	P2
Previous Values	12.6589	25.3179	2646.52	1968.78	-0.112575	0.0148744	-0.0270641	-8.572e-05	1e-07
Optimized Values	12.6521	25.3042	2644.48	1950.10	-0.109491	0.00939998	-0.0235374	-7.44037e-05	-0.000572976
Difference Previous / Optimized	-0.0068	-0.0137	-2.04	-18.68	0.003084	-0.00547442	0.0035267	1.13163e-05	-0.000573076

Distortion Grid



Camera Lens Distortion: Gray lines represent the zero distortion grid, and blue lines represent the real camera values.

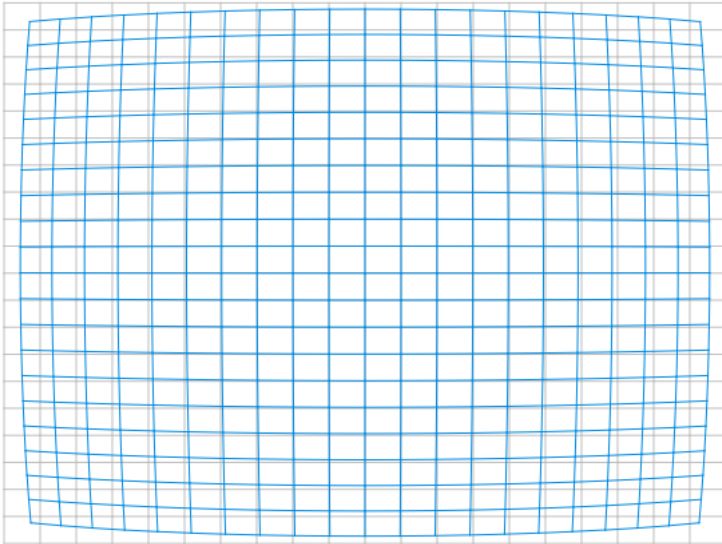
DJI M3M 12.29mm 5280x3956

Name:	DJI M3M
Model type:	Perspective
Image dimensions:	5280x3956 pixels
Sensor size:	18 mm
Number of photos:	75

Calibration Results

	Focal Length [mm]	Focal Length Equivalent 35 mm [mm]	Principal Point X [pixels]	Principal Point Y [pixels]	K1	K2	K3	P1	P2
Previous Values	12.6589	25.3179	2646.52	1968.78	-0.112575	0.0148744	-0.0270641	-8.572e-05	1e-07
Optimized Values	12.6341	25.2682	2640.20	1950.03	-0.109703	0.0108546	-0.0250377	-1.44474e-06	-0.000528194
Difference Previous / Optimized	-0.0248	-0.0497	-6.32	-18.75	0.002872	-0.0040198	0.0020264	8.42753e-05	-0.000528294

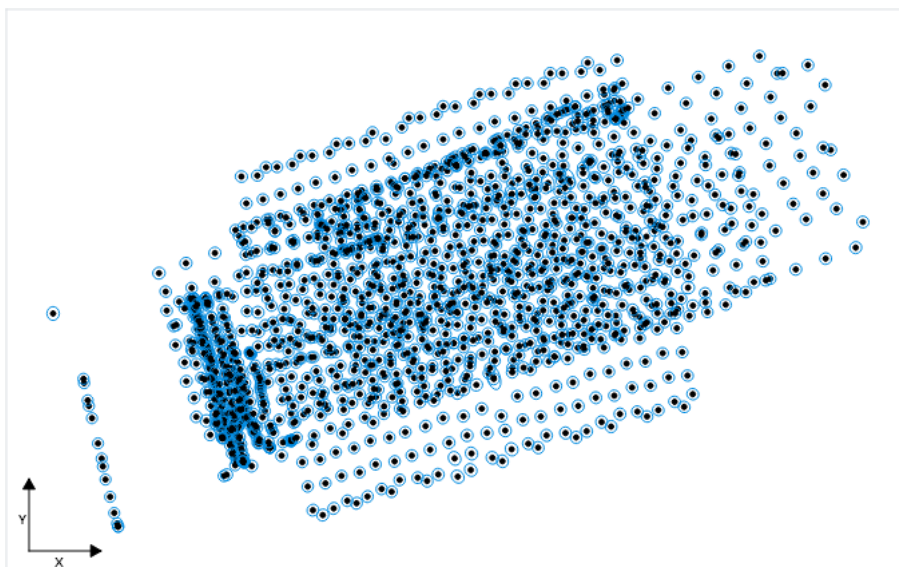
Distortion Grid

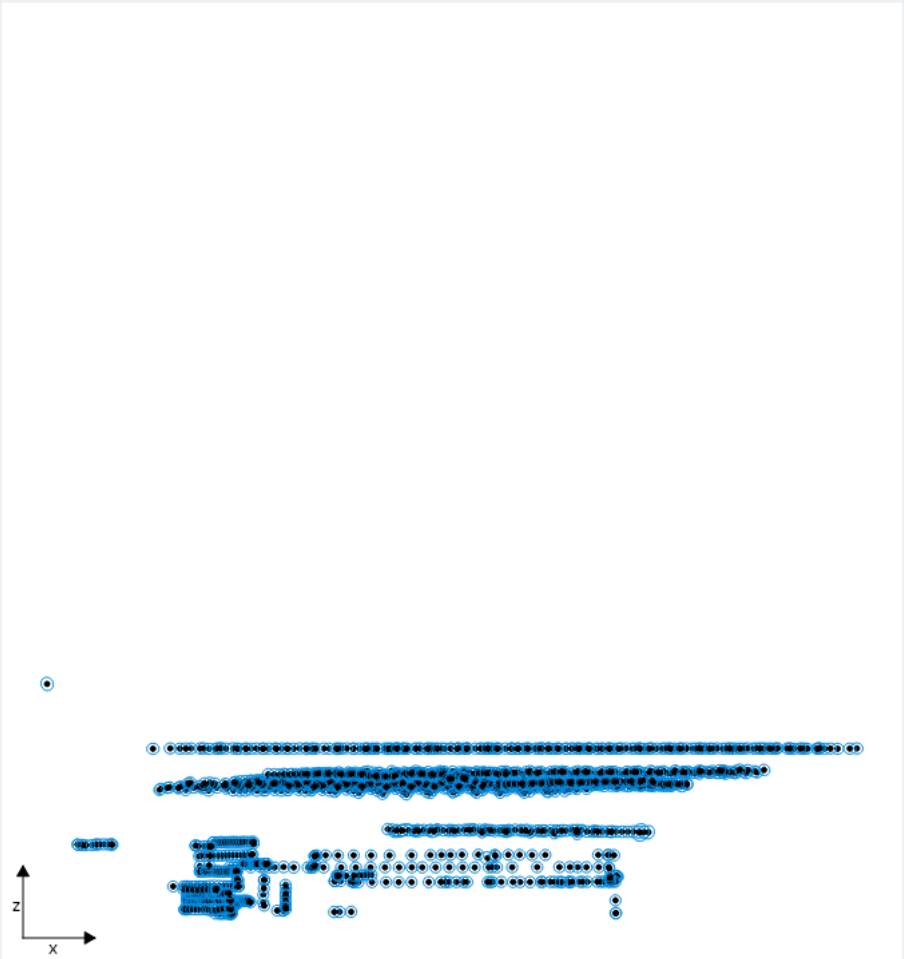


**Camera Lens Distortion:** *Gray lines represent the zero distortion grid, and blue lines represent the real camera values.*

## Photo Positions

### Photo Position Uncertainties



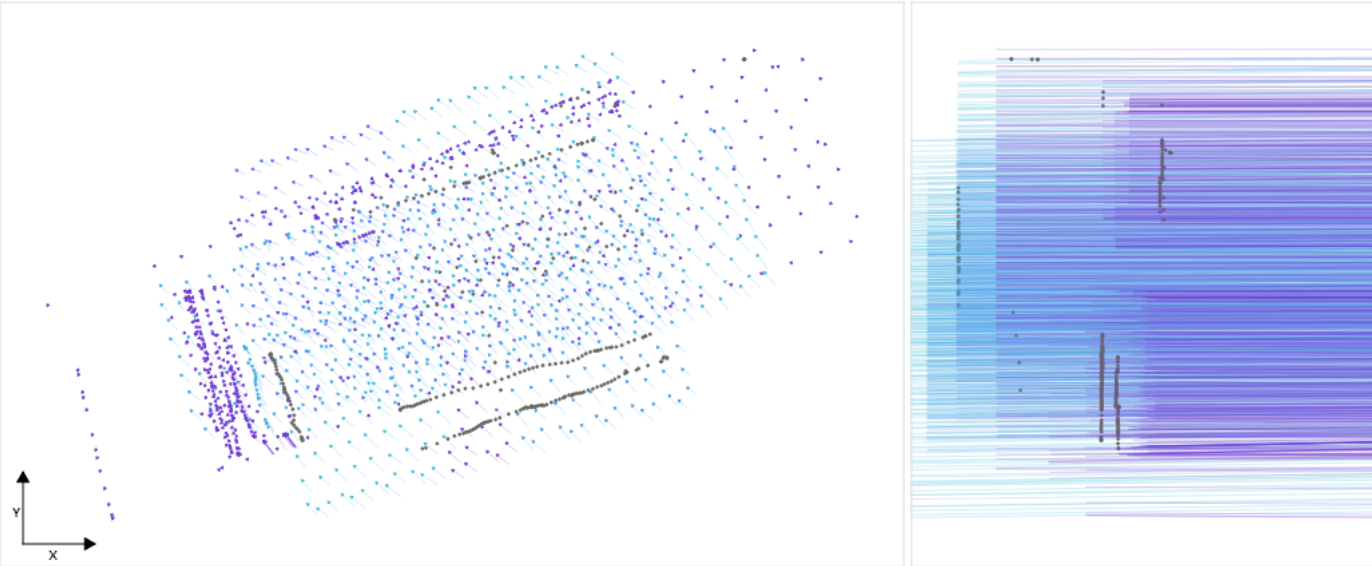


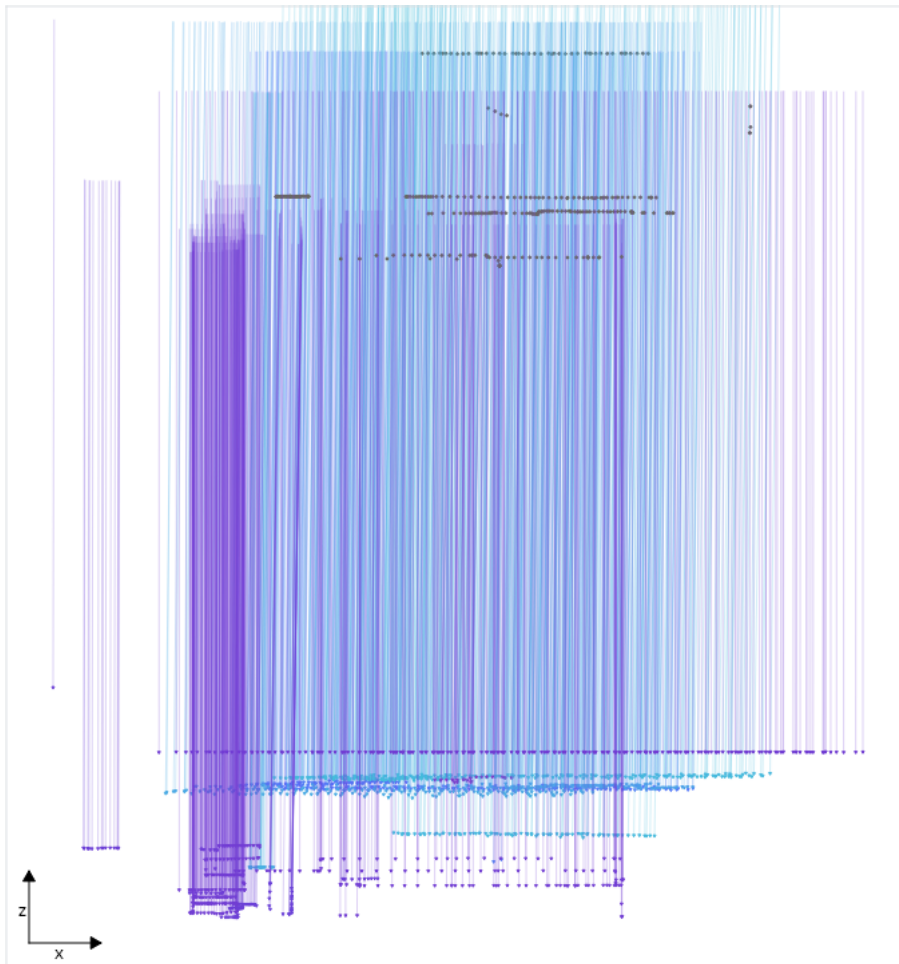
**Position Uncertainties:** Top view (XY plane), side view (ZY plane) and front view (XZ plane) of computed photo positions (black dots). Blue ellipses indicate the position uncertainty, scaled for readability. The minimum and maximum values, as well as the average value, can be found in the table below.

Position Uncertainties			
	X [meters]	Y [meters]	Z [meters]
Minimum	0.00005	0.00004	0.00006
Mean	0.00081	0.00088	0.00061
Maximum	0.01791	0.05522	0.00938

For more information on individual photos, please refer to the [Photos Report](#).

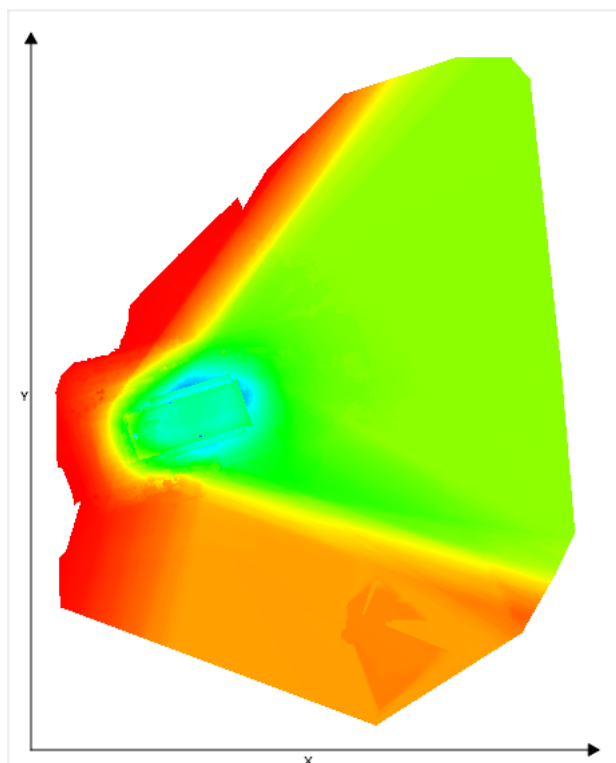
Distance to Input Positions

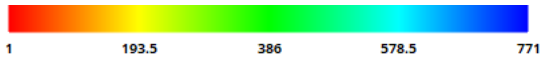




**Position Distance to Metadata:** Top view (XY plane), side view (ZY plane) and front view (XZ plane), with arrows indicating the offset between the metadata positions and the computed photo positions; all arrows start from the metadata positions and point toward the computed positions. Gray points • indicate uncalibrated photos that have metadata. Pink points • indicate calibrated photos that have no metadata. The values are in meters, with a minimum distance of 106.3296 meters and a maximum of 132.09758 meters. The median position distance equals 123.55983 meters.

## Scene Coverage





Number of photos seeing the scene: Top view (XY plane) display of the scene, with colors indicating the **number of photos** that potentially see each area.

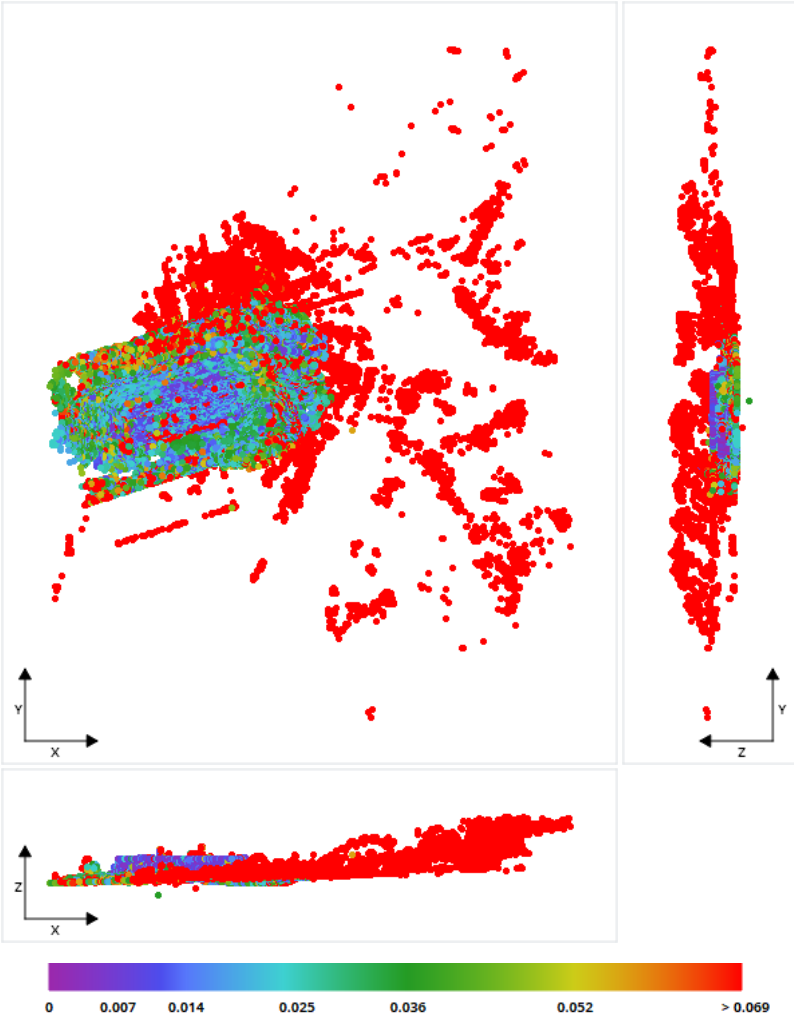
Photo Matching

Quality Measures on Tie Points

Generated Tie Points					
Number of Points	Median Number of Photos per Point	Median Number of Points per Photo	Median Reprojection Error [pixels]	RMS of Reprojection Error [pixels]	RMS of Distances to Rays [meters]
306199	4	841	0.73	1.14	0.01197

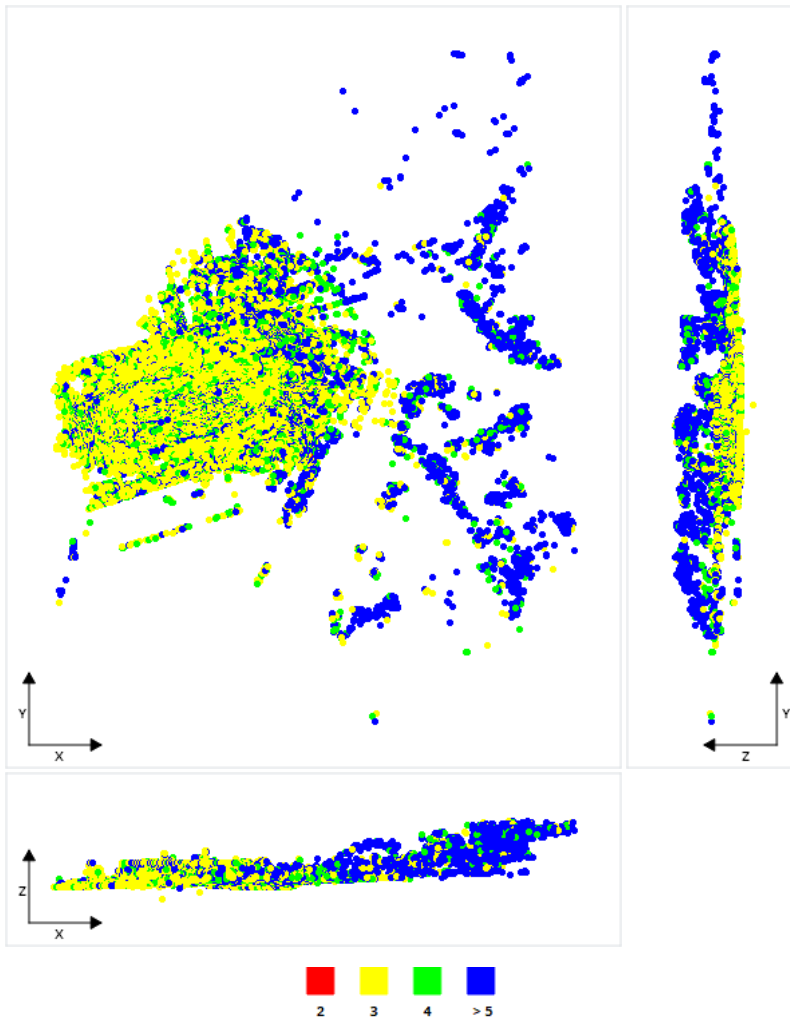
For more information on individual photos, please refer to the [Photos Report](#).

Tie Point Position Uncertainties



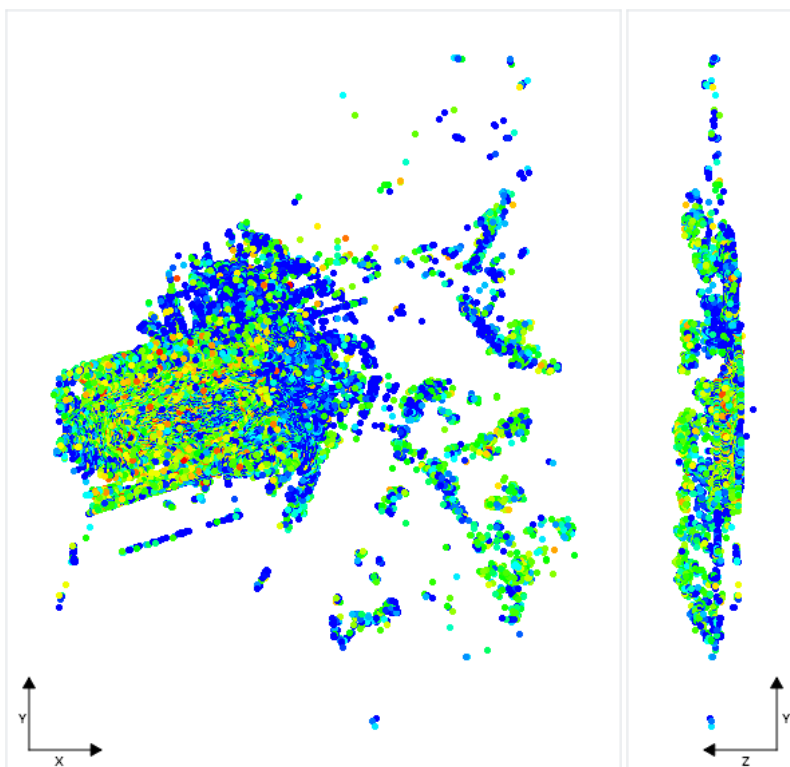
**Position Uncertainties:** Top view (XY plane), side view (ZY plane) and front view (XZ plane) displays of all tie points, with colors representing uncertainty in the individual point position. The values are in meters, with a minimum uncertainty of **0.00044 meters** and a maximum of **3.0877 meters**. The median position uncertainty equals **0.01357 meters**.

Number of Photos Observing the Tie Points

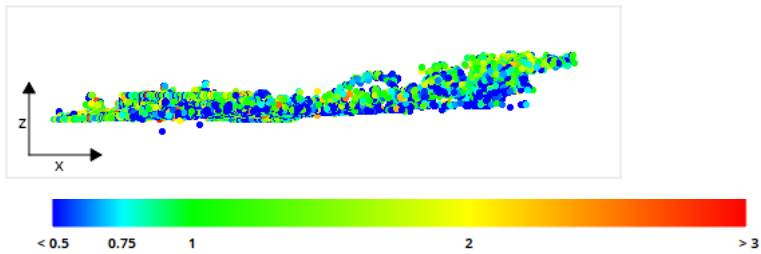


**Number of Observations per Tie Point:** Top view (XY plane), side view (ZY plane) and front view (XZ plane) displays of all tie points, with colors representing the number of photos that have been used to define each point. The minimum number of photos per tie point is 2 and the maximum is 96. The average number of photos observing a tie point is 5.

#### Reprojection Error

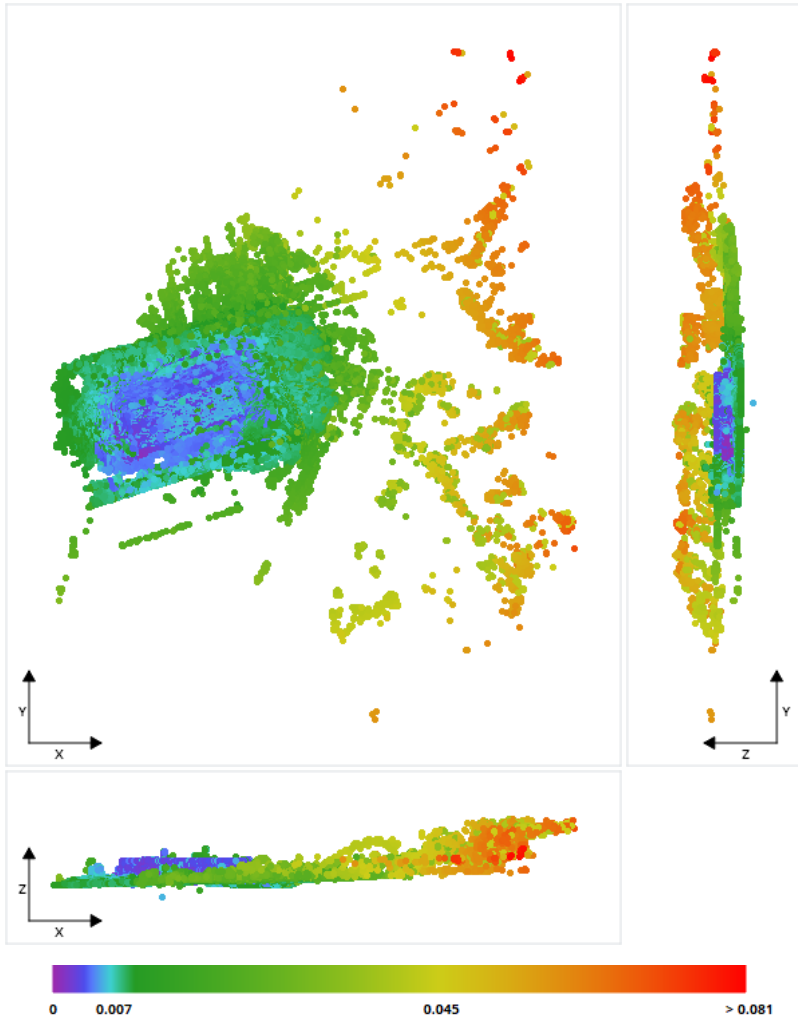






**Reprojection Errors per Tie Point:** Top view (XY plane), side view (ZY plane) and front view (XZ plane) displays of all tie points, with colors representing the reprojection error in pixels. The minimum reprojection error is **0.00 pixels** and the maximum is **3.42 pixels**. The average reprojection error is **0.99 pixels**.

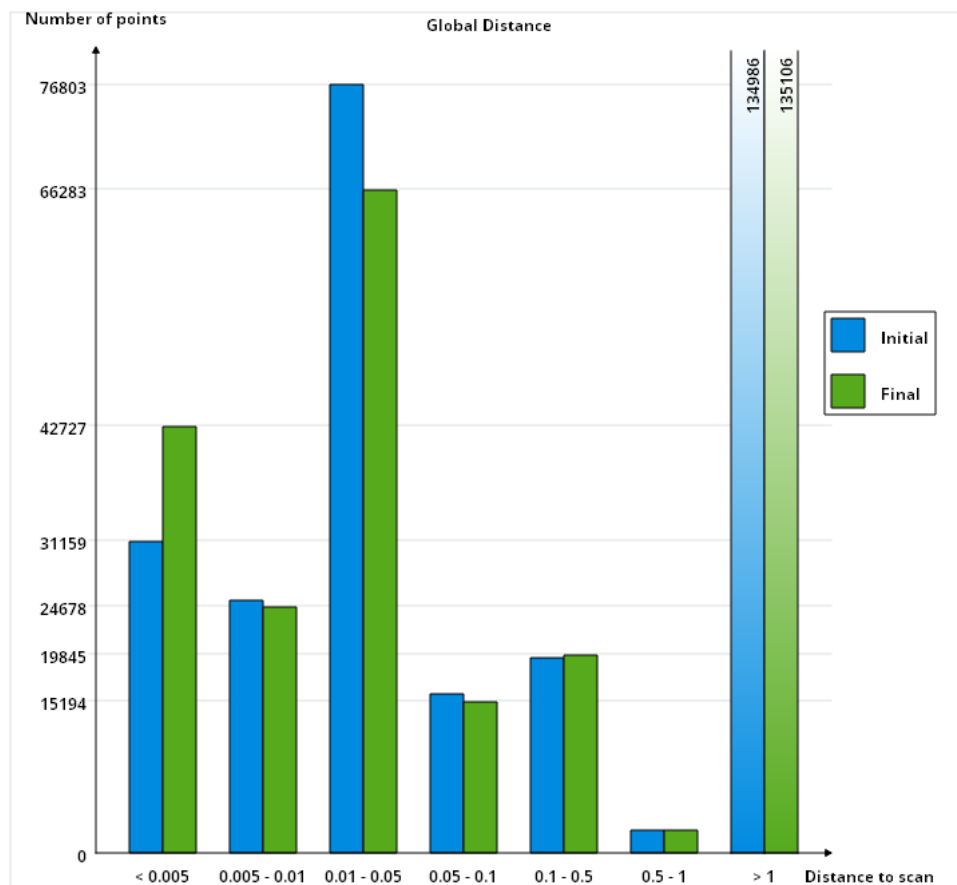
**Tie Point Resolution**



**Resolution:** Top view (XY plane), side view (ZY plane) and front view (XZ plane) displays of all tie points, with colors representing resolution in the individual point position. The values are in meters/pixel, with a minimum resolution of **0.0005 meters/pixel** and a maximum of **0.08062 meters/pixel**. The median resolution equals **0.00445 meters/pixel**.

**Distance to Point Clouds**

Distance between Tie Points Extracted from Photos and Scans				
	Initial values		Optimized values	
	Overlap (Number of points at < 50 cm)	Number of points at < 1 cm	Overlap (Number of points at < 50 cm)	Number of points at < 1 cm
NACEX_one_file	168826 (55.14% of the total number of tie points)	56485 (18.45% of the total number of tie points) (33.46% of the overlap)	168727 (55.1% of the total number of tie points)	67405 (22.01% of the total number of tie points) (39.95% of the overlap)
Global Distance	168826 (55.14% of the total number of tie points)	56485 (18.45% of the total number of tie points) (33.46% of the overlap)	168727 (55.1% of the total number of tie points)	67405 (22.01% of the total number of tie points) (39.95% of the overlap)



Details on Tie Point Distance to Point Clouds: Comparison between initial positions of the tie points, and the optimized values obtained after considering the point clouds.

## Surveys

Number of control points: 25. No control point is used as check point. Not used.

Number of user tie points: 3. No tie point is used as check point.

Number of positioning constraints: 0

## Control Points

Control Points Errors									
Name	Category	Accuracy [meters]	Number of Calibrated Photos	RMS of Reprojection Error [pixels]	RMS of Distances to Rays [meters]	3D Error [meters]	Horizontal Error [meters]	Vertical Error [meters]	
100	3D	Horizontal: 0.010; Vertical: 0.010	3 (3 marked photos)	9.84	0.01956	0.06897	X: -0.06197; Y: -0.02713	-0.01346	⚠
101	3D	Horizontal: 0.010; Vertical: 0.010	3 (3 marked photos)	6.26	0.01376	0.01425	X: -0.0076; Y: 0.00987	0.00693	⚠
102	Vertical	Horizontal: 0.01; Vertical: 0.01	3 (3 marked photos)	10.74	0.01685	0.0163		0.0163	⚠
103	3D	Horizontal: 0.010; Vertical: 0.01	3 (3 marked photos)	9.71	0.01604	0.02846	X: -0.02416; Y: 0.01482	0.00257	⚠
104	3D	Horizontal: 0.010; Vertical: 0.01	3 (3 marked photos)	2.47	0.00649	0.01541	X: 0.00971; Y: 0.01155	0.00313	⚠
106	3D	Horizontal: 0.010; Vertical: 0.01	3 (3 marked photos)	13.31	0.02031	0.03533	X: -0.03177; Y: 0.01103	0.01085	⚠
107	3D	Horizontal: 0.010; Vertical: 0.01	3 (3 marked photos)	21.03	0.03025	0.05078	X: -0.03367; Y: 0.02659	0.02716	⚠
108	3D	Horizontal: 0.010; Vertical: 0.01	3 (3 marked photos)	3.43	0.01259	0.01407	X: -0.00748; Y: 0.0011	0.01187	⚠
200	3D	Horizontal: 0.010; Vertical: 0.01	0 (0 marked photos)						
201	3D	Horizontal: 0.010; Vertical: 0.01	0 (0 marked photos)						
202	3D	Horizontal: 0.010;	3 (5 marked	5.28	0.01585	0.01674	X: -0.01103;	0.01192	⚠

		Vertical: 0.01	photos)				Y: -0.00404		
203	3D	Horizontal: 0.010; Vertical: 0.010	2 (5 marked photos)	24	0.07235	0.08641	X: 0.07773; Y: -0.00748	0.03699	⚠
204	3D	Horizontal: 0.010; Vertical: 0.01	3 (5 marked photos)	8.2	0.02299	0.02476	X: 0.018; Y: -0.01326	0.01064	⚠
205	3D	Horizontal: 0.010; Vertical: 0.01	0 (3 marked photos)						
300	3D	Horizontal: 0.010; Vertical: 0.01	0 (0 marked photos)						
301	3D	Horizontal: 0.010; Vertical: 0.01	4 (5 marked photos)	11.93	0.04441	0.05643	X: -0.03005; Y: 0.0401	0.02595	⚠
302	3D	Horizontal: 0.010; Vertical: 0.010	0 (0 marked photos)						
303	3D	Horizontal: 0.010; Vertical: 0.010	3 (3 marked photos)	24.85	0.08538	0.13744	X: -0.13291; Y: -0.00335	0.03481	⚠
304	3D	Horizontal: 0.010; Vertical: 0.01	3 (3 marked photos)	15.79	0.09468	0.25082	X: 0.24539; Y: 0.0242	-0.04592	⚠
305	3D	Horizontal: 0.010; Vertical: 0.01	3 (3 marked photos)	5.1	0.03969	0.04018	X: -0.00201; Y: 0.03987	0.00459	⚠
306	3D	Horizontal: 0.010; Vertical: 0.01	3 (3 marked photos)	21.69	0.04593	0.13307	X: -0.13232; Y: -0.01413	-0.00101	⚠
307	3D	Horizontal: 0.010; Vertical: 0.01	0 (0 marked photos)						
308	3D	Horizontal: 0.010; Vertical: 0.01	0 (0 marked photos)						
309	3D	Horizontal: 0.010; Vertical: 0.01	0 (0 marked photos)						
310	3D	Horizontal: 0.010; Vertical: 0.010	0 (0 marked photos)						
Global RMS				14.05	0.04371	0.08767	X: 0.08546; Y: 0.02043	0.02114	
Median				10.74	0.02299	0.04018	X: -0.01103; Y: 0.00987	0.01085	

No data are available

Horizontal and vertical errors are given according to each control point respective spatial reference system

#### User Tie Points

User Tie Points Errors				
Name	Number of Calibrated Photos	RMS of Reprojection Error [pixels]	RMS of Distances to Rays [meters]	
User Tie Point 1	4 (5 marked photos)	1.98	0.00483	⚠
User Tie Point 2	3 (5 marked photos)	2.98	0.01136	⚠
User Tie Point 3	4 (5 marked photos)	1.91	0.00726	⚠
Global RMS		2.34	0.00827	
Median		1.98	0.00726	

No data are available

Horizontal and vertical errors are given according to each control point respective spatial reference system